The Lattice Preferred Orientation of Olivine in Beni Bousera Ultramafic Massif, Morocco

by

Jessica R. Stanley

B.S. Earth, Atmospheric, and Planetary Sciences
Massachusetts Institute of Technology, 2008

Submitted to the Department of Earth, Atmospheric, and Planetary Sciences in partial fulfillment of the requirements for the degree of

Master of Science in Earth and Planetary Science

at the

Massachusetts Institute of Technology

September 2009

Author.....
Department of Earth, Atmospheric, and Planetary Sciences
June 22, 2009

Certified by.....
Oliver Jagoutz
Assistant Professor of Geology
Thesis Supervisor

Accepted by.....
Maria T. Zuber
E. A. Griswold Professor of Geophysics
Head, Department of Earth, Atmospheric, and Planetary Sciences

The Lattice Preferred Orientation of Olivine in Beni Bousera Ultramafic Massif, Morocco

by

Jessica R. Stanley

Submitted to the Department of Earth, Atmospheric, and Planetary Sciences on June 22, 2009 in partial fulfillment of the requirements for the degree of Master of Science in Earth and Planetary Sciences

Abstract

The roll of melt in deformation of the mantle is important for understanding mantle processes and evolution. The Beni Bousera Ultramafic Massif, northern Morocco, shows petrologic evidence that melt was an important part of its history. The massif, dominantly composed of spinel lherzolite with harzburgitic sections, has 10 to 100 meter scale zones which contain abundant pyroxenite dykes, dunite, harzburgite, and secondary lherzolite. These zones are interpreted as areas of focused melt percolation. Lattice preferred orientation (LPO) of olivine crystals from a sample transect across one of these zones was analyzed in comparison with LPO from the surrounding host lherzolite and harzburgite. The LPO from peridotites within the zone was slightly different from those outside the zone, and the LPO from the dunite analyzed was significantly different from the peridotites. Within the melt percolation zone, orientation of the olivine a-axis with respect to the mineral foliation indicates that strain increases towards the center of the zone and that shear sense changes across the zone. This suggests that focused melt flow can induce deformation in its host peridotite.

Thesis Supervisor: Oliver Jagoutz
Title: Assistant Professor of Geology

ACKNOWLEDGMENTS

I would like to thank my advisor, Oliver Jagoutz, for all his help and time, as well as the other members of my committee, Sam Bowring and Brian Evans. I would also like to thank Greg Hirth, Elizabeth Nadin, and Phil Skemer at Brown University for help with EBSD analysis. I would like to thank Pierre Bouilhol for sharing his microprobe data, Alison Piasecki for help in the field, Kyle Bradley for help with GIS, Sarah Gelman for editing and support, and everyone else at MIT who has shown interest and support. I would also like to thank Jessica Warren for help with pole figure projections and for providing the deformation mechanism map and paleopeizometer software. Finally, I would like to thank my family and friends for their continued encouragement.

Table of Contents

List of Figures

1. Introduction

Melt percolation and flow are important processes in the evolution of the Earth's mantle and crust. The presence of melt, even in small amounts can cause significant changes in the material properties of peridotite, by decreasing viscosity (Hirth and Kohlstedt, 1995) and causing melt-rich bands to segregate and concentrate strain (Holtzman et al., 2003). Melt channelization is also thought to be a important mechanism for melt extraction that is able to keep melts chemically isolated from the surrounding mantle (Kelemen et al., 1995; Suhr, 1999). Understanding melt percolation, segregation, and its relationship to deformation in the natural environment are important keys to understanding the evolution of the mantle and crustal processes. This thesis presents a petrographic and microstructural study of melt percolation zones and the host peridotite in the Beni Bousera Massif in northern Morocco. The data presented indicate deformation induced by channelized porous melt flow.

Beni Bousera is a large (~75 km^2) mantle peridotite now exposed in the Betic-Rif orogenic belt, part of the Alpine collision system. Earlier workers described Beni Bousera as a dominantly spinel lherzolite body with minor pyroxene dikes, which in part preserve evidence of high pressure (graphite pseudomorphs after diamond) (Pearson, 1989; Slodkevitch, 1982). Recent field studies (Gysi, 2007), however, have documented a larger lithological variability within the massif. In particular, Gysi (2007) found that pyroxenite dikes are not homogenously distributed throughout the massif; instead they occur in higher frequency in constrained tens to hundreds of meter wide zones. These zones show lithological

associations (dunite and harzburgite) indicating that they might represent zones of focused melt percolation. Field observations additionally indicate different deformation history for pyroxenite-rich zones and surrounding lherzolite: isoclinal folds and boudinage of pyroxenite layers are frequently observed within these zones, indicating strong deformation, whereas such structures are absent in surrounding host lherzolites which generally appear in the field as coarse and granular.

This thesis provides a field study of these zones and the surrounding peridotite, as well as a microstructural study of the high temperature deformation using electron backscatter diffraction (EBSD) to look at the lattice preferred orientation (LPO) of olivine crystals. We find evidence for melt percolation throughout the massif, and that heterogeneous zones represent areas of focused melt flow. We suggest that apparent difference in deformation between these zones and surrounding lherzolite is related to up-rise due to the density difference induced by melt percolation.

2. Geologic Background

The Beni Bousera Massif is located in the Rif mountain belt of Morocco that connects to the Betic Mountains of southern Spain across the straight of Gibraltar (Fig. 1). The Betic-Rif Arc contains several peridotite bodies including the Ronda Massif (southern Spain) and Beni Bousera Massif (northern Morocco).

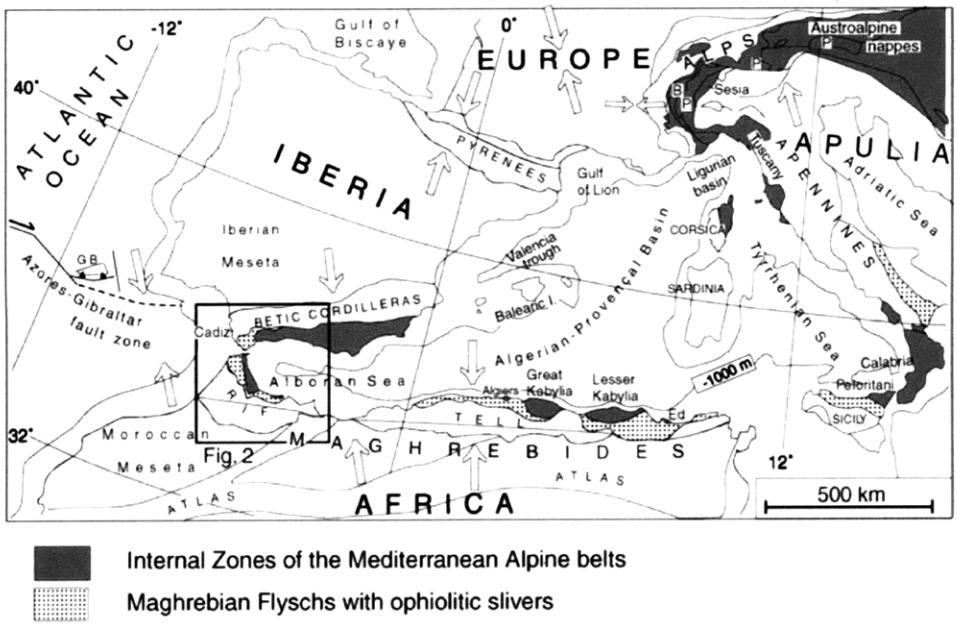

Figure 1. Shows the location of the Betic-Rif arc and the present day relative motion of the plates in the Mediterranean region. Arrows representing current day plate motion: (Balling and Banda, 1992; Buforn et al., 1995). Azores-Gibraltar fault zone: (Maldonado et al., 1999). From (Chalouan and Michard, 2004)

Structure

The Rif mountain range is structurally characterized by a complex nappe stack that was generally thrust towards the south and is divided into three major domains (Chalouan and Michard, 2004),(Figures 2 and 3) from the structural lower to higher: (1) The External Zone, which is a fold and thrust belt composed of pre-orogenic Upper Triassic to Lower-Middle Eocene sediments, followed by later

turbidite deposits (Chalouan et al., 2001), that have been detached from the African crust along Upper Triassic redbeds.

(2) The Maghrebian Flysch Nappes are thought to be the detached cover of the so-called Maghrebian Trough, thought to have formed in a small ocean separating the Internal Zones from Africa during the Jurassic and Early Miocene (Durand-Delga et al., 2000; Hoyes, 1989; Wildi, 1983).

(3) The Internal Zones contain carbonates, clastics, evaporates, metasediments and high grade schists and gneisses of continental origin derived from the Alboran terrain (Chalouan and Michard 2004). Beni Bousera is contained in the Sebtide Nappe, one of the three nappes that form the Internal Zones (Chalouan and Michard 2004).

Metamorphism

The majority of the Rif units have only been affected by low grade greenschist facies metamorphism (de Lamotte, 1985) which was dated at about 28 Ma by $^{39}Ar/^{40}Ar$ geochronology (Monie et al., 1984). However the parts of the Internal Zones shows Alpine aged (20 to 30 Ma) metamorphism, in some places high grade (Chalouan and Michard 2004). North of Beni Bousera in the area of the Beni Mezala ultramafics, there is evidence for high-pressure, low temperature (HP-LT) metamorphism, ranging from greenschist up to blueschist and eclogites facies (Bouybaouene, 1993; Chalouan and Michard, 2004; Goffe et al., 1996; Michard et al., 1997; Vidal et al., 1999). This was followed by retrograde isothermal decompression and subsequent decompression associated with cooling (Agard et al., 1999). The timing of the HP-LT event in the Beni Mazala region (north of Beni

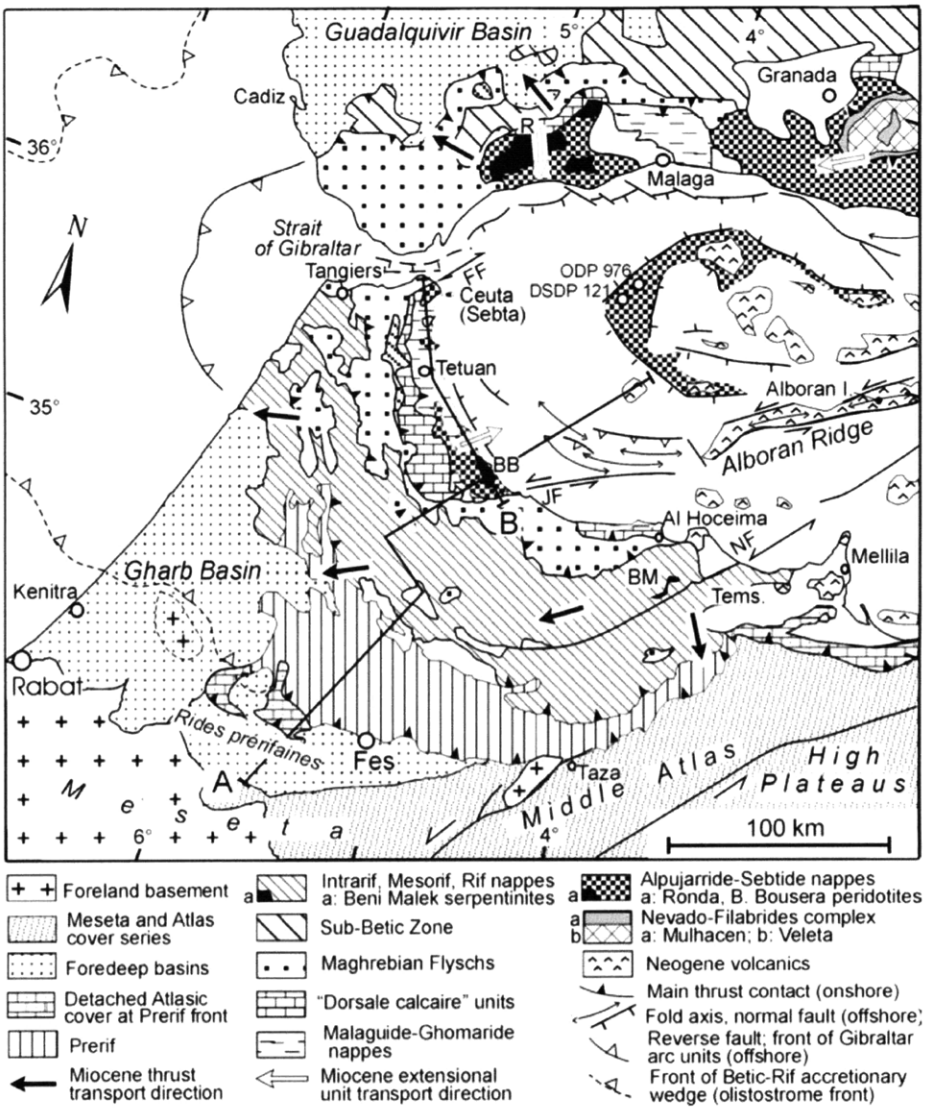

Figure 2. Geologic map of the Betic-Rif Region. A and B show traces of cross section in the following figure. BB is the Beni Bousera Massif, R is the Ronda Massif, and BM is the Beni Malek Massif. FF is the jebel Fahies fault, JG is the Jebha fault, and NF the Nekor fault. From Chaluan and Michard (2004), after Chalouan et al. (2001). Alboran basin: (Chalouan et al., 2001; Comas et al., 1999; Maldonado et al., 1999; MartinezMartinez and Azanon, 1997). Kinematic Directions: (Delamotte et al., 1991; MartinezMartinez and Azanon, 1997)

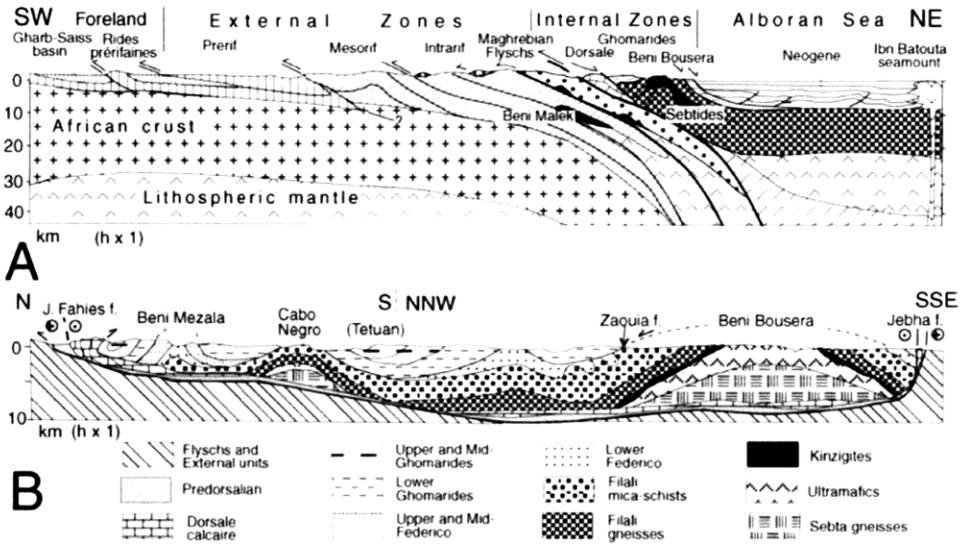

Figure 3. Interpretive cross section of the Rif Mountain belt (A) and the Internal Zones (B). The occurrence of the Sebta Gneisses under the Beni Bousera Massif is theoretically inferred from the presence of gneisses under the Ronda Massif. From Chalouan and Michard (2004).

Bousera) is not well constrained. K/Ar systematics of white micas yielded ages between 19.4+/-1.2 Ma and 27.4+/-0.6 Ma, and a green amphibole K/Ar age is 44.7+/-1.6 Ma (Montigny et al., 2004).

Beni Bousera and its surrounding units do not show evidence for HP-LT metamorphism. The Kinzigite rocks (granulite facies metapelites surrounding Beni Bousera) show peak pressures and temperatures of 800-850°C and 0.9-1.3 GPa (Bouybaouene et al., 1998). K/Ar biotite cooling ages cluster around 22+/-2 Ma (Montigny et al., 2004), which is interpreted as the onset of cooling after the climax of HT-LP (Alpine-related) metamorphism (Chalouan and Michard, 2004).

Tectonic Evolution

There are three proposed tectonic scenarios for this region. First: collision unrelated to subduction (Kornprobst and Vielzeuf, 1984; Montel et al., 2000; Platt and Vissers, 1989; Turner et al., 1999). Second: a single NW dipping subduction

zone connecting the Apennines to Gibraltar (Buforn et al., 1995; Caby et al., 2001; Calvert et al., 2000; Lonergan and White, 1997; Zeck, 1996). Third: two subduction zones, a SE-dipping one connecting the Alps to the Betics and a NW dipping one connecting the Apennines to the Rif, with a microcontinent in between(Andrieux et al., 1971; Chalouan and Michard, 2004; Chalouan et al., 2001; de Lamotte et al., 2000; Doglioni et al., 1999; Doglioni et al., 1998; Durand-Delga and Fontbote, 1980; Guerrera et al., 1993; Michard et al., 2002; Rehault et al., 1984; Torresroldan et al., 1986).

The tectonic evolution described here is based on the two-subduction zone scenario presented by Chalouan and Michard (2004), and is summarized in their figures (Fig. 4 and 5). The Alkapeca (Alboran-Kabylias-Peloritani-Calabrai) Block, a microcontinent containing the future Alboran domain as well as other related metamorphic domains found around the Mediterranean (Bouillin et al., 1986) is located between Iberia and Africa, east of its current day position (Fig. 4A). The Alkapeka Block is thought to have split off from the Apulian plate during extension of the Tethys (Michard et al., 1993).

At 80 Ma, convergence between the African and European plate began (Chalouan and Michard, 2004). In the Betic-Rif region, south-dipping subduction began in the Betics, on the north side of the Alkapeka microplate, related in the east to subduction in the Alpine chain (Chalouan and Michard 2004) (Fig. 4B, 5A). North dipping subduction and formation of the Rif Mountain belt began in the Oligocene, and was likely connected in the east to subduction Apennines (Fig 4C).

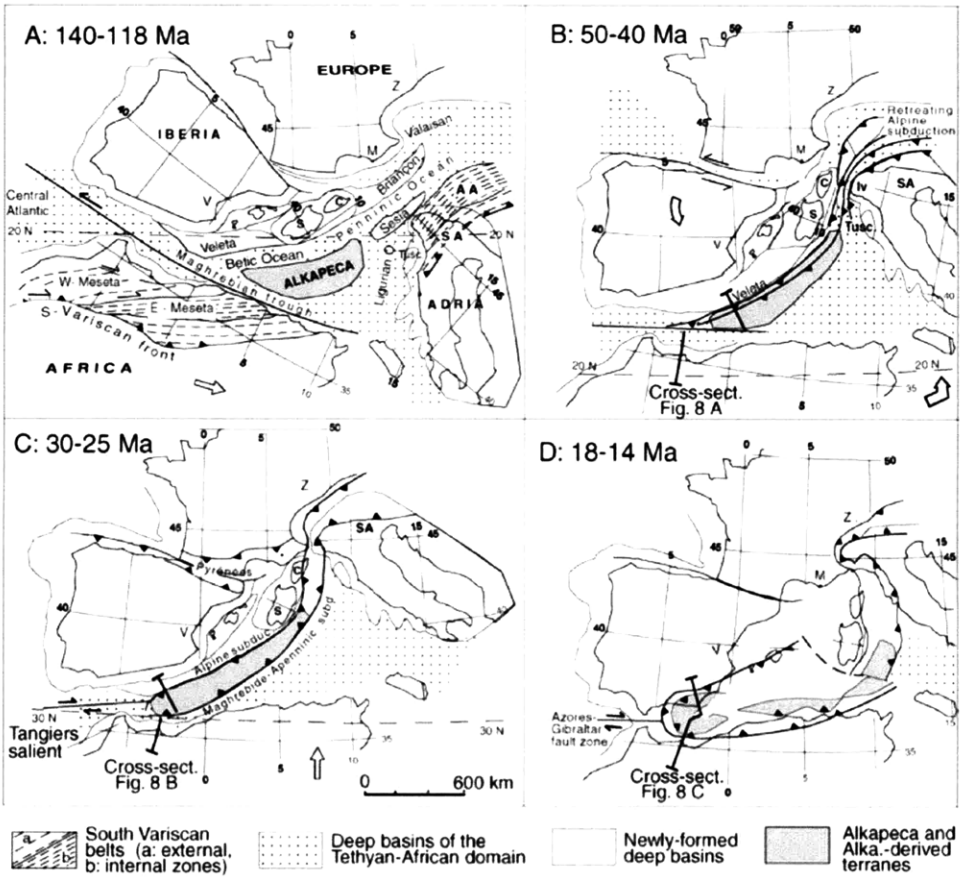

Figure 4. Tectonic evolution of the Betic-Rif region from Chalouan and Michard (2004). Displacements are shown by arrows with respect to Europe (Dercourt et al., 1993; Roest and Srivastava, 1991; Savostin et al., 1986). AA: Austroalpine, C: Corsica, Iv: Ivrea Zone, M: Marseilles, SA: South Alpine, S-M: Sesia-Margna, Tusc: Tuscany, V: Valencia; Z: Zurich. Western Alps: (Froitzheim et al., 1996; Stampfli et al., 1998). Panel D: (Bouillin et al., 1998; Faccenna et al., 1997).

Depending on the poorly constrained date for HP-LT metamorphism in the Rif, there is more than one interpretation of how the Maghrebian subduction progressed (5B and 5C) (Chalouan and Michard 2004).

Subduction rollback toward the southeast triggered extension in the overriding Alkepeka block, with the Alborian domain moving toward Morocco (Figure 4D) (Chalouan and Michard, 2004; de Lamotte et al., 2000; Gueguen et al., 1997; Lonergan and White, 1997; Maldonado et al., 1999; Verges and Sabat, 1999). The western end of the Maghebrian subduction zone rotates over time, becoming

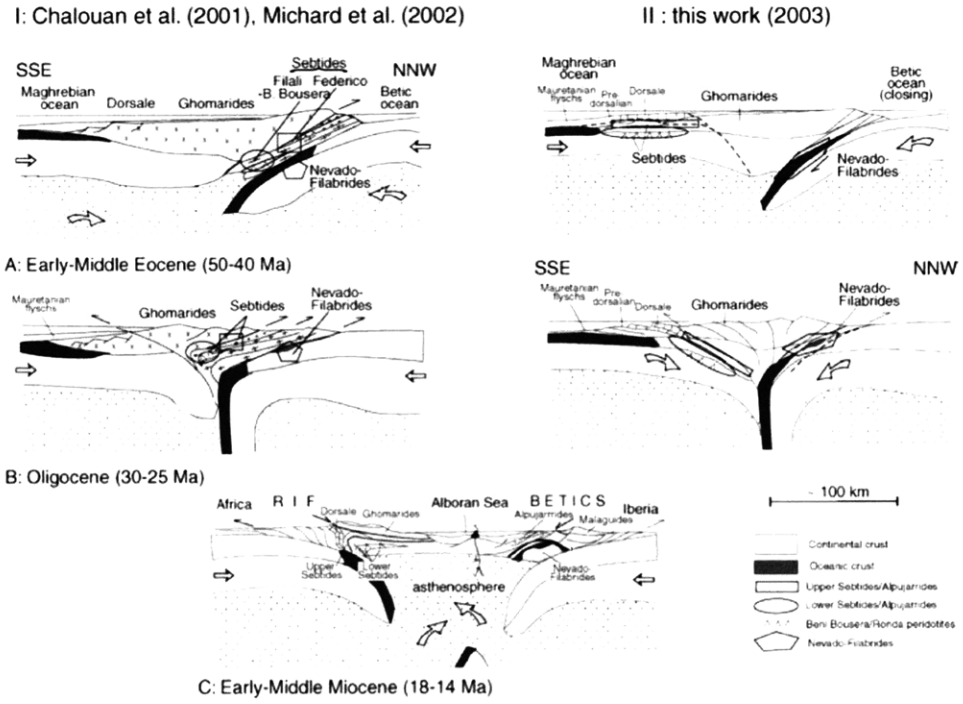

Figure 5. Two cross section scenarios for the tectonic setting presented in Figure 4 depending on the poorly-constrained age of HP-LT metamorphism, from Chalouan and Michard (2004).

north-south trending, and then likely connecting with the Betic-Alpine subduction in the north (Fig 4D) (Chalouan and Michard, 2004; Favre, 1995; Menvielle and Lemouel, 1985).

From the late Oligocene to middle Miocene, backarc spreading caused extreme extension and the collapse of the internal orogen (Figs. 4D and 5C) (Chalouan and Michard, 2004; Chalouan et al., 2001; Chalouan et al., 1997; Comas et al., 1999; Garciaduenas et al., 1992; Maldonado et al., 1992; Watts et al., 1993). This is supported by cooling ages from the internal units being clustered around 22+/-2 Ma (Montigny et al. 2004).

The Miocene-Pliocene was a period of compression, followed by a period of extension (Chalouan and Michard, 2004). In Pliocene-Pleistocene, there is another

period of compression resulting in post-nappe synclines in the central Rif (Chalouan and Michard, 2004).

Pressure-Temperature-Time Evolution

Platt et al. (2003) constrain the P-T-t evolution of the Ronda and Carratraca massif and surrounding units. Their study included samples from peridotites and surrounding gneisses up to unmetamorphosed sediments. They document a P-T-t relationship (Figure 6), which suggests that all structural levels saw isothermal exhumation paths or heating during exhumation, with cooling not starting until shallow crustal depths (10-15 km) (Platt et al., 2003). The radiogenic ages document that exhumation occurred rapidly, as ages from U-Pb zircon, ^{39}Ar-^{40}Ar hornblende and muscovite, and zircon fission track are very similar within error (around 20 Ma) (Figure 7). K-Ar biotite ages from the kinzigite rocks surrounding Beni Bousera are similar at 22+/-2 Ma (Montigny et al., 2004). It is thought that the rapid exhumation occurred during post-orogenic extension and crustal thinning. Geologic evidence indicates the crust is about a third as thick as it was before extension, and Platt et al. (2003) attempted to model this and the P-T-t data. The observed temperature increase during exhumation can either be explained by heating due to radiogenic decay in a thickened crust, or by lithospheric delamination. Modeling of the P-T-t evolution indicates that lithospheric delamination at 67.5 km provides the best fit to the data (Platt et al., 2003).

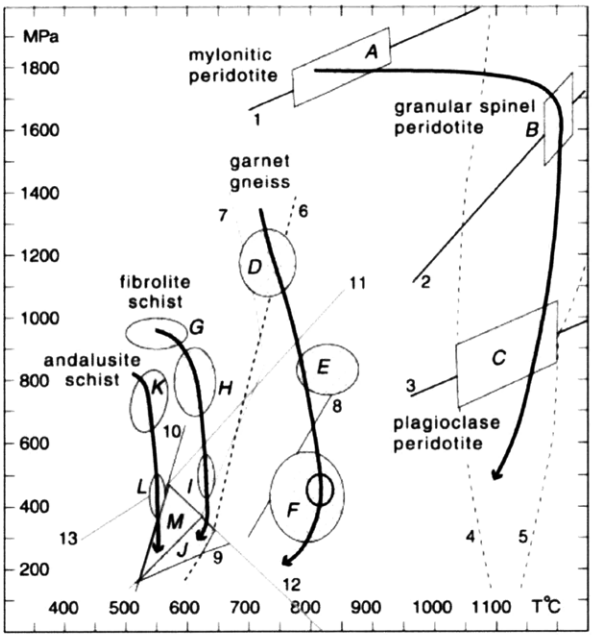

Figure 6. Pressure-Temperature evolution for the Ronda massif and surrounding units, from Platt et al. (2003). Note how little cooling occurs as pressure significantly decreases. A, B, and C are for the different facies of the Ronda peridotite, interpretation based on Van der Wal and Vissers (1993) and Lenoir et al. (2001). D:Grt-cpx cores in a mafic boudin from the surrounding garnet gneiss, E:Grt-hbl-pl in mafic boudin, F-Grt-opx-pl in mafic boudin, data for D-F from Platt et al (2003). G: Grt-St-Ky-Pl-Rt in the fibrolite schist, H:Grt-St-Ky-Bt-Ms in fibrolite schist, I: Grt-Sil-Bt-Ms in fibrolite schist, J:And-Bt-Ms in fibrolite schist. K: Grt-St-Ky-Bt-Ms in andalusite schist, L: Grt-St-And-Bt-Ms in andalusite schist, M:St-And-Bt-Ms in andalusite schist. Data for G-L from (Argles et al., 1999).

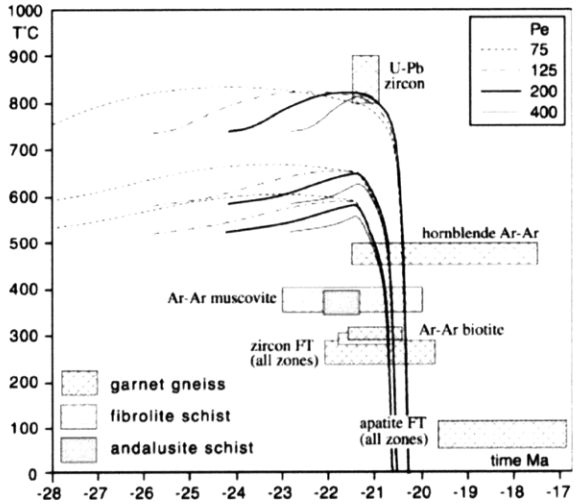

Figure 7. Radiometric data for crustal envelope of the Ronda massif plotted with the results of P-T-t modeling from Platt et al (2003). Note how fast the cooling is. The different lines represent different Peclet numbers used in the model during the stretching phase, they favor Pe=200, shown in bold. The fission track ages are means of all the data for the 3 metamorphic zones, and thus may underestimate the true variance.

Peridotite Emplacement

The emplacement of the peridotite massifs in the western Mediterranean is not well understood. There are two alternate overarching interpretations, each with variations: Emplacement of ultramafite as tectonic slivers, or emplacement as a diapir. The first, favored by Chalouan and Michard (2004), Kornprobst (1974), Reuber et al. (1982), Michard et al. (1991) and others, suggest that the Beni Bousera and Ronda massifs were brought to crustal levels during the Tethyan rifting, and emplaced as tectonic slivers during the Paleogene period of collision and compression. Reuber et al. (1982) interprets the contact of Beni Bousera with the surrounding Kinzigite gneisses as a ductile shear zone related to tectonic thrusting (Fig. 8). The supporters of this emplacement mechanism suggest that the internal units along with the ultramafic massifs were thrust up from the middle of the Alboran basin, based on paleomagnetic rotations and gravity anomaly data (Fig. 9).

Van der Wal and Vissers (1993) argue that extensional emplacement in the crust does not account for the complex pressure-temperature histories for the Ronda massif, and present a scenario in which emplacement is related to subduction and slab break (Figure 10). In this model early uplift is related to Jurassic extension (not shown). Paleogene subduction then led to cooling, but slab break off in the Oligocene led to further uplift and heating. Finally, extension and collapse of the internal orogen in Oligocene-Miocene emplaced the massifs in the crust (Vanderwal and Vissers, 1993).

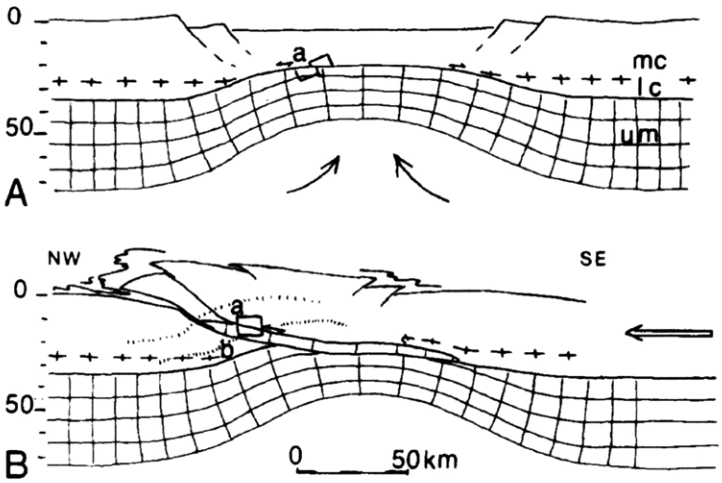

Figure 8. Model for emplacement of the Beni Bousera Massif from Reuber et al. (1982). A: Extension causes uplift the upper mantle (um) with massif protolith (a) from lower crust (lc) to middle crustal (mc) depths. B: Thrusting allows decoupling of massif from upper mantle and brings it farther up into the crust.

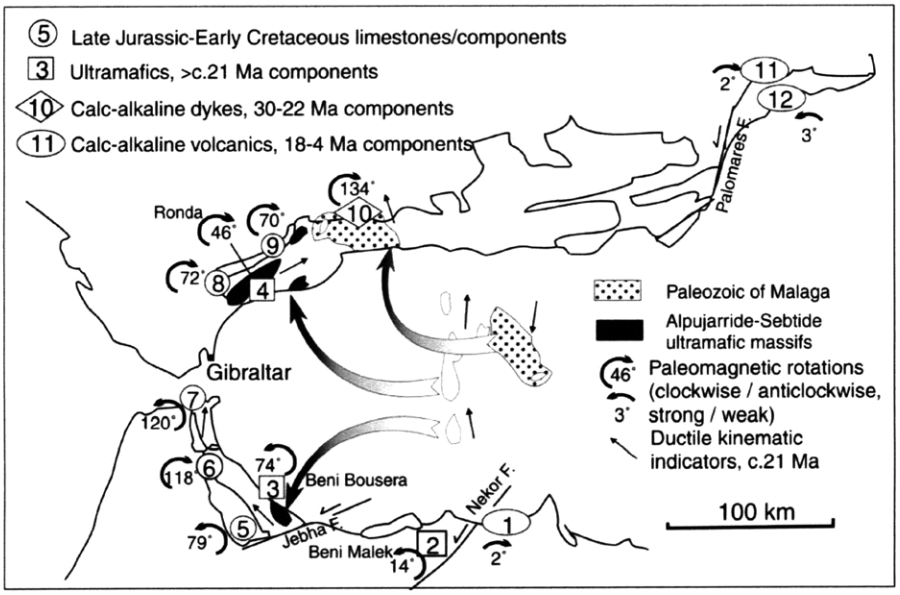

Figure 9. The inferred origin of the thrust nappes and ultramafic massifs from the approximate location of the pre-Miocene orogen, as supported by paleomagnetic rotations. From Chalouan and Michard (2004). Paleomagnetic references: 1:(Najid et al., 1981), 2:(Elazzab and Feinberg, 1994), 3:(Saddiqi et al., 1995), 4:Feinberg 1996* 5-9:(Allerton et al., 1994; Platzman, 1992; Platzman et al., 1993), 10:(Calvo et al., 2001; Platzman et al., 2000), 11-12: (Calvo et al., 1997).

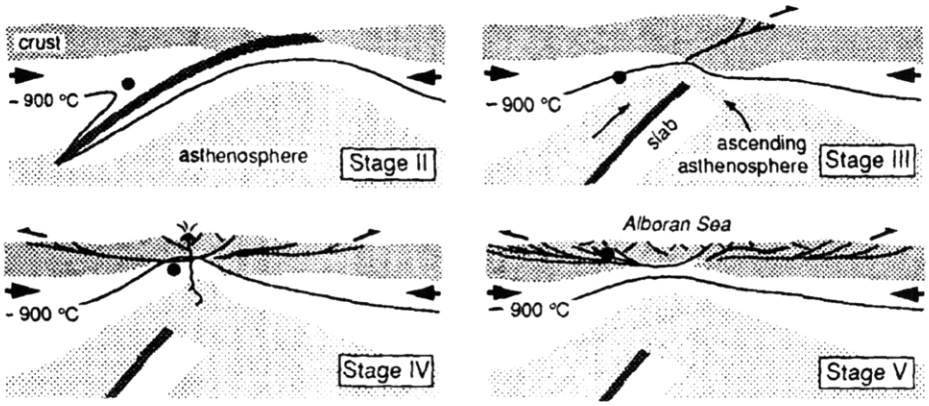

Figure 10. Tectonic emplacement involving a subduction zone and slab break off from Van der Wal and Vissers (1993). After original uplift into the crust (not shown), Stage II: Subduction in the Cretaceous to Paleogene causes cooling. Stage III: Slab detachment in Oligocene leads to uplift and heating. Stage IV: Extension and collapse in Oligocene to Miocene lead to emplacement in the crust. Stage V: Thermal subsidence and the formation of the Alboran Sea.

Based on the P-T-t data and modeling, Platt et al. (2003) suggest that the peridotites were emplaced in the crust through a series of ductile normal faults which reached down into the lithospheric mantle, and subsequent thrusting of the external thrust belts. Their sequence is shown in Figure 11, and requires a specific geometry for the extensional structures, but does account for the massifs' emplacement during a period of extension.

Others (Loomis, 1972; Montel et al., 2000; Obata, 1980) favor an origin for the massifs from a mantle diapir. Loomis (1972) bases his argument on contact metamorphism and metamorphic isograds in the Kinzigite gneisses surrounding the Ronda massif. He argues that the diapir was grounded in a hot asthenospheric root, and was driven up into the crust by buoyancy forces (Fig. 12). Obata (1980) uses his calculated P-T paths to support a diapiric origin, but calculates an uplift rate of 1m/yr for 1200° to 800°C based on cooling rates and crystallization, and notes that the viscosity of the massif would be too high to achieve this rate, so later emplacement must have had some tectonic involvement. Similar in some ways to

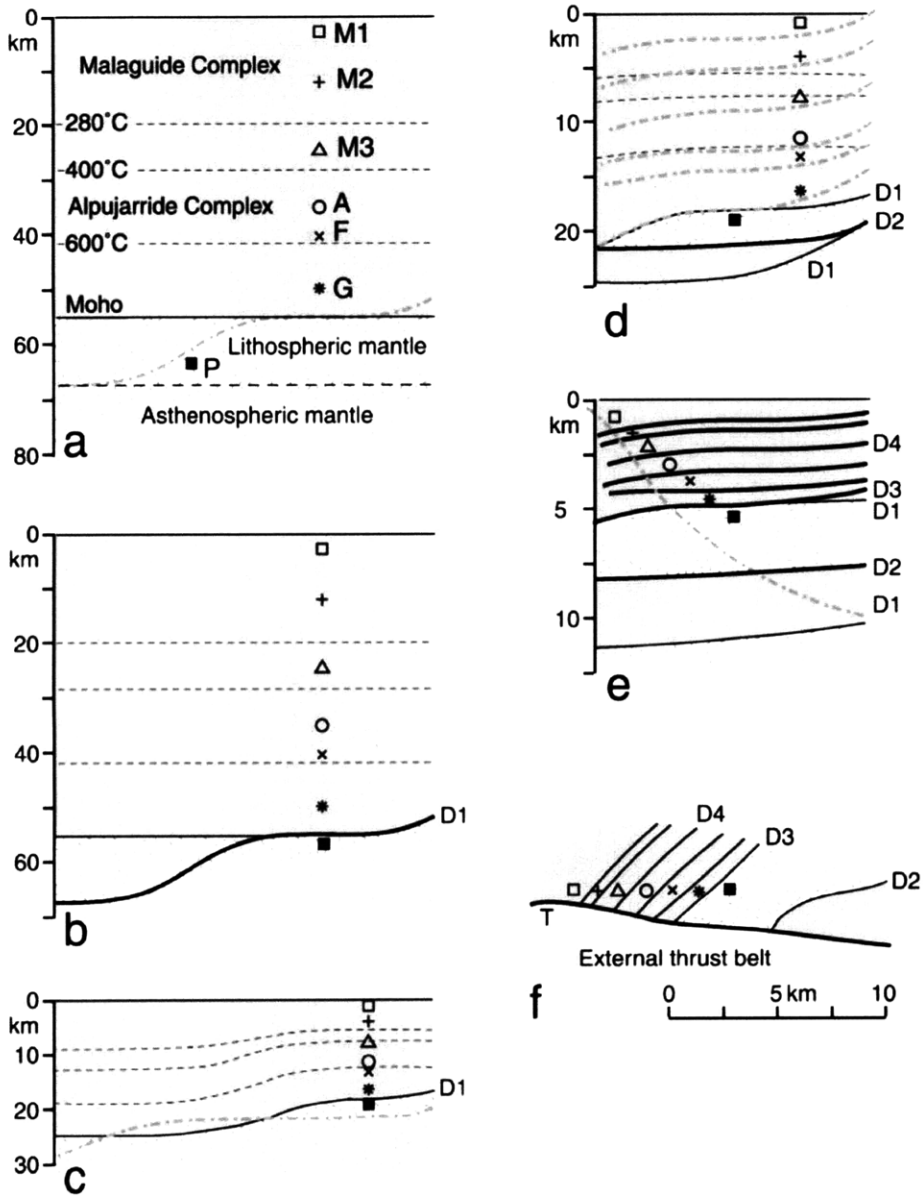

Figure 11. Illustration of the emplacement mechanism envisioned by Platt et al. (2003). The grey units are the overlying metamorphic units, the box labeled P represents the peridotite massif. Bold lines are active faults, dashed grey lines are future faults. a) Situation before thinning begins. b) D1 is the first ductile extensional detachment, which becomes the upper contact of the peridotite with crustal rocks. c) situation at 21Ma when the crust has been thinned by a third. d) the second extensional detatchment, D2 brings the periodtite into contact with the crustal rocks on its lower contact (scale is twice that of a-c). e) situation at 20 Ma with continued crustal thinning. f) the whole sequence is thrust on to the Iberian margin, producing the arrangement seen today. From Platt et al. (2003).

Obata, Montel et al. (2000), based on geochronological arguments, infer that the mantle rocks were emplaced in the lower crust as a diapir, and then thrust up, while still hot, toward the surface causing some contact metamorphism (Fig. 13).

Obviously, the orgin of the ultramafic massifs in the western Mediterranean is still debated, and one of the compelling reasons to study these rocks.

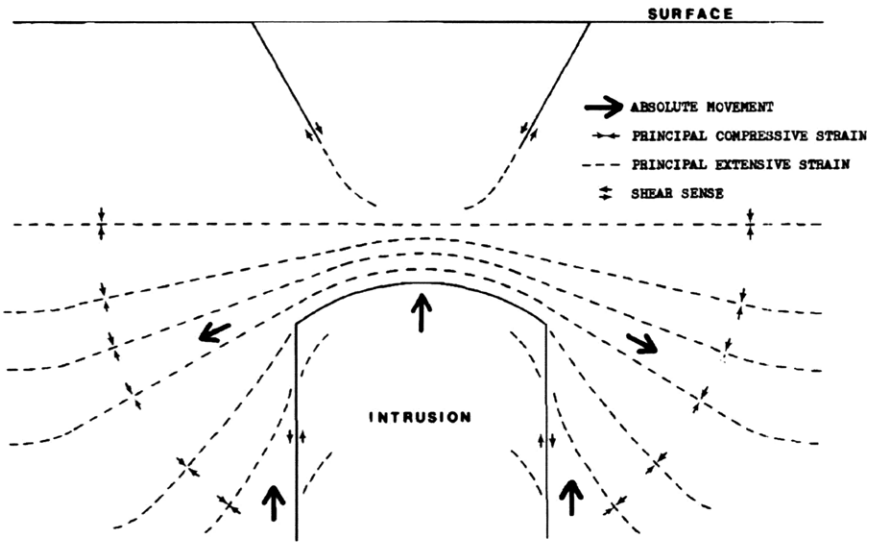

Figure 12. Schematic diagram of diapiric intrusion model from Loomis (1972). Extensional features are expected at the surface, as is a foliation drag (dotted lines).

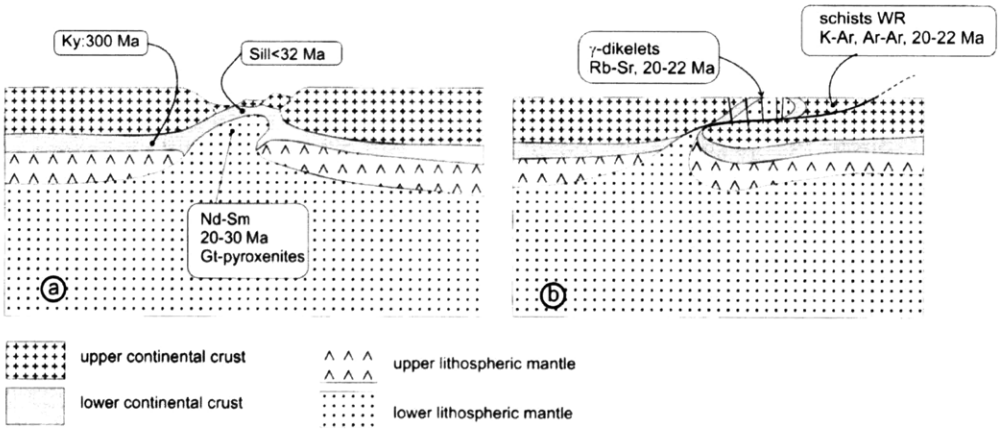

Figure 13. Model of peridotite emplacement from Montel et al (2000) based on geochronology and analogue models (Beslier and Brun, 1991), modeled after Kornprobst and Vielzeuf (1984). a) lower lithospheric mantle intrudes upper mantle and lower continental crust during extension. b) compression brings mantle rocks to the surface

3. Field Observations and Petrology

Field and Thin Section Observations

Field observation focused on a north to south transect across the massif complemented by observations made near the contact between the massif and the host rock and elsewhere in the massif. In the field rocks were classified through their modal mineral content and texture. Rocks were categorized into lherzolite, harzburgite, dunite, or pyroxenite based on the ternary diagram shown in Figure 14 (Streckeisen, 1976).

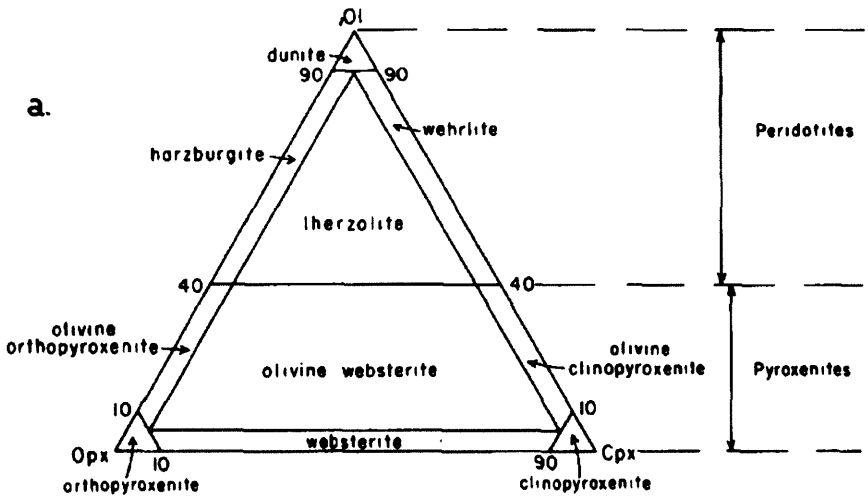

Figure 14. Ternary diagram for the classification of rocks with more than 90% mafic minerals (Streckeisen, 1976).

Textural observations were made on the basis of grain size, shape, and arrangement (texture, fabric) within the rock. Separation based on textural criteria can locally be challenging due to poor exposures or weathering. Additionally, solid state deformation might obliterate older textures.

Conventional thin sections from samples taken in the field were studied with a petrologic microscope. Petrographic observations focused on mineral content,

grain size and shape, and the nature and age relationship between intermineral contacts.

Major Rock Units and Associations

Nich Lherzolite

Shown in green on map and cross section, Plates 1 and 2*. Named after a type locality at 35°16'12.012"N, 4°52'6.144"W.

Fertile lherzolite characterized by large spinel crystals. Modal composition varies locally, but typically about 40-60% olivine, 5-15% spinel, 15-25% orthopyroxene, and 15-20% clinopyroxene, based on field observations. Orthopyroxene is often light to dark brownish (depending on weathering), while clinopyroxene is generally bright green. Texture is granular, and normally is characterized by an olivine matrix surrounding regularly distributed grains of pyroxenes and spinel. The Niche Lherzolite generally shows little to no macroscopic deformation features, and a foliation is hard to see. This unit is generally found in homogeneous outcrops and forms a major unit in the massif. A typical texture is shown in Figure 15.

In thin section, fractured and often serpentinized olivine surrounds large (3-5 mm), rounded, oblong opx and smaller cpx and spinel grains. Opx is generally more rounded, whereas cpx and spinel are more often exteneded and alligned with foliation. Both opx and cpx show exsolution lamellae of the opposite pyroxene. The olivine grain size is generally bimodal and variable, with larger relict olivine porphroblasts (several milimeters), and smaller neoblasts (tenths of mm). The

Figure 15. Typical Nich Lherzolite texture. Orange colored mineral is olivine, black flecks are spinel, green is clinopyroxene, and grey is orthopyroxene.

Nich shows evidence for several generations of melt-rock reactions circling around the olivine, opx peritictic according to the reation:

$$ol+melt1 = opx +melt2$$

Both reaction direction are observed. Poikiolitic opx with olivine inclusions indicates that the opx grew at the expense of olivine. On the other hand olivine and spinel have concave contact relation ship and embay the opx and therefore are interpreted to consume it on the grain boundary (Figure 16). This is espacially true for samples from the central part of the Niche units. Whereas, close to the contact with the Porphyric harzburgite, the Niche lherzolite is characterised by decreasing modal abundance of cpx and to a lesser extend opx indicating that both pyroxenes are being consumed by melt producing reaction(s). In the contact zone the edges of the pyroxene grains are often embayed by olivine, and grains cut by olivine veins

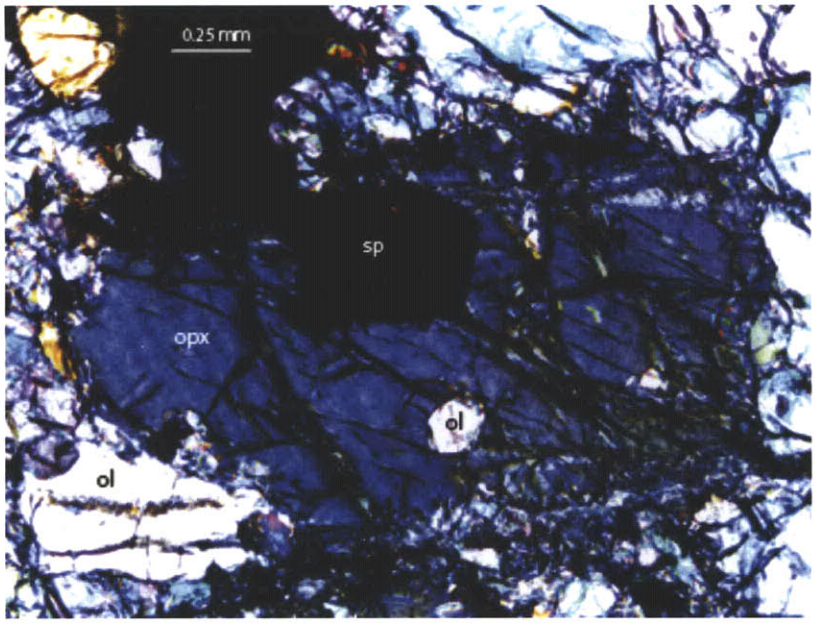

Figure 16. Thin section of the Nich Lherzolite showing multiple stages of melt-rock interaction. Opx (blue, center) has inclusions of olivine (white, center), but it's boundarys are being embayed by spinel (black) and later stages of olivine (white and multicolored).

(Fig 17). Spinel crystals are dark and amoeboid shapped, and appears to be growing interstitially between the olivine and opx (Fig 18). Foliation intensity is often more apparent in thin section than would be expected from the texture of the hand samples.

Porphyric Harzburgite

Shown in yellow (homogeneous Porphyric) or orange (part of a heterogeneous zone) on the accompanying map and cross section (plates 1 and 2)

Harzburgite that has an average modal composition 50% olivine, 5% spinel, 5% clinopyroxene, 40% orthopyroxene, as estimated in the field. However, it commonly shows significant modal variation within outcrops, ranging locally from 85% olivine to 85% opx creating foliation parallel banding defined by variations in modal content of orthopyroxene and olivine (Fig 19). The cpx and spinel composition seem to vary less. The Porphyric harzburgite has an olivine matrix

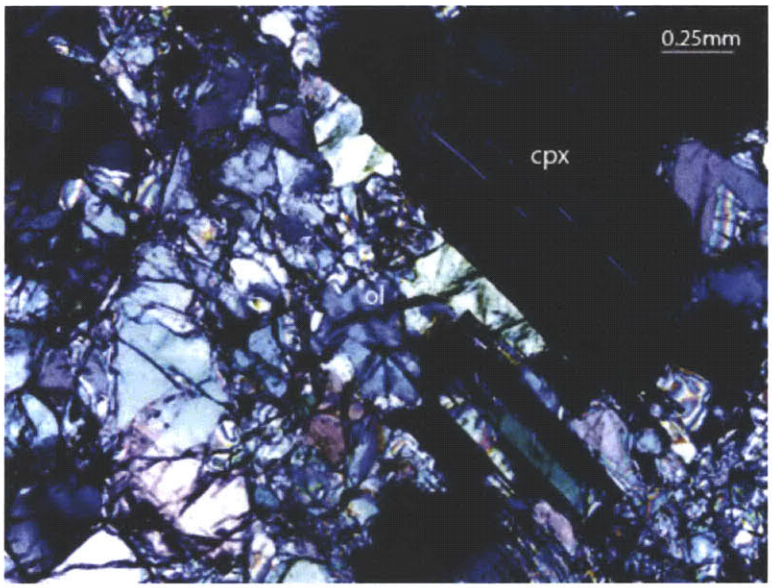

Figure 17. Thin section of Nich Lherzolite. Cpx grain (in extinction) has been split by olivine (bright colors). Olivine also embays the cpx in the upper right.

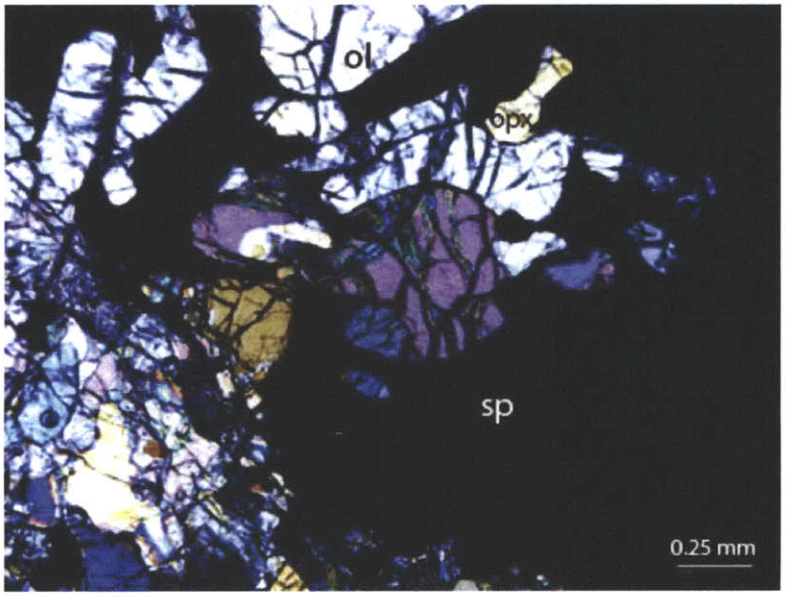

Figure 18. Thin section of Nich Lherzolite. Large spinel grain (black) shows amoeboid shape engulfing olivine (colors) and opx (light grey).

surrounding rounded, ellipsoidal (porphyric) orthopyroxene grains generally 5-10 mm across and 2-6 mm wide (Fig 20). It is can be associated with pyroxenite dikes and dunite.

In thin section large (several mm), rounded, elongate opx grains show wide (~.1 mm) exsolution lamellae (Fig 21) of cpx, and are surrounded by fine-grained (average .6 mm) fractured olivine. When spinel and cpx are present they show small grain size (generally around 1 mm). Inter mineral contact relationship

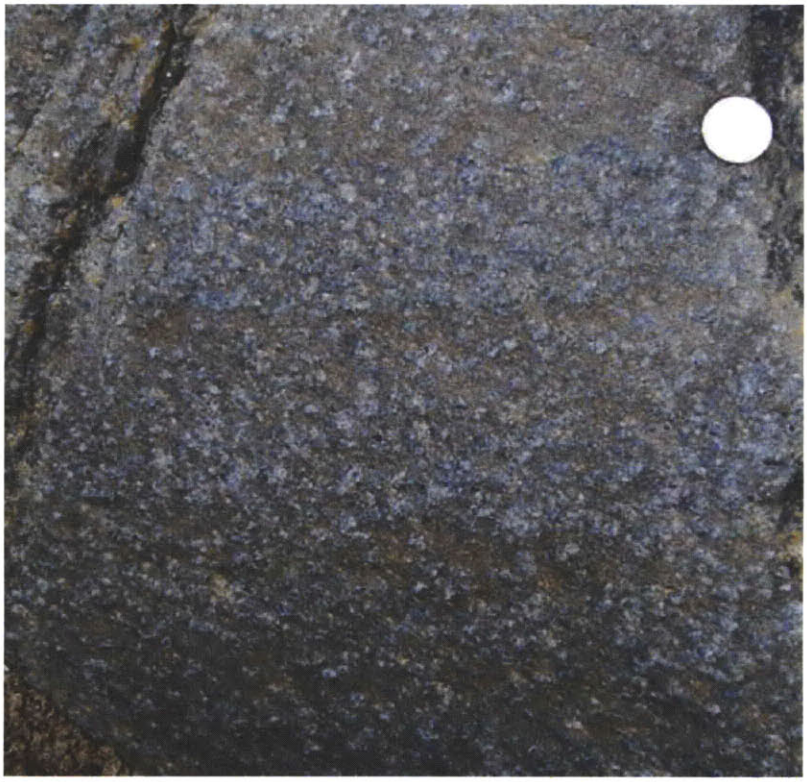

Figure 19. Porphyric harzburgite texture showing compositional banding. Orange matrix is olivine and grey mineral is opx, black specs are spinel.

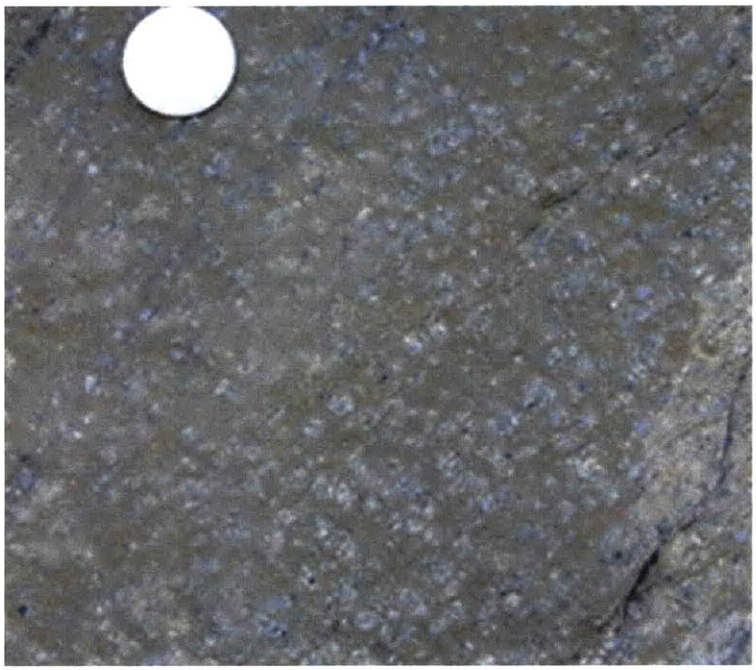

Figure 20. Porphyric texture as seen in the field, orange background is olivine, grey mineral is the opx, notice the ellipsoid shape.

indicate that the olivine grows at the expense of cpx According to the reaction

$$cpx + melt1 = ol + melt2$$

The contact relation between the opx and the olivine is hard to discern. Many of the large opx grains have olivine inclusions, indicating that opx grew originally at the expense of olivine. However, the intermineral contact relations between ol and opx are unequivocal and often difficult to discern. It appears that opx and ol show mutual replacive relationship, similar to those observed in the Nich lherzolite. There are clear examples of large opx with an almost poikilitic texture which grows at the expense of olivine and consuming grains at their edges (Fig 22). However, good examples of olivine splitting large opx grains and consuming them along exsolution lamellae (Fig 23) are found too.

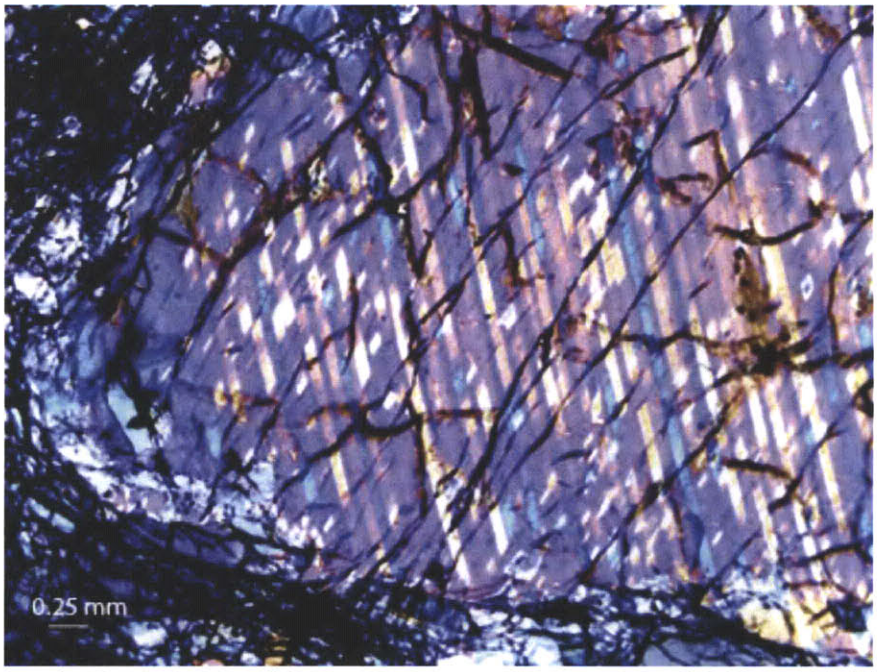

Figure 21. Porphyric texture in thin section. Large opx egg (purple) shows wide exsolution lamellae of cpx (orange) and is surrounded by small olivine grains.

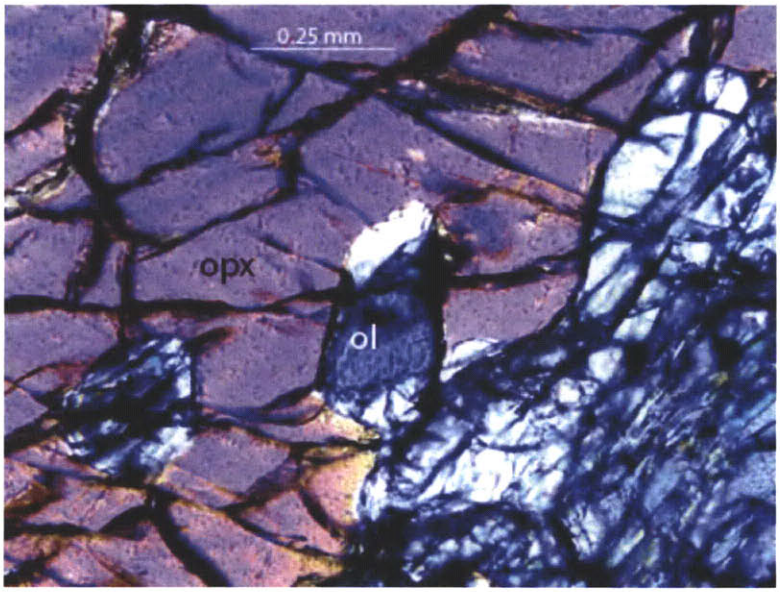

Figure 22. Porphyric texture in thin section. Edge of large opx grain (purple) surrounding and consuming neighboring olivine grains (blue).

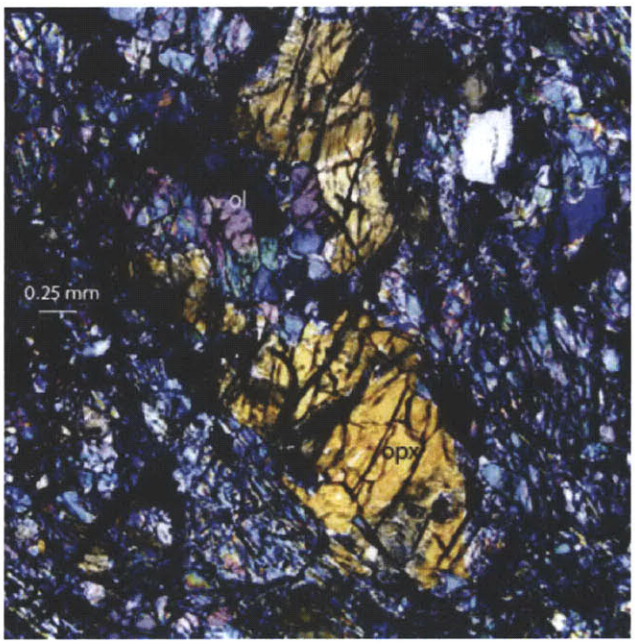

Figure 23. Porphyric opx grain (orange) being cut by smaller olivine grains (blue, green purple).

Heterogeneous Zones

Shown in orange on the map and cross section (plates 1 and 2). The heterogeneous zones are characterized by a large lithological variability observed often over only a few meters. The dominant lithologies that make up the heterogeneous zones are outlined below. Additionally, heterogeneous zones are often associated with the Porphyric Harzburgite, which however also forms mapable units outside of the heterogeneous zones.

Figure 24. Example of interstitial texture in a honeycomb lherzolite. Orange is ol, notice how it is surrounded by grey and green opx and cpx grains.

Honeycomb Peridotite

The Honeycomb Peridotite is either a harzburgite or lherzolite with a modal composition that is generally 60% olivine, 5% spinel, 10% clinopyroxene, and 25% orthopyroxene, but can vary significantly locally, with as much as 90 % olivine. Regardless of modal abundances the honeycomb peridotites is characterized by a texture of pyroxenes (~1 mm) which occur interstitially between individual olivine grains, which are generally 2-5 mm wide (Fig. 24). The unit occurs both on outcrop scale, and as small meter sized bodies within single outcrops associated with other facies such as the Porphyric Harzburgite, dunite and pyroxenites.

In thin section the pyroxenes lack the wide exsolution lamellae found in the Porphyric Harzburgite and Nich Lherzolite. If exsolution lamellae are present, they are thin, though the pyroxenes are generally smaller than in the Nich Lherzolite or Porphyric Harzburgite (1mm as apposed to 3-6mm). Texturally pyroxenes grow at

the expense of olivine. Pyroxene-olivine co-mineral contacts are either sharp edges splitting olivine grains (Figure 25) or irregular whereby pyx engulfs olivine grains. Pyroxenes occur interstitially on grain boundaries between larger olivine grain boundaries, frequently in triple junctions. Based on these textural observations pyx in the honeycomb peridotites are clearly largely secondary growing at the expenses of olivine (Figure 25). Sometimes cpx seems to be the dominantly growing mineral (as opposed to opx), suggesting that some of this unit may be re-infiltrated harzburgite rather than re-infiltrated dunite.

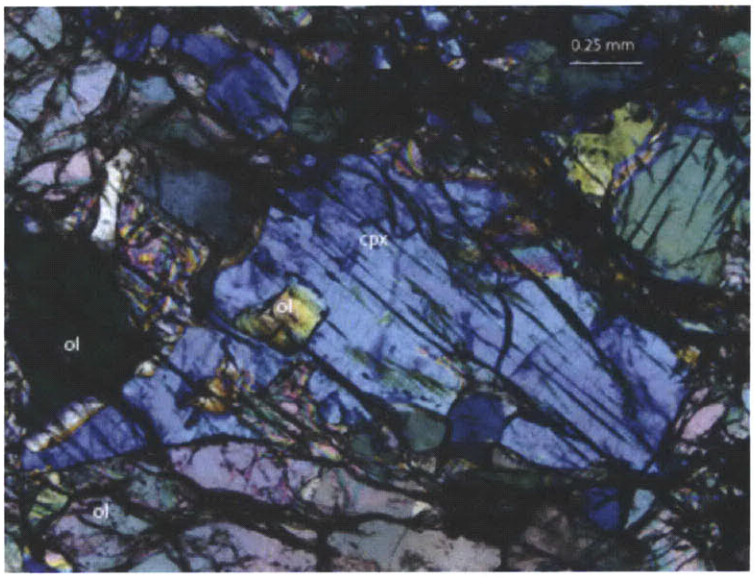

Figure 25. Bright blue cpx grain, center, is interstitial and interpreted as secondary. It splits the surrounding olivine grains along grain boundaries, and has olivine inclusions.

Dunite

Modal composition ranges from 100% to 90% olivine, with the other constituents (if present) being pyroxenes and spinel. Usually occurs as sharply constrained dike-like features, partly folded or diffuse patches within other rocks, usually Porphyric Harzburgite or honeycomb lherzolite, and is often found in close proximity with abundant occurrence of pyroxenite dikes (see later). The contact

relation of the dunite with the surrounding rock varies; it can either be in well-defined dikes (Fig 26), or diffuse or irregular shapes and patches (Fig. 27).

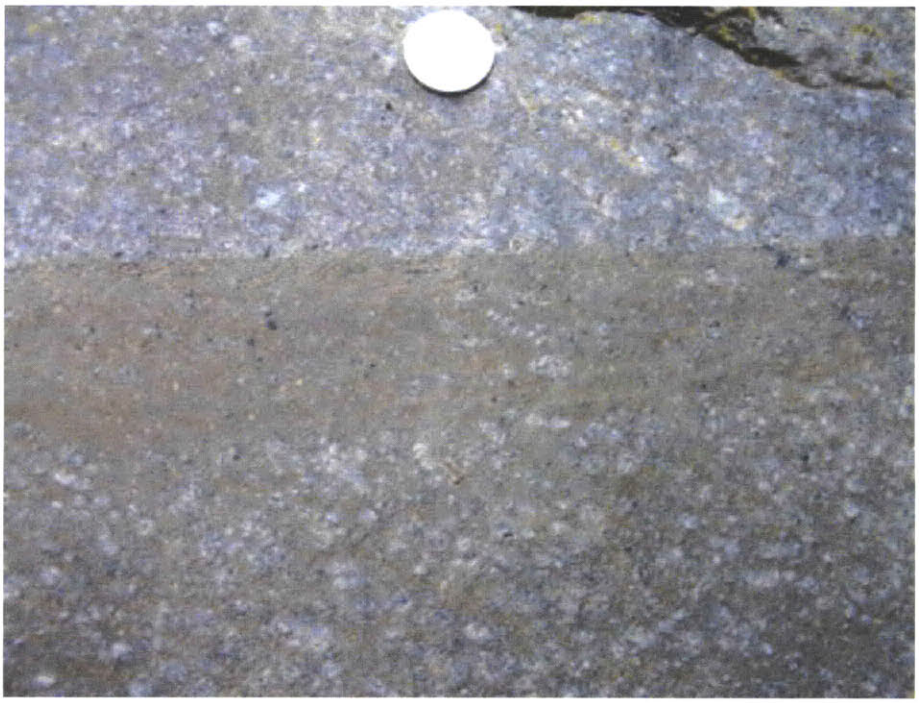

Figure 26. Well defined dunite dike (orange) in Porphyric harzburgite. Notice the sharpness of the contact.

Figure 27. Irregularly shaped dunite (orange) in olivine-rich Porphyric Harzburgite. The bottom contact is well defined but irregularly shaped with respect to foliation. The top is a much more diffuse contact, where the opx (grey) more gradually becomes dominant.

Pyroxenite Dikes

Gysi et al (2007) identifies four types of pyroxenites in the massif: garnet bearing pyroxenites, spinel websterites, garnet metagabbros and Cr-diopside websterites (described in next section). Full details of the pyroxenites are beyond the scope of this thesis, and the interested reader is referred to Gysi (2007) for a detailed study.

In southeast corner of the massif pyroxenites contain graphitized pseudomorphs after diamond (Pearson, 1989; Slodkevitch, 1982). Garnet is found in the south of the massif, often with kelyphite reaction rims. Pyroxenites are generally found concordant with the foliation and occasionally isoclinal folds hinges (Fig 29) and boudins (Fig. 30) are observed. They range from cm to m wide, and are usually found in groups of more than one at a time (Fig 31). Generally associated with harzburgite, dunite, honeycomb texture, and Cr-diopside patches.

Figure 28. Isoclinally folded pyroxenite dikes. Bottom of folded layer is outlined in black. Photo faces south, and foliation runs parallel to pencil (horizontal across picture).

Figure 29. Boudinaged pyroxinite dike. Foliation runs horizontal across picture, and lineation is parallel to the pencil.

Figure 30. Group of pyroxenite dikes as found in a heterogeneous zone. Pyroxenites define the foliation.

Cr-Diopside and Spinel Patches

Groupings of about 60% chrome rich diopside and 40% spinel which occur in patches and small veins. Generally fine grained, patches are usually 2-3 cm wide and irregularly shaped. Veins are up to 3 cm wide and often not completely continuous. Patches are often found with dunite surrounding them within another type of peridotite.

These Cr-Diopside patches are not solely associated with heterogeneous zones, though they are much more common there. They can be found elsewhere in

the massif, sometimes even in relatively granular sections of Nich Lherzolite, often in vein form.

Boarder Facies Lherzolite

This and other border facies are colored red on the map and cross section, plates 1 and 2.

This lherzolite has a modal composition of 60% olivine, 5% spinel, and 15 % clinopyroxene, and 20% orthopyroxene as estimated in the field. It is distinguished from other lherzolites based on the presence of very large orthopyroxene grains, up to 3 cm long by 0.5 cm wide, which are quite deformed (Fig. 31). The clinopyroxene is smaller and rounded, possibly less affected by the deformation, based on the grain shape. This unit is found on the edge of the massif, near the contact with the Kinzigites, and is associated with dunite and large garnet pyroxenite dikes.

Figure 31. Large opx grain (grey, above coin) in Boarder Facies Lherzolite. Surrounding orange material is olivine.

In thin section shows a fine-grained olivine matrix surrounding large elongated opx (several cm long) and smaller (1-3 mm) nearly equant cpx. Cpx is generally rectangular and looks to be absorbing olivine around its edges, so it is likely growing, and appears to have grown after much of the deformation which caused the opx to become so elongated (Fig 32). The opx shows wide (0.05 mm) exsolution lamellae and a slightly poikilitic texture with olivine inclusions, indicating that it is also probably growing with respect to the olivine grains (Fig 33). The olivine is quite deformed, showing both relic large grains and recrystallized neoblasts.

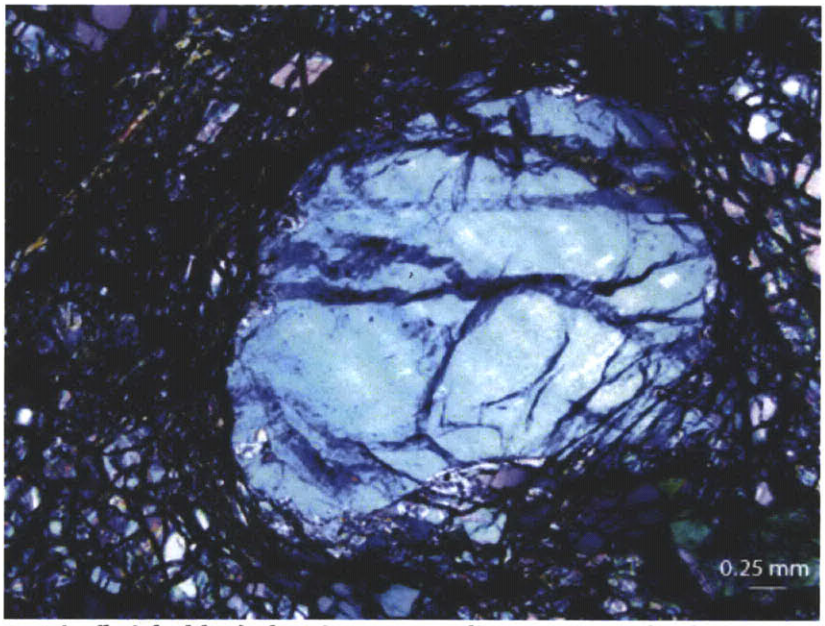

Figure 32. Cpx grain (bright blue) showing equant dimensions and sub-rectangular shape. In the lower left corner it has absorbed some small olivine grains.

Figure 33. A large, extended opx grain (purple and orange) in thin section showing slightly deformed exsolution lamellae and inclusions of olivine (light blue) at the top of grain.

Transect Up Valley Sidi Yahia Aârab

Detailed field observations were made in a north to south oriented valley (Sidi Yahia Aârab) transecting the massif. Exposure in Sidi Yahia Aarab is generally good through most of the river, the river rocks and cliffs provide ample outcrops for observation. Overall foliation and pyroxenite banding in this valley strike roughly east west and dip gently to the south (around 20°) so a north to south transect up the valley translates to moving up section. Lineation in the valley generally trends north-south, plunging south down dip (Fig. 34). The nice exposure in the valley, and its cross-cutting nature allow for good observation of the nature of the contacts between the rock units. The geological cross sections made along this valley is shown in Plate 2. The details of the units and their mutual contact

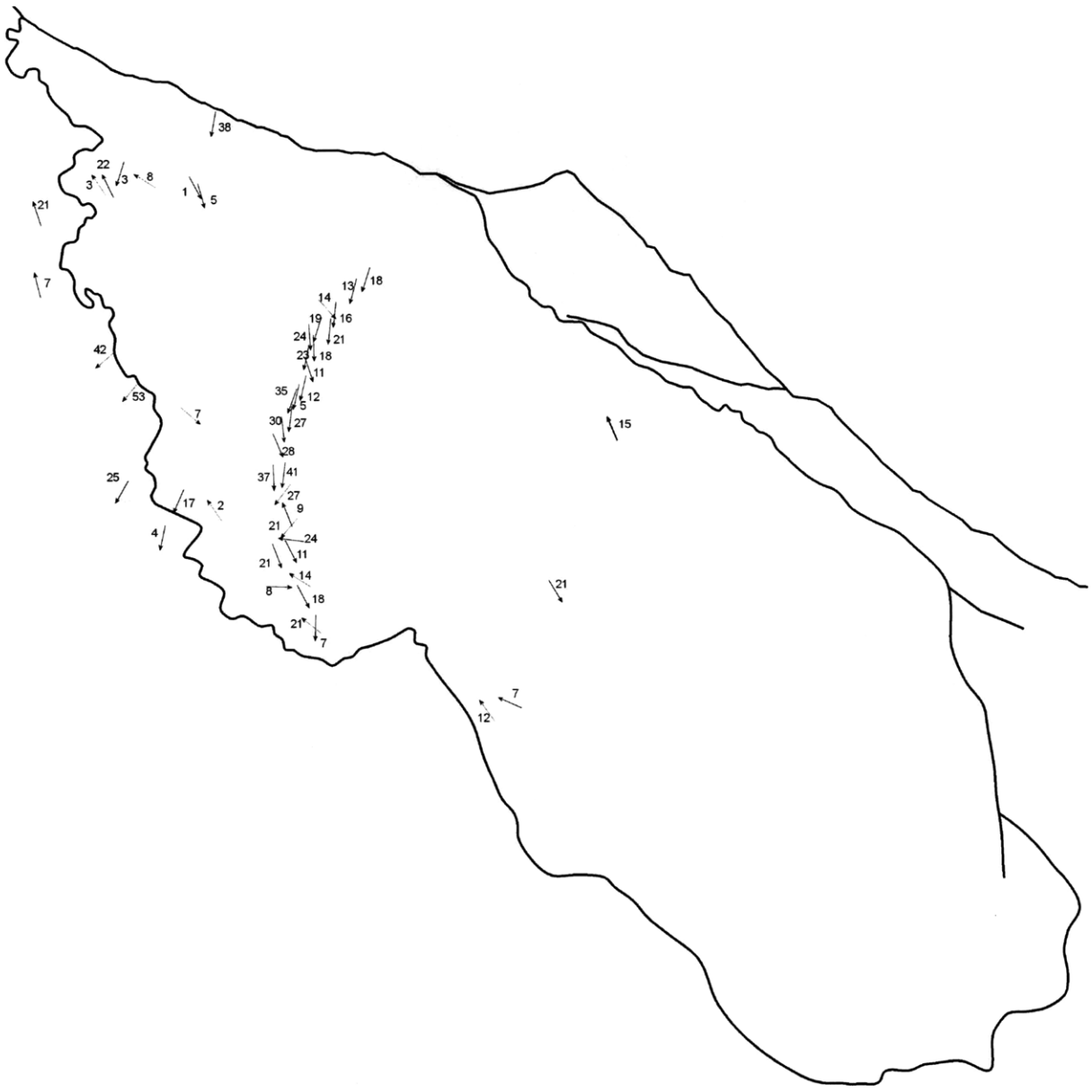

Figure 34. Lineation map of Beni Bousera. Area with the most data is the Valley Sidi Yahia Aârab. In that valley lineation generally trends north-south.

relationships are described below. Notes in brackets are to help identify the unit on the cross section.

At the base of the section [farthest north, in green] is Nich Lherzolite, which is poorly exposed, but likely more than 300 m thick. This is followed by a foliated lherzolite [green with dashes], with locally quite strong deformation. It has the

same mineralogical composition as the Nich Lherzolite down section, especially large spinel. A planar fabric associated with the deformation, where elongate pyroxenes define the strong foliation, overprints the granoblastic texture of the Nich Lherzolite.

The sheared lherzolite is followed by the first and one of the largest Heterogeneous Zones, which is dominated by harzburgite and pyroxenite dikes [orange on the cross section, moving south]. The lowermost portion of this heterogeneous section is olivine-rich honeycomb lherzolite (with less than 15% pyroxene). Also with this unit are a few foliation parallel pyroxenite dikes (less than 15 cm wide) and cpx-spinel patches are observed. The direct contact between the sheared lherzolite and the ol-rich honeycomb lherzolite is not exposed.

Further south, up section within the heterogeneous zone, the abundance and the width (up to a meter wide), of pyroxenite dikes increases and the host rock becomes dominantly the Porphyric Harzburgite associated with some amount of honeycomb harzburgite. Pyroxene and olivine content in the Porphyric Harzburgite are variable, and a foliation parallel banding defined by modal variations in olivine and opx is developed. Macroscopically the peridotites appear not as strongly deformed as the underlying Nich lherzolite section. However, pyroxenites are isoclinally folded with fold axes parallel to lineation (Fig. 28). There are cpx-spinel patches which are surrounded by dunite. Dunite is generally not always concordant with foliation here, and in one instance contains isoclinally folded spinel strings (Fig. 35).

Figure 35. Isoclinally folded spinel strings (black) in dunite (orange). Found in the northern Heterogenous Zone.

Following the pyroxenite-rich section, there is a section of honeycomb harzburgite, also quite variable in terms of modal mineralogy, but overall more homogenous than the previous section. It has some cpx-spinel patches generally with diffuse contact to the host, sometime occurring as 2-3 cm wide veins concordant to foliation. The honeycomb harzburgite gradationally changes to Nich Lherzolite [green with honeycomb symbols], with the cpx at first being associated only with patches and veins, and becoming evenly distributed. The Nich Lherzolite section still has some more olivine-rich portions, which exhibit a honeycomb texture. There are also still some diffuse veins rich in cpx and spinel.

This short (about 30 m wide) period of lherzolite is followed by another very heterogeneous section [orange] dominated by harzburgite and pyroxenite dikes. The dikes are concordant with foliation and up to a meter thick. There are again isoclinally folded dikes. The harzburgite is of both the Porphyric and honeycomb varieties, the more the Porphyric sections tend to have a higher modal abundance of

pyroxene than the honeycomb sections which tend to be more olivine-rich. The modal variation in pyroxenite content and texture define a foliation parallel banding. Foliation is not strong and a mineral lineation slightly more developed.

This is followed by another gradational section that transitions from harzburgite to Nich Lherzolite. At first cpx is only found in Cr-diopside patches, but a gradual change (over 10-20 m) in modal composition and texture cpx becomes evenly distributed, and the harzburgite texture is lost. This section [green with yellow sections] is transitional from harzburgite into the Nich Lherzolite which is initially not homogeneous and lacks some characteristics of the Nich Lherzolite: there are sections, sometimes within outcrops of Nich Lherzolite, which are honeycomb textured lherzolite or Porphyric harzburgite. Textural and modal compositional changes in lithology are pronounced on the meter to decameter scale. There are also cpx-spinel patches and veins, which tend to have fairly diffuse edges. This section is about 70 m thick.

This is followed by a section, 20-30 m wide, of extremely deformed lherzolite [green with dashes], fairly similar to the sheared lherzolite north of the Heterogeneous Zones, which has the high spinel content typical of the Nich Lherzolite. A strong deformation fabric is well defined by elongate pyroxenes. This marks the beginning of a fairly thick section, around 300 m, of dominantly lherzolitic lithologies [green]. It is not completely homogeneous, modal composition sometimes varies, creating banding. The host rock is similar to the Nich Lherzolite, but there are pockets of honeycomb texture, occasionally Porphyric Harzburgite, and sporadically lherzolite which displays opx grains resembling the texture of the

Porphyric Harzburgite. These lithologies are often not laterally continuous along strike, and they tend to grade one into another and vary on the decameter scale. Visible deformation intensity also varies, some sections have little to no foliation, while others show a distinct foliation.

Moving up river, the cpx-spinel patches become more common, and the Porphyric Harzburgite [yellow] becomes more frequent until it becomes dominant, though there are still sections of Nich Lherzolite, and intermittently olivine-rich honeycomb textured lherzolite. Small, less than 10 cm wide pyroxenite dikes begin to occur, as well as dunite dikes with cpx-spinel strings along foliation. This more heterogeneous section culminates in an outcrop with 10 to 15 pyroxenite dikes over about 3 meters of section, all 5 to 10 cm wide [orange]. Host peridotite is mostly porphyric harzburgite with large variability in the opx content throughout the outcrop. There is also a section of dunite just above the pyroxenite dikes. Moving up section pyroxenites and dunite dikes become less common and smaller in diameter, and the host rock becomes a very spinel-rich porphyric harzburgite.

The spinel-rich porphyric harzburgite has a gradational contact with the Nich Lherzolite [green] above it. Close to the contact the Nich Lherzolite is more variable in composition than the typical Nich Lherzolite. Some portions are a lot more olivine rich than others, and cpx content varies significantly such that there are sections which are harzburgitic and have faint porphyric texture, and there are pockets of the porphyric harzburgite. There are still a few small pyroxenites (less than 5 cm wide), and cpx-spinel patches and veins. Cpx-spinel patches are more common in the olivine rich sections of the lherzolite.

This grades into a thick section (~400 m) of fresh, undeformed, relatively uniform Nich Lherzolite. There is still some compositional variability but it is one of the more uniform sections in the transect. The rock can be very fresh with little serpentinitization.

The following section is a very thick section of the Porphyric Harzburgite. The composition ranges from sections which are more than 70% olivine to sections which are up to 60% opx on the decimeter to meter scale, though there are little to no true pyroxenites or dunite with sharp contacts to the host. The compositional variability creates foliation parallel banding. The more dunitic portions are often finer grained and more deformed than the opx rich harzburgite. The contact between the Nich lherzolite and the porphyric harzburgite is gradational over about 3 meters of section; there is a gradual decrease in modal amount of cpx from Nich lherzolite to harzburgite and a change of texture.

The thick section of Porphyric Harzburgite is interrupted by a brief section of dunitic rock with 80% to 90% olivine and minor amounts of opx, cpx and spinel [orange]. There are diffuse cpx-spinel patches and veins throughout the rock. The dunite has a gradational contact with the Porphyric harzburgite above, such that there are patches and layers of dunite alternating with the harzburgite. The harzburgite layer starts out quite heterogeneous with these dunite layers or foliation concordant dikes, which sometimes have pyroxenite bands inside them (Fig. 26). There are also cpx-spinel patches and veins.

This interlude is followed up-section by a return to the Porphyric Harzburgite as before (yellow). At the base of the section just above the dunitic

section there is also variation in the cpx content, such that some cpx-rich places (5-10%) could be considered a cpx-poor lherzolite [green]. Foliation strength, as judged by pyroxene elongation varies thought this section of porhyric harzburgite, but all lithologies are foliated, with the strongest foliation found at the top (southern end) of the section.

There is another interlude of a small section of extremely coarse-grained lherzolite [orange], with pyroxenes up to 3 cm long (Figure 36). It is deformed, with the pyroxenes generally having an aspect ratio of at least 3:1. Modal composition in this unit is about 55% olivine, 5% spinel, 20% opx and 20% cpx. There are also some small Cr-diopside-spinel patches, 1 to 2 cm across, with the usual grain size.

Next there is a return to the Porphyric Harzburgite, in which pyroxenite dikes (beginning to contain macroscopically visible garnet) begin to appear, with increasing frequency moving up section. The harzburgite contains a noticeable amount of spinel 3-5%, and often cpx up to 5%. Compositional variation again creates a foliation-parallel banding.

Pyroxenites begin to become more common and wider (up to 1 meter), and the host rock changes to the border facies lherzolite [red] with large, deformed opx and smaller, less deformed cpx. This is followed by a brief period (about 10 m thick) of deformed lherzolite [green with dashes], which is similar to the other sections of highly deformed lherzolite.

Close to the edge of the massif, there is one more heterogeneous section with many pyroxenite, as well as gabbroic dikes. These are boudinaged (Fig. 29) and contain garnet with little to no kelephyite rims. There are layers, as well as large

Figure 36. Coarse grained Lherzolite. Green mineral is cpx, brown mineral is opx, surrounding orange mineral is olivine, and black dots are spinel.

patches (0.5 to 1 m wide) of dunite, which contain smaller (1-3 cm) cpx-spinel patches. The surrounding peridotite is generally deformed, opx-rich harzburgite. Just above this section is a lherzolite with a very strong lineation and larger opx grains.

Finally, just before the contact with the surrounding Kinzigites, there is a 20 meter wide zone of serpentine. This weathers a distinctive green color, and is visible continuously along the upper contact of the massif.

Geologic Map

The geologic map, Plate 1, is based on own field observations, and complemented with observation from previous studies (Draoui, 1992; Gysi, 2007; Kornprobst et al., 1975; Reuber et al., 1982). Summaries of the Reuber and Draoui maps can be found in the field trip guide by Kornprobst et al. (1995), though Reuber's is also published separately. As mentioned the most detailed and complete

observations from this study were made in the valley Sidi Yahia Aârab, and other parts of the massif, in particular the southern part, have been extrapolated in this study's map. The map has been split into 5 sections for ease of discussion, shown in Figure 37.

Section 1 is primarily Nich Lherzolite, but with pockets and sections of Porphyric Harzburgite and small heterogeneous zones. This section is difficult to map in detail because the lithology changes quickly from Nich Lherzolite to porphyric harzburgite with little regard to foliation. It is likely that there are other patches of porphyric harzburgite within Section 1 that have not been mapped, or are too small to represent on the map.

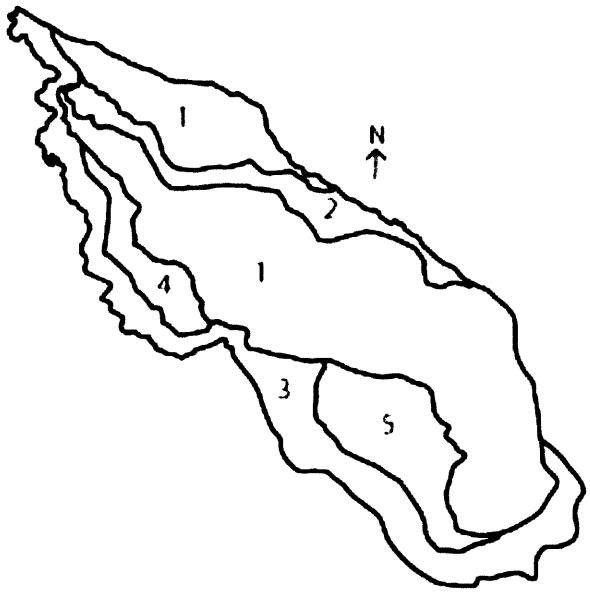

Figure 37. Geologic regions described in text, compare to full geologic map, Plate 1.

Section 2 is one of the more extensive heterogeneous zones where much of the EBSD analysis (presented below) was focused. It seems to have more pyroxenites toward the western part of the massif while the outcrops observed in the eastern side were characterized more by dunite than pyroxenites.

Section 3 represents the Border Facies, which is characterized by Border Facies peridotite texture as well as garnet pyroxenites, dunite, and in one section pyroxenites with graphite pseudomorphs after diamond. It is essentially a heterogeneous zone that includes Border Facies texture and garnet pyroxenites. It also includes several sections of what have been described as garnet dunite, which have been interpreted as extremely mechanically-mixed pyroxenites (Kornprobst, 1974). Its extent has not been well mapped in all places, especially in the southern portion of the massif.

Section 4 represents the homogeneous Porphyric Harzburgite observed in the cross section. Such a thick section was not observed in the other valleys visited, and therefore is not likely to circumvent the whole massif, and would need to be mapped more carefully to know its full extent. Similar to Section 1, this section also can contain heterogeneous zones.

Section 5 is shown as harzburgites by Reuber and Draoui, however not well described. Pearson (1989) looked at the pyroxenites in this region to understand the petrogenesis of the diamond pseudomorphs, and describes pyroxenites. However Pearson also disagrees with Reuber et al.'s (1982) interpretation of the whole area as harzburgite, indicating that he observed fresh lherzolite. Because of

the presence of pyroxenites, harzburgite, and lherzolite, this section is interpreted on this map as a large heterogeneous zone.

Contacts of the major units within the massif are generally gradational. For instance, the contact between Nich and Porphyric generally grades over several meters, with the gradual development of distinctive opx texture and loss of cpx. Contacts between the granular peridotites and heterogeneous zones are also gradual, marked by the increase in harzburgite and honeycomb textures. The contacts between pyroxenite dikes and peridotites, however, are often sharp and well defined.

The external contacts of the massif with the surrounding rocks are more varied and difficult to discern. The eastern edge has been mapped as a northeastern dipping normal fault. The western and southern contact with the Kinzingite gneisses is inherently related to the debated peridotite emplacement mechanism. The published map by Kornprobst et al. (1975) labels this contact as intrusive, but Reuber et al. (1982) interpret the contact as a ductile shear zone from thrusting. The contact itself is poorly exposed, generally extremely weathered and heavily serpentinized. In some places the contact appears to dip shallowly and follow topography, but in others it dips quite steeply (for example the southwest).

Chemistry

Samples BB-08-30, a Nich Lherzolite, BB-080-47, a porphyric harzburgite, and BB-08-45, a dunite were analyzed on the electron microprobe for major element geochemistry for the major minerals. This section is not meant to provide a full analysis and interpretation of the major element geochemistry in Beni Bousera, it is simply meant to present some basic relationships to give a flavor of the massif and to help support the rock unit groupings made in the field. Overall the chemistries of the porphyric harzburgite and Nich Lherzolite appear similar, but the Dunite shows pronounced different chemistry.

Spinel

For Cr-spinel, the Mg #, Mg/(Mg+Fe) and the TiO_2 weight percent were plotted against Cr #, Cr/(Cr+Al) (Figs. 38 and 39). The dunite has a much lower Mg # and much higher Cr #. In general the TiO_2 weight percent ranges from 0.018 to 0.124, and does not show much correlation with Cr #.

Clinopyroxene

For cpx, Mg # was plotted against Al_2O_3 weight percent, and Aluminum with a coordination number of 4 against Aluminum with a coordination number of 6 (Figs. 40 and 41). Mg # ranged from .890 to .905 for the Porphyric Harzburgite, .904 to .916 for the Nich Lherzolite, and .929 to .938 for dunite. Al_2O_3 weight percents were higher for the harzburgite and lherzolite than the dunite. The dunite also had a lower ratio of aluminum in 6-fold coordination to aluminum in 4-fold coordination. Al^{VI} is a measure of jadeite content, the high pressure form, so a low Al^{VI}/Al^{IV} indicates lower pressure.

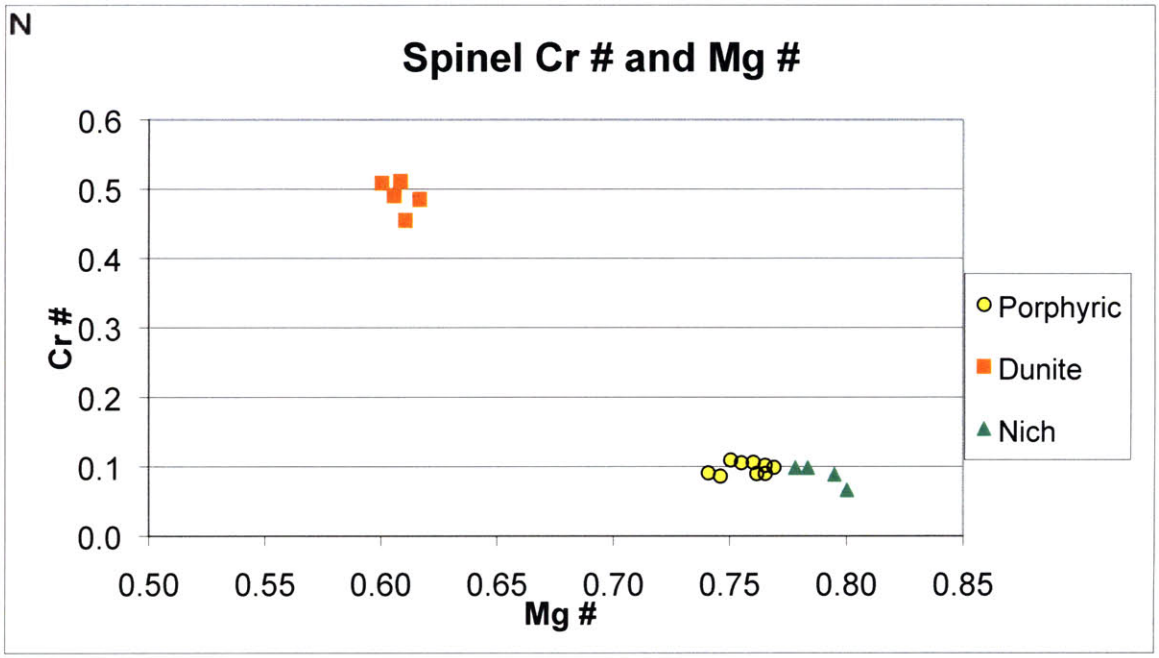

Figure 38. Cr # and Mg # in spinel from samples analysed on the elecron microprobe. The dunite sample is significantly different from the Porphyric Harzburgite and Nich Lherzolite.

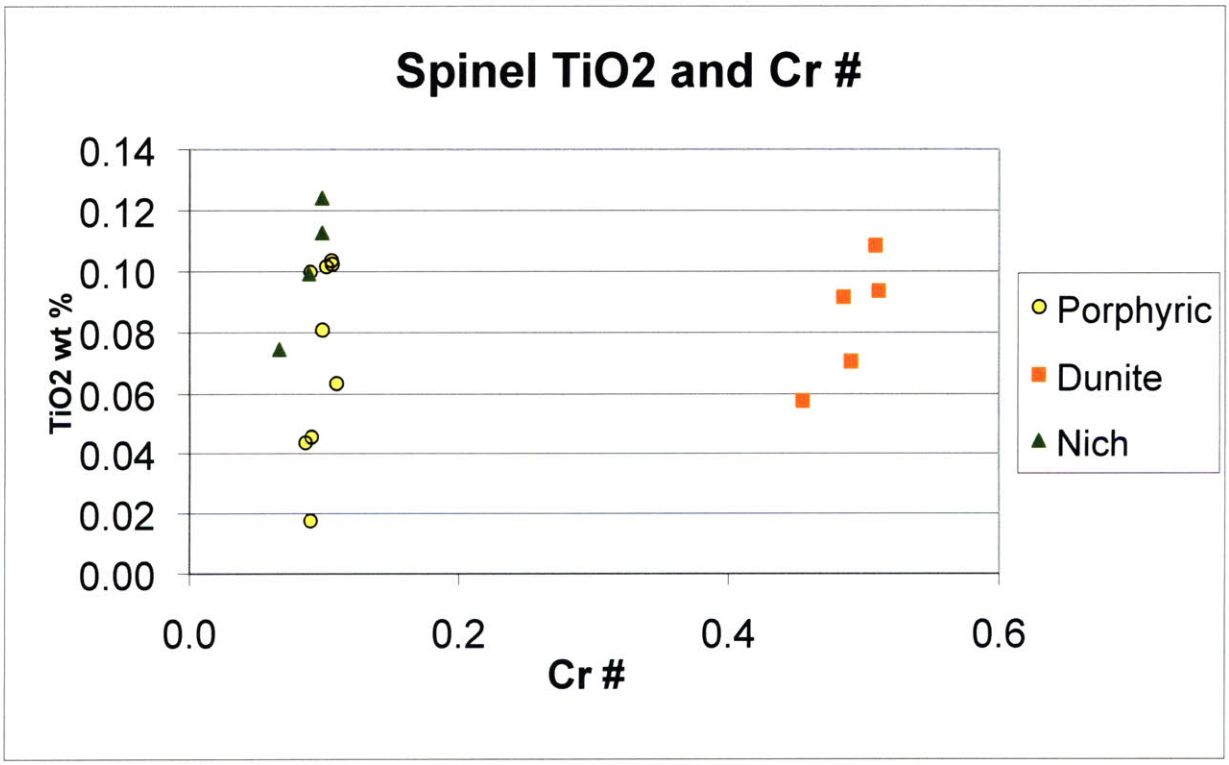

Figure 39. TiO_2 weight % and Cr # for spinel. Again, the dunite is quite different from the others, though not as much in TiO_2 as Cr #.

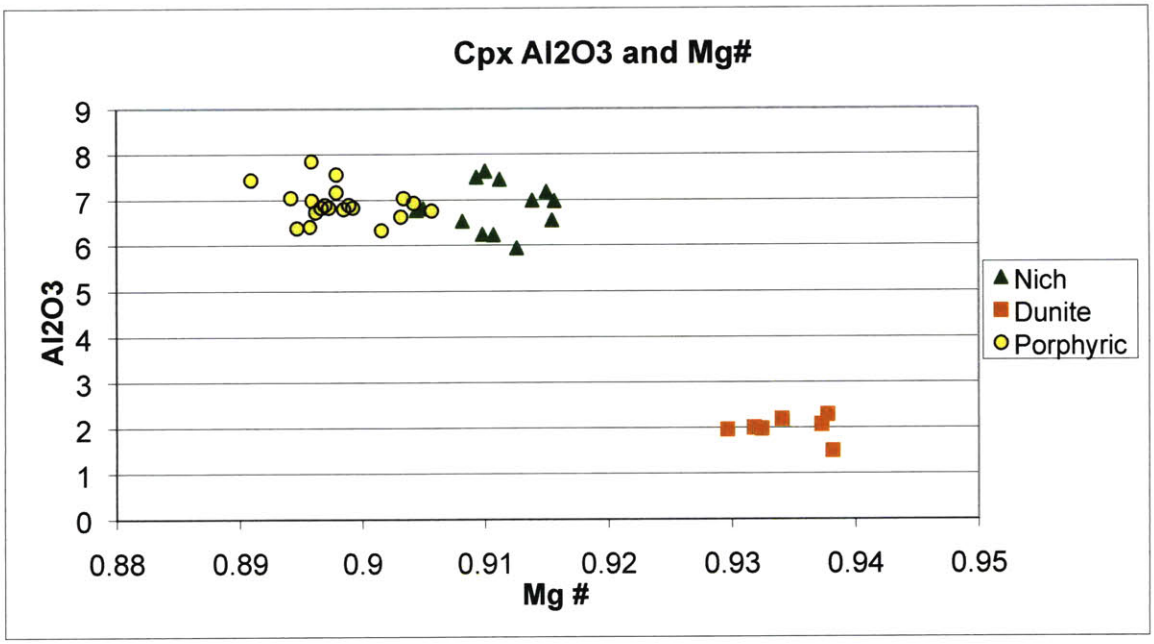

Figure 40. Cpx Al2O3 against Mg #. The Porphyric Harzburgite and Nich Lherzolite have similar Al2O3 contents, with the Nich having slightly higher Mg#. The dunite is separate with higher Mg # and lower Al2O3 content.

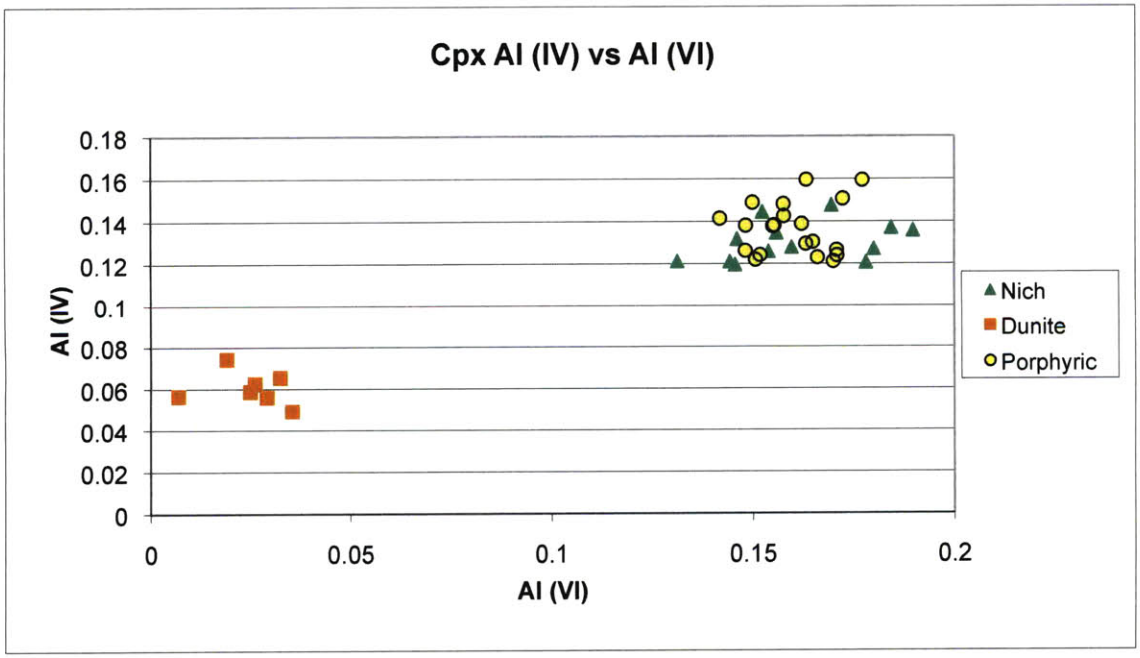

Figure 41. Al(IV) against Al(VI) for cpx. The Porphyric Harzburgite and Nich Lherzolite are similar, but the dunite has a lower Al(VI)/Al(IV) ratio, and generally lower Al content.

Orthopyroxene

Al_2O_3 and Mg # were also plotted for orthopyroxene (Fig. 42), with similar results as for pyroxene, though much more of a overlap and spread of Al_2O_3 content for the Nich Lherzolite and the Porphyric Harzburgite. Mg# range from .890 to .900 for the Porphyric Harzburgite, from .893 to .899 for Nich Lherzolite, and .915 to .919 for the dunite.

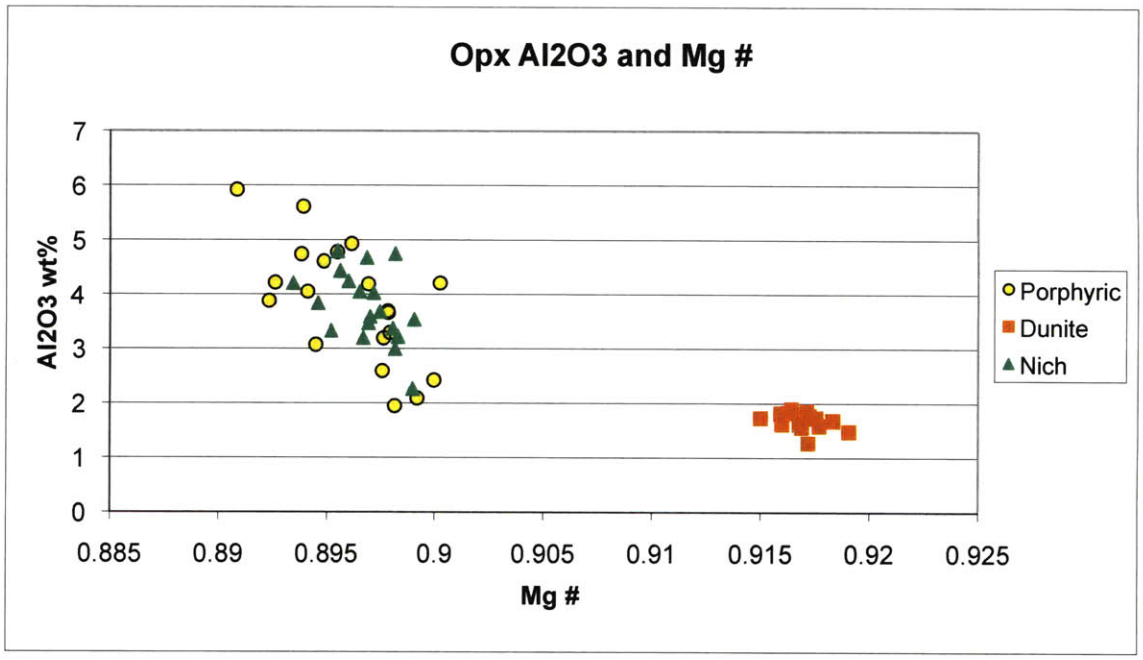

Figure 42. Al2O3 against Mg # for opx. The Porphyric Harzburgite and Nich Lherzolite fields overlap, but the dunite is different.

Olivine

For olivine, NiO weight percent was plotted against Mg # (Fig. 43). NiO content was not extremely different for the lithologies, but Mg # ranged a bit. Mg # was from .885 to .892 for the Porphyric Harzburgite, from .888 to .893 for the Nich Lherzolite, and from .910 to .913. Again overall the Nich Lherzolite and the

Porphyric Harzburgite were not extremely different, but the dunite is separate on the plot.

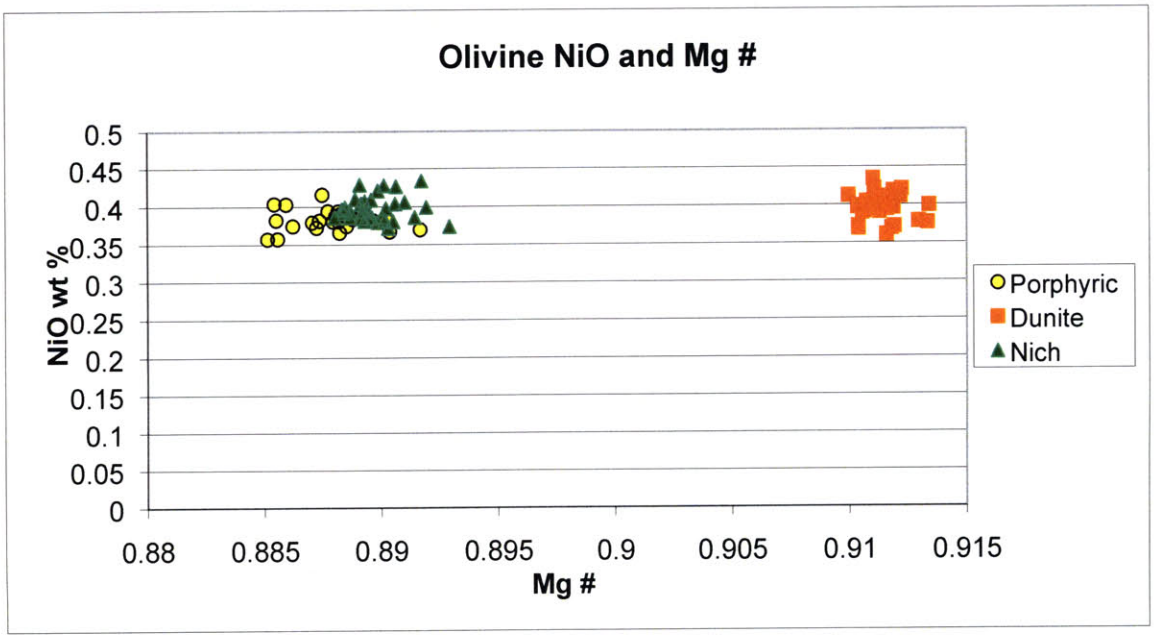

Figure 43. NiO weight percent against Mg # for olivine. The Nich Lherzolite and Porphyric Harzburgite plot fairly close together, and the dunite is separate, however they all have similar weight % NiO, it is mostly the Mg# which differentiates them.

Field and Petrology Interpretations

Field and thin section observations indicate that a there was a significant amount of melt present in the peridotites in Beni Bousera during its history. Thin sections also point to melt-rock reactions, likely several generations (Figures 44 and 45). The presence of dunite, harzburgite, lherzolite, and pyroxenites all outcropping within meters of each other indicates a complex history and melt rock interaction at increasing and decreasing melt mass. Experimental studies have shown that melts formed at high pressures become saturated with olivine with decreasing pressure (Stolper, 1980), thus some melt migration will cause the dissolution of pyroxene and precipitation of olivine, thus the formation of dunite (Kelemen, 1990). Under similar principles of different melts becoming saturated in different phases at different pressure conditions, it is also possible to form harzburgite by melt-rock reaction (Kelemen et al., 1992). Secondary lherzolites can also be formed by enrichment through reaction with percolating melts (eg. Beyer et al., 2006; Le Roux et al., 2007; Muntener et al., 2004).

Based on field evidence, the Nich Lherzolite is interpreted to be the oldest of the units, and all other units are interpreted as the result of melt rock reactions at various stages of melt interaction. One might imagine a textural evolution, starting with the Nich Lherzolite, small amounts of reaction leading to the Porphyric Harzburgite. Thin sections of the Nich Lherzolite close to the contact with the Porphyric Harzburgite show conclusively that olivine is replacing pyroxene. This trend could continue to form dunite. Pyroxene formation is the result of the opposite reaction due to the reaction of the peridotites with a silica-saturated melt,

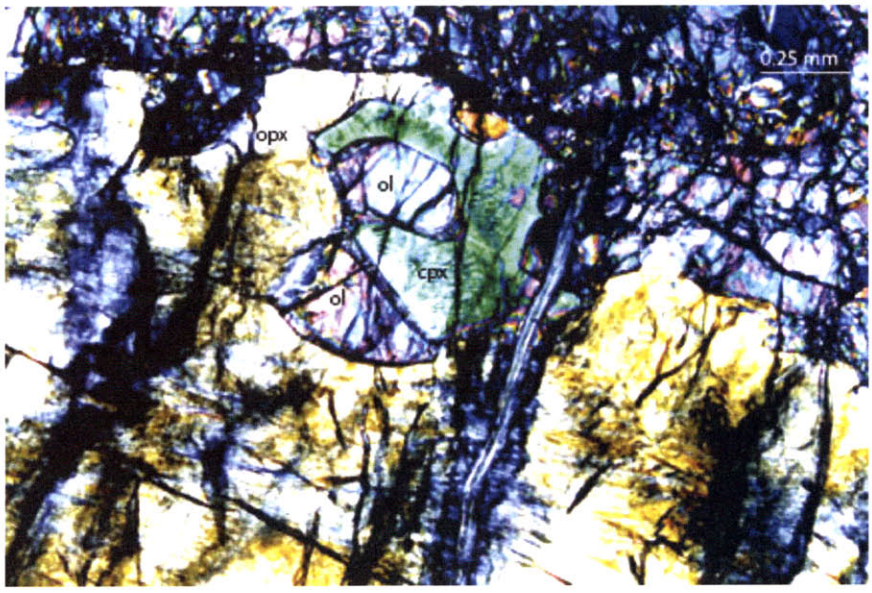

Figure 44. A Nich Lherzolite (BB-08-37) in thin section showing multiple generations of melt interaction. Center shows two olivine grains (white/blue), one of which is surrounded by a cpx grain (green). A large opx grain (orange, lower half of picture) then consumes the cpx and the other olivine inclusion, while at the latest stage olivine embays and consumes the opx and cpx.

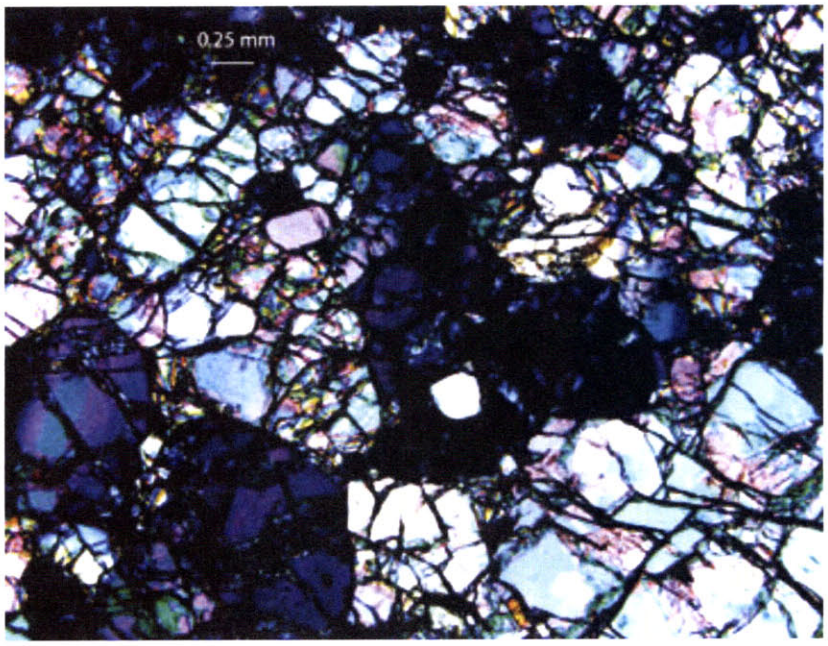

Figure 45. This secondary lherzolite (BB-08-9) shows an olivine grain (white, center) included within another olivine (extinct, center) indicating several generations of olivine.

and crystallizing pyroxene resulting in a honeycomb texture. The re-infiltration process appears to occur at any stage in the Niche Lherzolite to dunite evolution, so secondary lherzolites can be found that contain both relic large opx grains, and small secondary ones on grain boundaries, interpreted as infiltrated porphyric harzburgites. Certainly additional chemistry needs to be done to fully understand the evolution of the textures found in Beni Bousera, but there is a complex history resulting from multiple waves of melt infiltration at changing pressure and temperature conditions.

The heterogeneous zones show the most evidence for melt infiltration: dunite, secondary lherzolites, harzburgite and pyroxenites. These zones are interpreted as larger scale melt channels. Melt channels of focused porous flow have been suggested as a method of melt extraction from the mantle and a method of keeping melts chemically isolated (Kelemen et al., 1995; Suhr, 1999).

This interpretation of the heterogeneous zones as melt channels and the presence of melt throughout the massif influences the drawing of the map and cross section. Heterogeneous zones and harzburgites have been interpreted as channel networks seen in map view or cross-section, this is supported in part by the changes in porphyric harzburgites and Nich Lherzolites in some sections with little regard to foliation or linearity, thus it is possible that these represent insipient channels and that parts of the map view are somewhat like a cross section of a trees roots. This is probably not the only interpretation available and much more detailed mapping would be necessary to know if this is truly the case.

4. Lattice Preferred Orientation (LPO)

LPO Formation and Measurement

A lattice preferred orientation (LPO) in rocks is a type of texture or fabric where many of the mineral grains have the same or similar mineral orientations in space. Stress and deformation in the dislocation creep regime cause an LPO to form, so an LPO can give information about the deformational history of a rock.

Measurement: Electron Backscatter Diffraction (EBSD)

One method of measuring LPO, and the method used in this thesis, is Electron Backscatter Diffraction (EBSD), which uses the electron beam from a scanning electron microscope (SEM) to create diffraction pattern which can be linked specific minerals and their orientation. In EBSD analysis, a sample is placed at an angle to the electron beam produced in a scanning electron microscope (SEM) (Fig. 46). The electron beam is scattered by the sample material both elastically and inelastically in a variety of possibly manners, and the resulting image is captured on a phosphor

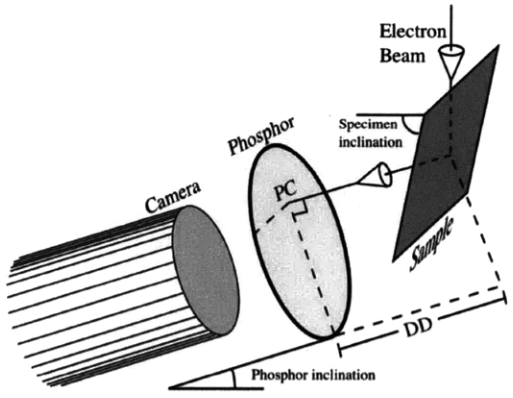

Figure 46. Experimental setup for EBSD imaging inside the sample chamber. DD designates the distance from source point to phosphor. From Prior et al. (1999).

screen (Prior et al., 1999). Bands and bright spots on the image produced (Fig 47) can be related to specific lattice planes and zone axes, and used to identify the mineral and its orientation relative to the sample axes. Each image gives the full crystallographic orientation of a point in a sample (Prior et al., 1999)If many points are taken for each sample, both the statistical distribution of orientations and the differences between them (misorientations) can be considered (Prior et al. 1999). Statistical distributions of orientations are generally either presented as pole figures or inverse pole figures. Pole figures display the poles to specific lattice planes on a stereonet relative to the sample reference orientation. Inverse pole figures show the lineation or pole to foliation of the sample relative to the crystallographic axes for the mineral (Prior et al. 1999). Data in this thesis is presented as pole figures.

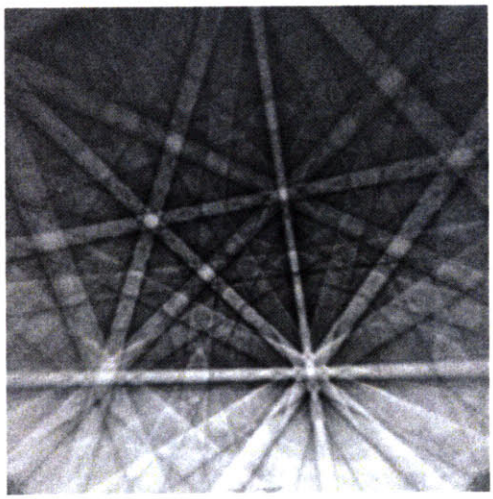

Figure 47. . EBSD image of experimentally deformed halite. Lines and intersections can be correlated to lattice planes and crystallographic axes From Wenk (2002).

There are indices that attempt to quantify fabric strength: the J-index (Bunge, 1982), and the M-index (Skemer et al., 2005). Both the M-index and J-index are calculated for our samples. The misorientation angle between two grains is the

angle of rotation around a common axis required to bring two grains into crystallographic alignment. The misorientation index (M-index) compares the distribution of misorientation angles between all possible grain pairs with the distribution expected from a randomly oriented sample. The difference between these two distributions is expressed as an index between 0 and 1, with 0 indicating a random fabric, and 1 a fabric with all crystals perfectly aligned (Skemer et al., 2005). The J-index is the second moment of the orientation distribution function (ODF). The ODF is the distribution of the crystallographic orientation data in Euler angle space (Bunge, 1982). J index ranges from 0 to infinity and increases with fabric strength.

LPO Formation

For LPO to be a useful tool in understanding the deformational history of a rock, it is important to first understand how a LPO texture forms in a rock. Dislocation creep is the most important mechanism by which an LPO forms, but recrystallization and dissolution and growth of crystals in the presence of fluids are also significant (Wenk, 2002). Modeling the deformation under dislocation glide in a polycrystalline solid is very complex and heterogeneous; individual dislocations move within individual crystals along slip systems, dislocations interact and cause hardening, and crystals interact with their neighbors (Wenk, 2002). Most models do not take into account all of these affects, and make large generalizations, but still provide useful information

In addition to modeling, rock deformation experiments have shown that stress, temperature and water content can change what type of LPO pattern is

produced. The LPO pattern is dominated by the pattern produced by the easiest slip system, and the easy system changes based on conditions of deformation (Karato et al., 2008). Figure 48 shows the different patterns produced by olivine. The most common, A-type fabric is produced by slip in the [100] direction on the (010) lattice

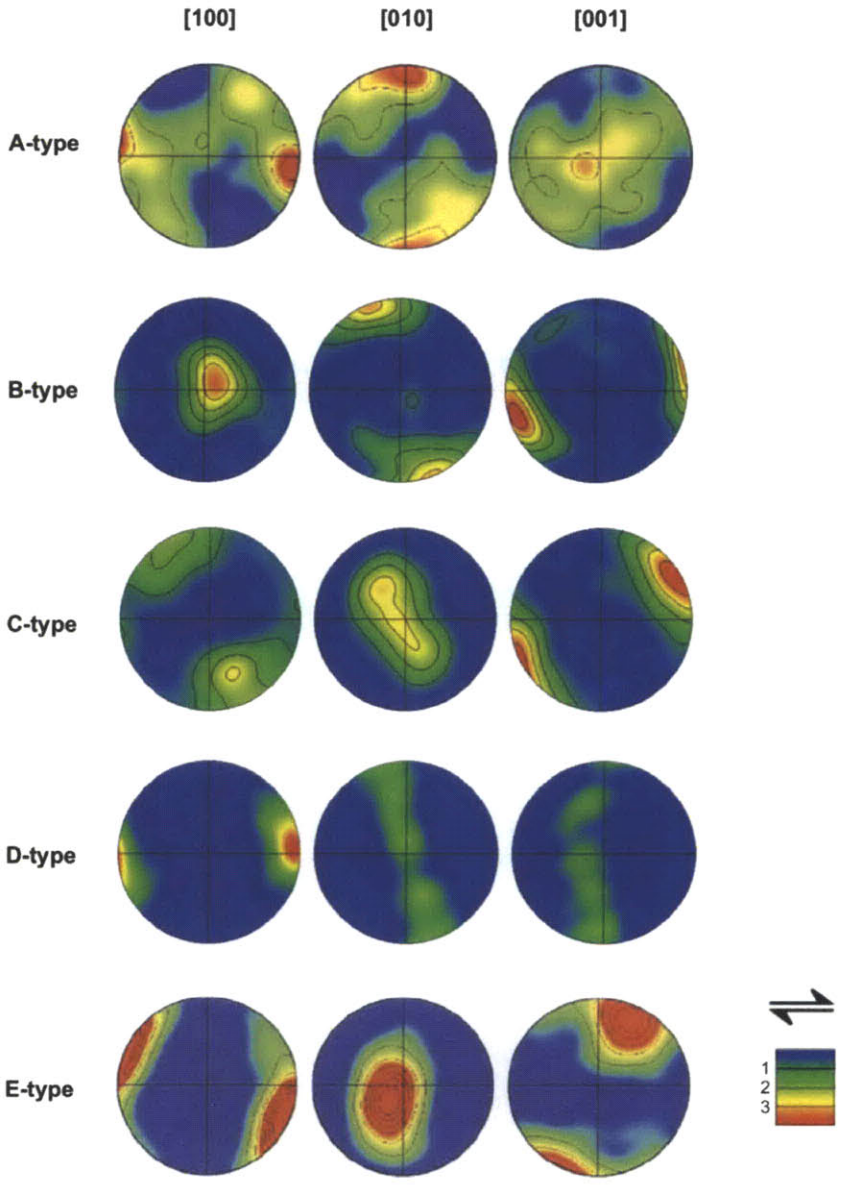

Figure 48. Pole figures of the a, b and c axes of olivine produced experimentally under different conditions. The horizontal axis is the shear plane, and shear sense is dextral. Contours are multiples of a uniform distribution. Notice the girdle in the D-type pattern caused by slip on multiple plains. From Karato et al. (2008) after Jung et al (2006).

FABRIC TYPE	A-fabric	B-fabric	C-fabric	D-fabric	E-fabric
SLIP SYSTEM	[100] (010)	[001] (010)	[001] (100)	[100] {0kl}	[100] (001)

Table 1. Olivine slip systems associated with the different fabric types.

plane, Table 1 shows the possible olivine fabric types and their slip systems. The LPO pattern produced depends on three variables: Temperature, expressed as T/T_m, where T_m is melting temperature, which is a function of pressure; Stress (σ), expressed as σ/μ, where μ is viscosity and a function of both temperature and pressure; and water content (Karato et al., 2008). Figure 49 shows the regions for each pattern type on a graph with the three variables as axes.

These categorizations are a bit simplistic, and there are many other variables which can effect the specific LPO, but it categories are nice for ease of discussion.

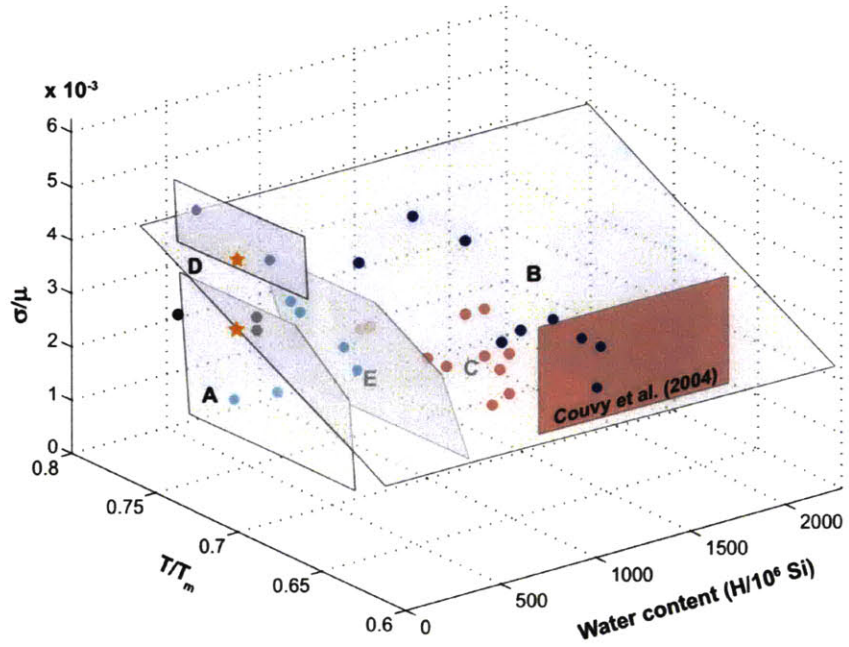

Figure 49. Shows the regions in which certain olivine LPO patterns are formed (corresponding to the patterns in Figure 8) in ($T/T_m(P)$, $\sigma/\mu(P,T)$, C_W) space. From Karato et al. (2008) after Couvy et al., (2004)

Analytical Methods

Oriented peridotites samples were taken from in situ bedrock outcrops where foliation and lineation measurements were made. Every attempt was made to get the freshest, least serpentinized sample, but completely fresh samples were not always possible. Thin sections were cut perpendicular to foliation and parallel to lineation (XZ section), keeping track of the geological orientation. Samples were mechanically polished to .5 μm and then placed on a Vibromet automated polisher with colloidal silica for at least four hours, generally overnight.

Carbon coated samples were analyzed using the JOEL 845 SEM operating at 20 kV with Oxford Instruments EBSD acquisition and HKL software at Brown University. For each sample, 40-100 points were manually chosen and analyzed, known to be different grains, followed by semi-automated points for a total of between 500 and 800 points were analyzed. Semi-automated points were chosen on the SEM image before analysis, thought to be different grains, and then chosen points were indexed automatically. Automated indexing was scanned visually as it occurred, and there was some redundancy in grains measured, but not generally more than 3 points from one grain, and often only one point per grain. Points with greater than 1° mean angular deviation (MAD) were discarded. The orientations of crystallographic axes were plotted on stereonets to make pole figures for interpretation. Forsterite, enstatite and diopside were all analyzed, but only forsterite had enough grains to make a meaningful pole figure. Fabric strengths were quantified using the M-index (Skemer et al., 2005) and J-index (Bunge, 1982).

Results

Olivine pole figures from the ten samples analyzed are shown below. They are grouped in to three categories: Ones near the heterogeneous zone, ones in granular peridotites, and a dunite. All are shown as multiples of a uniform distribution (MUD) on equal-area lower-hemisphere projections. All pole figures have set maximum at 6 unless they have a higher maximum, so the shading is somewhat comparable between figures. The contour interval is 1 for all figures. Pole figures shown here have the lineation along the horizontal axis, north to the left and the geographic up direction at the top. The pole figures are also plotted on the cross section, Plate 2, for comparison with the geology. Pole figures were created with the Careware software by David Mainprice: http://www.isteem.univ-montp2.fr/PERSO/mainprice/

Heterogeneous Zone

The patterns associated with the heterogeneous zones are generally A-type fabric, as defined by Karato et al. (2008), with the <100> aligning with the lineation, the <010> axis perpendicular to the foliation, and the <001> perpendicular to the lineation within the foliation plane. This indicates deformation in the dislocation creep primarily in simple shear on the [100] (010) slip system, under dry conditions.

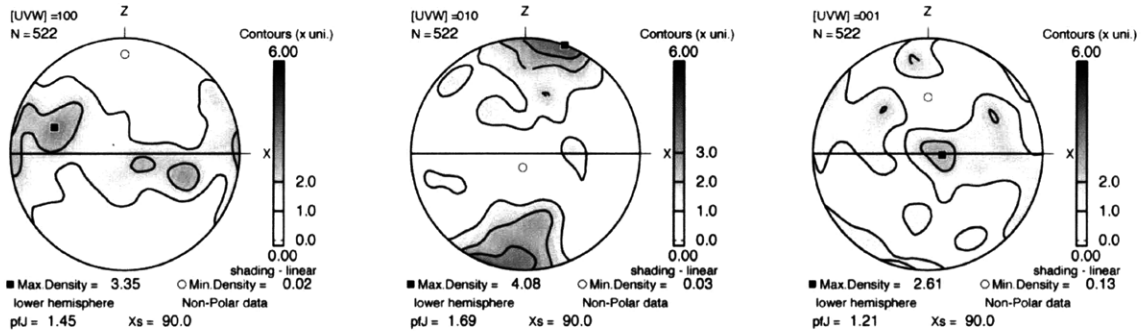

BB-08-31b: Deformed lherzolite north of melt zone. M-index = 0.064, J-index = 4.78, maximum density = 4.08.

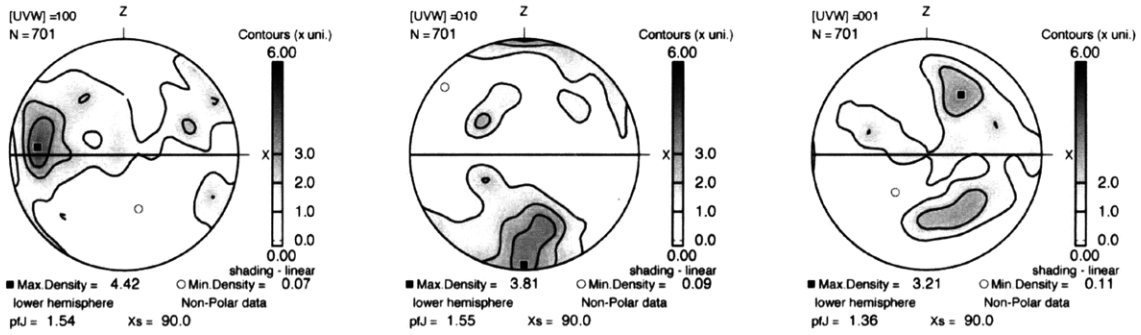

BB-08-35: Deformed lherzolite north of the melt zone. M-index = 0.065, J-index = 4.90, maximum density = 4.42.

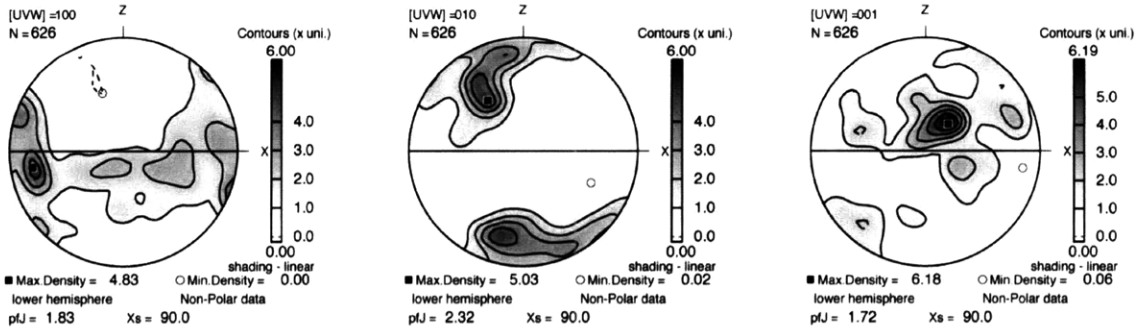

BB-08-9: Honeycomb lherzolite, within the heterogeneous zone, just south of the center. M-index = 0.14, J-index = 8.86, maximum density = 5.20.

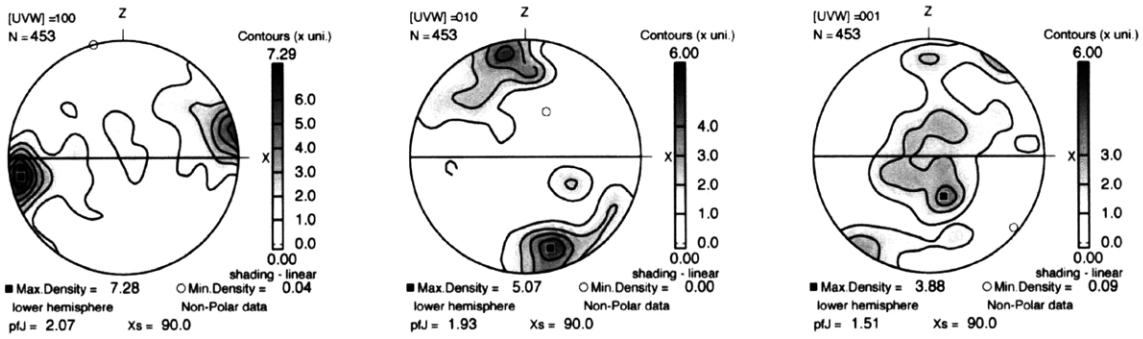

BB-08-18: Transitional lherzolite, within the heterogeneous zone, toward south side. M-index = 0.12, J-index = 7.25, maximum density = 7.28.

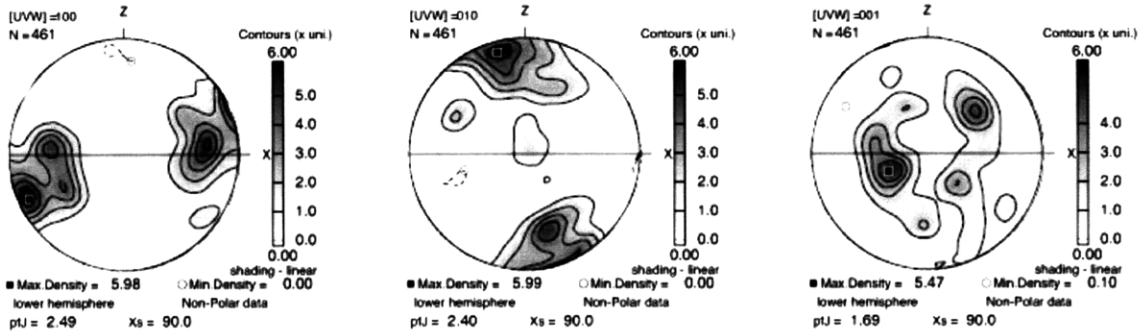

BB-08-23: Honeycomb lherzolite, just south towards the edge of the heterogeneous zone. M-index = 0.16, J-index = 9.78, maximum density = 5.99.

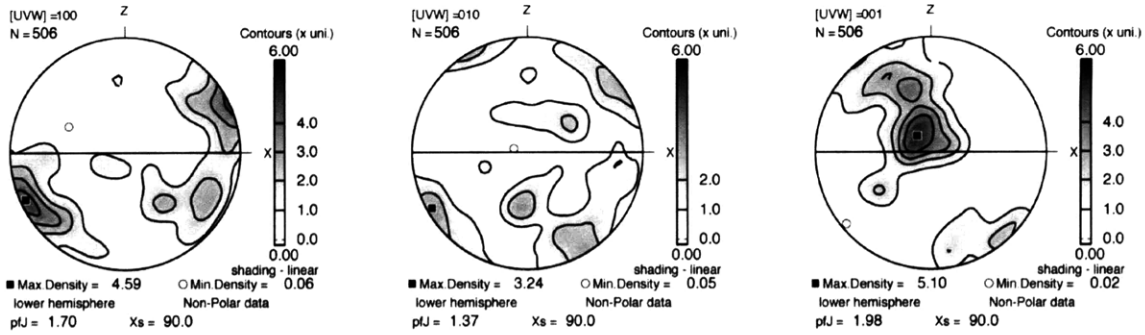

BB-08-13: Deformed Lherzolite on the southern edge of the heterogeneous zone. M-index = 0.066, J-index = 6.43, maximum density = 5.10.

Figure 50. LPO patterns from the heterogeneous zone in the north of valley Sidi Yahia Aârab.

Granular Textures

The LPO patterns for the granular Nich Lherzolite and Porphyric Harzburgite are similar to the A-type fabric in the heterogeneous zone, but they have slightly more of a girdle on the <100> and <001> axes. Thus the <010> axis is aligned perpendicular to foliation, and the <100> and <001> axes are contained within the foliation plane, indicating more of a uniaxial compression component to the deformation.

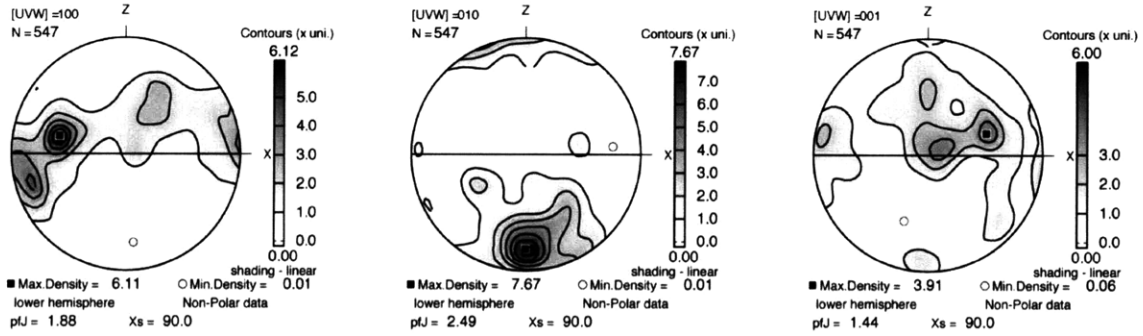

BB-08-49b: Nich Lherzolite from the homogenous section in the south central part of the massif. M-index = 0.13, J-index = 7.59 maximum density = 7.67.

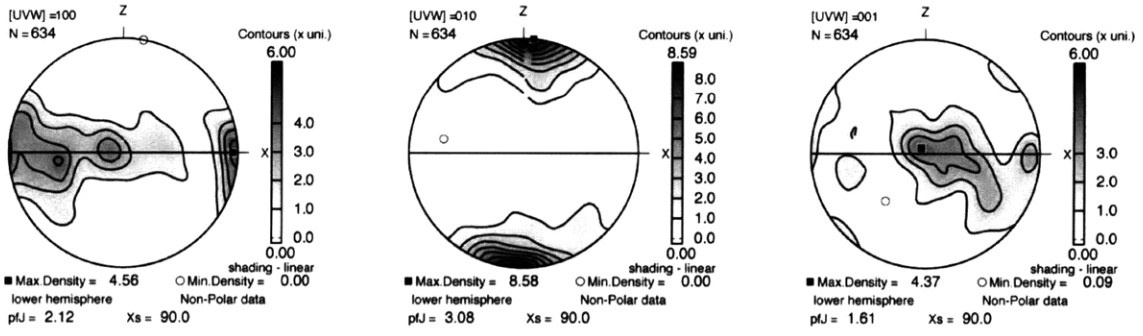

BB-08-10: Nich lherzolite from the section south of the heterogeneous zone. M-index = 0.19, J-index = 8.10, maximum density = 8.58.

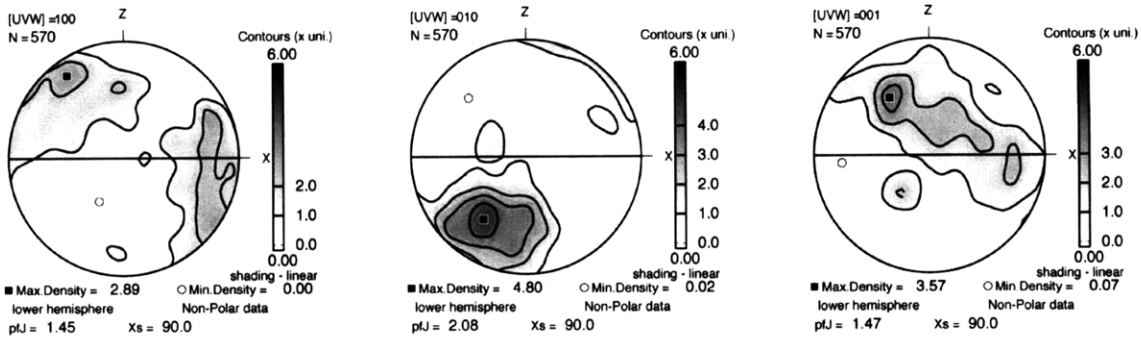

BB-08-47: Porphyric Harzburgite from section towards the south of the massif. M-index = 0.12, J-index = 5.16, maximum density = 4.80.

Figure 51. LPO from granular textured rocks, Porphyric Harzburgite and Nich Lherzolite from Valley Sidi Yahia Aârab

Dunite

The one dunite sample produced a different LPO from the others, a B-type fabric by the Karato et al. (2008) classification. This is characterized by the <100> axis in the foliation plane perpendicular to lineation, the <010> axis perpendicular to the foliation plane, and the <001> axis aligned toward the lineation, indicating primarily simple shear with slip on the [001] (010) system. Karato et al. (2008) attribute this pattern to having higher water content, however Holtzmann et al. (2003) also find this pattern in their experiments where melt has segregated into melt-rich bands.

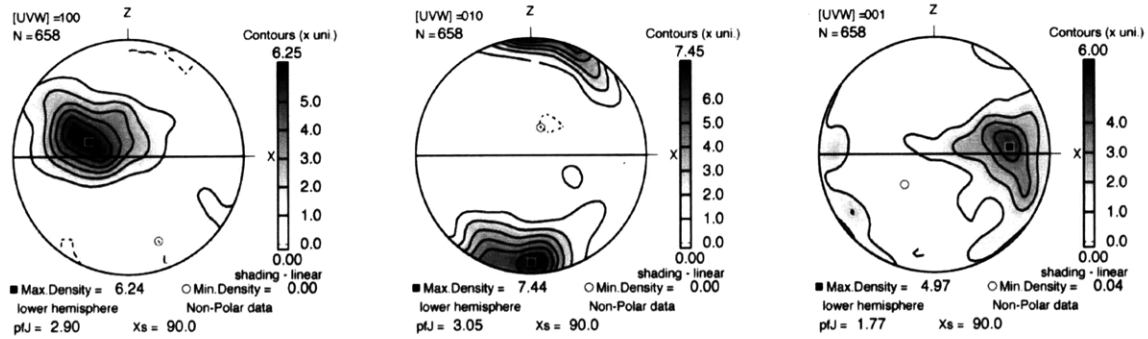

BB-08-46: Dunite from a heterogeneous zone within the Porphyric Harzburgite. M-index = 0.26, J-index = 9.44, maximum density = 7.44.

Figure 52. LPO pattern from a dunite in the south of valley Sidi Yahia Aârab.

5. Discussion

LPO Patterns

There are a few general observations that can be made from these patterns, the first is to split the patterns into two main categories: the peridotites and the dunite. The peridotite category could perhaps be split into two sub-groups, those with a- and c-axis girdles and those with point maxima, but the distinction is far less clear. With a few exceptions, the patterns are not very strong, and the patterns from the "deformed lherzolite" sections bounding the northern heterogeneous zones have particularly low M-indices. There also is a change a change in the orientation of the <100> axis with respect to the foliation plane across the heterogeneous zones.

The dunite shows the pattern-type most different from the others. Two explanations for this pattern-type from experimental studies are 1) high water content (Karato et al., 2008) and 2) high melt content (Holtzman et al., 2003). In this case the high melt content interpretation is favored as there is strong petrological evidence for melt presence. Additionally other the other samples analyzed show dry fabric patterns, so it seems unlikely that there was a much higher content in this one dunite than in the rest of the massif. Since it is only the dunite that shows a different pattern, perhaps phase interaction is important. Laboratory studies show that the addition of enstatite to olivine aggregates decreases the strength of the aggregates (Hitchings et al., 1989; Ji et al., 2001). Recently Sundberg and Cooper (2008) found that reactions between olivine and orthopyroxene produced an LPO in the diffusion creep regime. We do not see the pattern they find, thus conditions are likely not right for the production of this fabric in the Beni

Bousera samples, but it indicates that phase interaction can be an important component of a deformation fabric.

The distinction between the girdled and non-girdled fabric is much more subtle, and depends somewhat on the way in which the data are presented. It therefore does not make a very strong argument, but it does seem that the ones which have a little bit more of a girdle on both the a- and c-axis are the granular peridotites (BB08-10,47,49b). BB-08-9 and BB-08-31b do also show a bit of a girdle on the a-axis, though in the case of BB-08-9 the C-axis shows more of a point maxima. In BB-08-31b, the pattern is weak, so it is hard to discern whether it is truly a girdle or just part of the weak pattern. Girdles on both axes indicate more uniaxial compression in the deformation, and therefore could indicate that there was slightly less shearing in the granular peridotites than those associated with the heterogeneous zone.

LPO Strength

The weakness of the patterns by experimental standards is perhaps best explained by the fact that these are natural rocks, and nature is more complex than a laboratory or model. There are likely several factors contributing to the weakness including, interaction of multiple phases, likelihood of overprinting a previous LPO, and perhaps the presence of melt itself. Le Roux et al. (2008) find consistently weaker LPO fabric in the melt-infiltrated sections of the Lherz Massif than in the melt-free regions. Interestingly they also find more field evidence for deformation (strong mineral-alignment foliation, boudinage of websterite layers) in the areas with melt-percolation and weaker LPO. They suggest that this could be because of

greater amounts of diffusion-accommodated creep or grain boundary sliding. Lower deviatoric stress, and the presence of fluids can increase the likelihood of deformation by diffusion creep. Le Roux et al. (2008) note that a large temperature or stress gradient is unlikely on the tens of meter scale, and suggest that it larger melt flux is more likely the cause. They also note that larger melt volume can assist grain boundary sliding (Le Roux et al., 2008; Rosenberg and Handy, 2001; Scott and Kohlstedt, 2006). This suggests that melt could be a factor influencing the strength of LPOs. There is good geologic and petrologic evidence for melt presence in the Beni Bousera samples, and it likely contributed to the LPO pattern strength.

The dunite sample also has the strongest pattern in terms of M-index, so it is possible that the presence of additional phases is important in LPO strength, though the dunite also likely saw high melt contents. In Tommasi et al.'s study of the Murray Ridge peridotite, they also find significantly stronger LPO their dunite samples as compared to the harzburgites, and attribute this to either faster grain boundary migration or strain localization due to higher melt content (Tommasi et al., 2006). In fact they use the strengthening of their dunite LPO in conjunction with the change in slip systems they see from harzburgites to dunites together with the diffusive nature of the harzburgite-dunite contact to argue that the melt percolation and high temperature deformation occurred at the same time (Tommasi et al., 2006). The same Beni Bousera dunite also shows a diffuse boundary, stronger LPO and change in slip system, however the slip systems at play are different than the ones found by Tommassi et al. (2006).

A-axis orientation

Models (Kaminski and Ribe, 2001; Tommasi et al., 2000; Wenk and Tome, 1999), experimental results (Bystricky et al., 2000; Zhang and Karato, 1995), and field evidence (Warren et al., 2008) indicate that the olivine a-axis (100) aligns with the shear plane with increasing shear stain. The direction of offset of the a-axis also indicates the shear sense direction.

In the sample transect across the heterogeneous zone, there is both a decrease in the angle from the foliation plane to the a-axis toward the center of the heterogeneous zone and a switch in the direction of a-axis offset from the foliation. In our interpretations the foliation is used as a measure rather than the shear plane because in natural samples the exact shear plane is generally unknown. Therefore it is important to try and understand the relationship between the shear plane, a-axis and foliation. Figure 53 shows a diagram of the model predictions of a-axis alignment with the shear direction, experimental results, and the natural results from Warren et al. (2008). The lines for VPSC and DRex represent models for LPO evolution, and it appears that the DRex model (Kaminski and Ribe, 2001), which takes in to account recrystallization, fits the experimental data best, and the shape of the curve of the natural data. This approaches the direction of the shear plane much faster than the FSE (finite strain ellipsoid) curve, which is representative of the foliation. The a-axis from the natural samples approach the shear direction by about 300% strain, but the finite strain ellipsoid doesn't reach the shear direction until 800-1000%. This indicates that if a decrease in the angle between foliation.

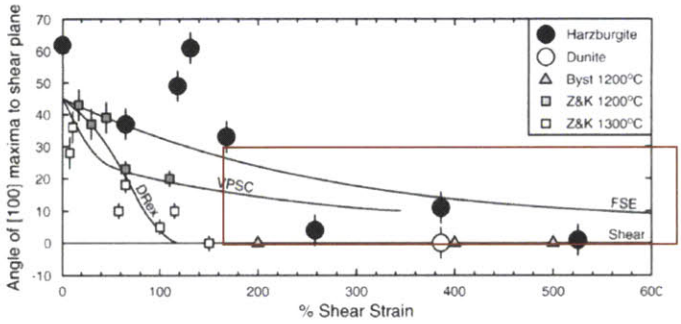

Figure 53. Model prediction of the a-axis maxima to the shear plane in comparison with experimental and natural results. Models are VPSC, viscoplastic self-consistent(Tommasi et al., 2000), DRex which includes recrystallization (Kaminski and Ribe, 2001), and FSE, the finite strain ellipsoid. Experimental results are Zhang and Karato (1995) and Bystricky et al. (2000). Points labeled Harzburgite and Dunite are natural samples from Warren et al. (2008). The red box shows where the Beni Bousera samples are likely to plot. Figure from Warren et al. (2008).

and a-axis is apparent, the a-axis is likely close to the shear plane, and the foliation is rotating toward the shear plane.

In our samples, the angle between the a-axis and the foliation plane decreases towards the center of the melt zone. Figure 54 shows a plot of the angle between the a-axis (best Euler 1 angle pole) and the foliation plane. Thin sections were visually checked to make sure mineral alignment foliation was horizontal in thin sections. The center of the zone is taken as just to the north of sample BB-08-9, where field evidence indicated the most intense heterogeneity. Distances to the south is taken to be and counter-clockwise rotations are considered positive for plotting. There is a distinct positive trend across the heterogeneous zone.

Plate 2, the cross-section shows the pole figures in relation to the geology, and it can be seen that the pole figures to the north of the heterogeneous zone (BB-08-31b and BB-08-35) have a-axis maxima rotated clockwise from the foliation, which if we take the a-axis as close to the shear plane indicates top to the south or

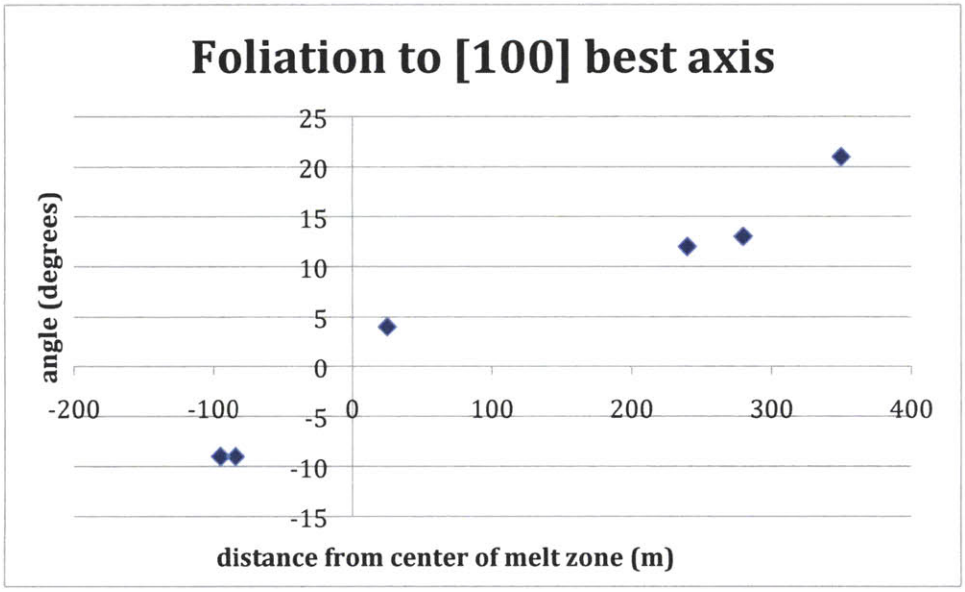

Figure 54. Plot showing angle between a-axis and foliation plane against distance from the center heterogeneous zone. Positive distance is south of the melt zone. There is a positive trend across the heterogeneous zone. Counter-clockwise is a positive angle. Angles were measured visually from the location of the best E1 (Euler angle) pole given by the PFch5 pole figure plotting software by David Mainprice.

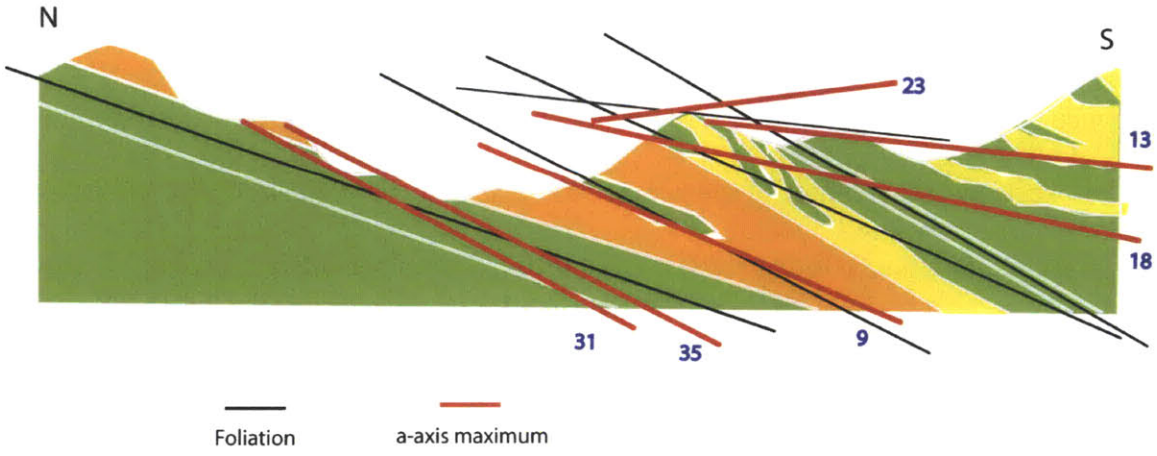

Figure 55. Simplified cross section showing orientation of the a-axis (red) relative to the foliation (black). With the exception of sample 23, they rotate towards the orientation of sample 9 and the foliation as they move into the heterogeneous zone. Sample 23 is a bit strange because the foliation in that location is nearly horizontal, whereas the others are fairly consistently dipping at ~20°.

dextral shearing. Samples just south of the heterogeneous zone show counter-clockwise offset, indicating top to the north or sinistral shearing. Figure 55 shows a simplified version of the cross-section with the orientation of the a-axis and the foliation displayed.

Inspection of Figure 55 reveals that the a-axis maxima actually appears to rotate towards the foliation rather than the other way around. It seems possible that in this case the foliation plane was already aligned close to the shear plane and that the a-axis orientation is catching up. Relatively consistent foliation orientation throughout the heterogeneous zone and the massif indicates that this might be the case; perhaps foliation became aligned with the shear plane during a preceding diffusive regime which did not form an LPO. If this is the case the shear senses indicated by the LPO are the opposite, with a sinistral sense indicated in the north and a dextral sense to the south of the heterogeneous zone, but it does not change the interpretation that there is a change in shear sense across the zone.

The angle between the a-axis maximum and the foliation indicates that the shear sense changes across the heterogeneous zone, and that strain increases toward the center of the zone. The most obvious explanation for this is that the heterogeneous zone had movement relative to the rest of the massif. Depending on the interpretation of the shear plane, the shear senses indicate that the zone is either moving up or down relative to the surrounding rocks in the current reference frame, but either way, the change in shear sense indicates that it is not just a straightforward shear zone.

Deformation Mechanism Maps and P-T Path

Field evidence indicates that areas with high melt flux show strong deformation indicated by isoclinally folded and boudinaged pyroxenite dikes. To assess whether melt flux and deformation are related and therefore the source of the LPO, we investigate the P-T conditions under which the LPO formed, and compare them to the available thermobarometry data that constrain the P-T history massif. It is generally assumed that LPO is formed only by deformation in the dislocation creep regime and not in the diffusion creep regime (Wenk, 2002). The transition between dislocation creep and diffusion creep is dependant on P, T grain size, and stress. Dislocation creep and diffusion creep are related with olivine flow laws of the form:

$$\dot{\varepsilon} = A\sigma^n d^{-p} f_{H_2O} \exp\left(-\frac{E^* + PV^*}{RT}\right)$$

where $\dot{\varepsilon}$ is strain rate, A is a pre-exponential constant, σ is differential stress, n=1 for diffusion creep and n=3 to 5 for dislocation creep, d is grain size, and p=3 for diffusion creep, and p=0 for dislocation creep, f_{H_2O} is water fugacity, E* is activation energy, P is pressure, V* is the activation volume, R is the ideal gas constant, and T is temperature(Hirth, 2002) .

Ideally we would be able to constrain some of these variables to understand which mechanisms were operating in Beni Bousera. Geothermometry and barometry provide constraints on P and T, while the observed averaged grain size was used to constrain d. The A-type LPO patterns are generally interpreted to

reflect anhydrous conditions (Karato et al., 2008), so water fugacity can be neglected.

The observed average grain size of olivine was used to estimate the paleostress condition using a paleopiezometer (Fig 56) (Karato et al., 1980; Vanderwal et al., 1993). Average grain sizes were counted using the grain intercept method (Underwood, 1970). Average grain size ranged from .4 to .9 mm; the average for each sample is presented on Plate 2. There was generally somewhat of a bimodal distribution for olivine, and often irregular grain shapes, so it unclear how representative these averages are, but they allow at least general placement on a paleopiezometer (Fig 56). The paleopiezometer indicates a differential stress of around 10 MPa. We use these stress and grain size constraints to investigate under which P, T conditions Beni Bousera resided in the dislocation creep or diffusion creep regime. It is, however, worth noting that these paleopiezometers are calibrated for deformation in the dislocation creep regime, thus are not necessarily valid for diffusion creep.

The dominant olivine deformation regime depends on stress, temperature, grain size and to a lesser extent on pressure. The relationship between deformation mechanism and the different parameters is illustrated in 2 dimensions on deformation mechanism maps, where any two variables on the axes and the other two held constant. We investigated the dependence of the deformation regime in stress-grain size space, and calculated a variety of deformation maps for different temperature and pressure conditions inferred from Beni Bousera (Gysi et al. in prep), to investigate the changes in dominant deformation mechanism for different

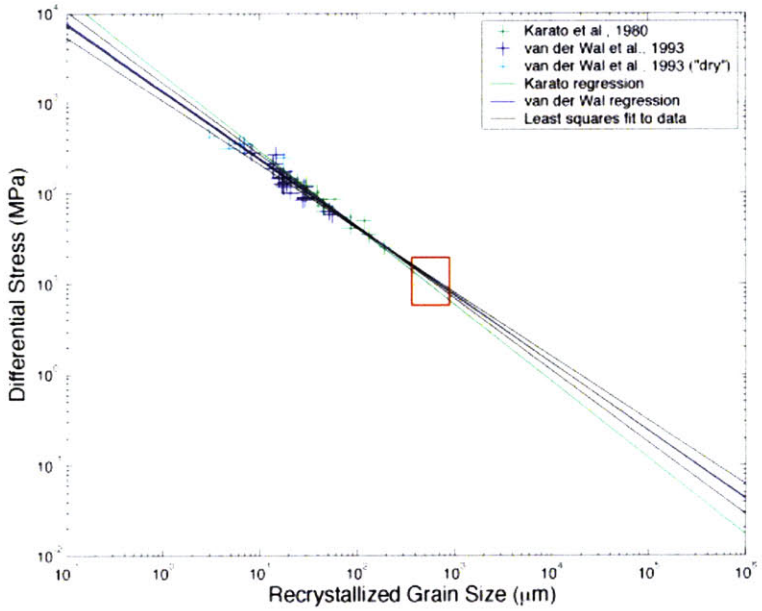

Figure 56. Paleopiezometer calculated from experimental results of Karato et al. (1980) and van der Wal et al. (1993). Both the published regression lines and the least squares fit to the data are shown. Red box shows location of Beni Bousera samples from approximate average grain sizes. After Warren (2009).

periods in Beni Bousera's history (Fig 57). Deformation mechanism maps were created with the program OlivineDeformationMaps by J. M. Warren, and is based on the flow laws from Bai et al (1991), Evans and Goetze (1979), and Hirth and Kohlstedt (2003). As we consider the deformation related to melt infiltration we used the P-T conditions as constrained by Gysi et al. (in prep) for the emplacement of pyroxenites dykes. These authors noted four types of pyroxenites dykes in the massif, three of which are though to be the result of magmatic crystallization process at high pressure and therefore associated with melt flux: (1) Garnet websterites, which give temperatures of 1000-1100°C at 20-30 kbar (Gysi et al. in prep). The deformation mechanism map for olivine at these P-T conditions is presented in (Fig. 57a) and using the above derived grain-size stress dependency it

is apparent that under these P-T conditions olivine would deform dominantly in the diffusion creep regime, which would not result in the LPO recorded in our samples.

(2) Spinel websterites, for which Gysi et al. (in prep) inferred temperatures of about 1000°C at pressures of 16-18 kbar. Similar to the conditions inferred for

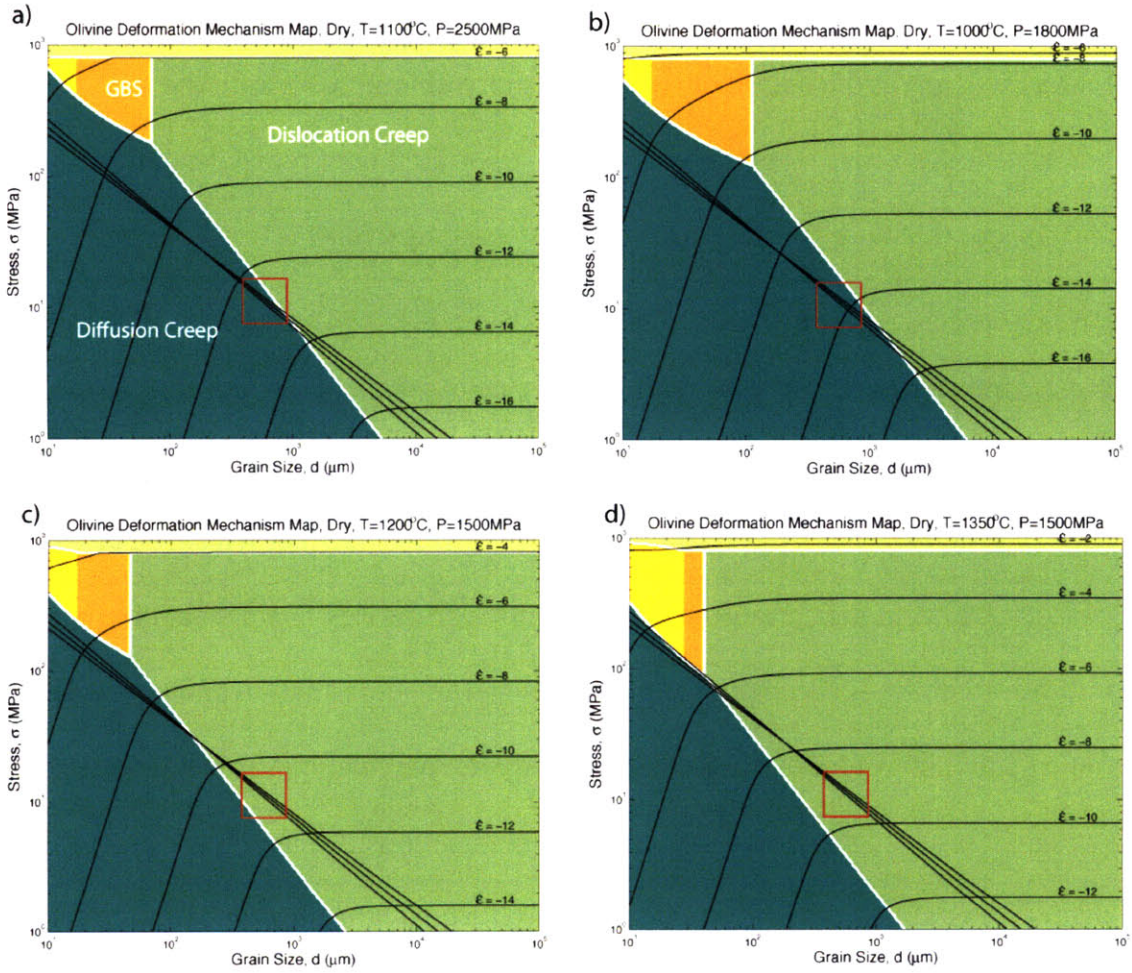

Figure 57. Dislocation mechanism maps for conditions recorded at different stages of Beni Bousera's history. Blue area is Diffusion Creep, green is Dislocation Creep (responsible for LPO formation) and yellow is a region of Grain Boundary Sliding (GBS). Strain rate contours are plotted, as are the regression lines from the piezometers (shown in Figure 1). Red box indicates the region of Beni Bousera samples. a) and b) indicate deeper parts of the massif's history, at about 75km and 54km depth, respectively, and both show deformation in the diffusion creep regime. c) and d) represent different temperature extremes for the influx of the Cr-diopside veins and patches at about 45km depth. These both give deformation in the dislocation creep regime, though fairly close to the boundary. Deformation Mechanism maps created the program OlivineDeformationMaps ©2007 by J.M. Warren based on the flow laws from Bai et al. (1991), Evans and Goetze (1979), Hirth and Kohlstedt (2003), Karato et al. (1980), and Van der Wal et al. (1993).

the garnet pyroxenites the calculated deformation mechanism map (Fig 57b) also indicates that these P-T conditions predict dominant diffusion creep deformation, and thus we conclude that this event is not responsible for the LPO in our samples.

(3) Cr-diopside-spinel patches appear to be the latest feature based on crosscutting relations and deformation intensity observed in the field. They are found throughout the massif but are much more ubiquitous within the heterogeneous zones where they are often associated with replacive dunite. Gysi et al (in prep) calculate temperatures for these ranging from 1200 to 1350°C at pressures of 14-16 kbar. The deformation mechanism maps (Figs. 57c and 57d) for these conditions predict deformation of olivine in the dislocation creep regime, which would form a LPO. So we infer that the measured LPO pattern at least in the heterogeneous zones is the result of deformation associated or triggered by a melt percolation event that produced the Cr-spinel websterites. Field evidence indeed indicates that areas with high melt flux show strong deformation and my results indicate that strain increases with increased melt percolation. The older garnet pyroxenites are highly deformed, whereas the Cr-diopside patches are less deformed or appear largely undeformed. Accordingly the observed LPO pattern is likely contemporaneous or pre-dates the infiltration associated with the formation of the Cr-Diopside veins.

Additionally under the assumed LPO-forming conditions associated with the Cr-Diopside veins the deformation mechanism maps indicate high strain rates. Strain rate exponents range from -9 to -11 (Figs 57c and 57d) compared with exponents of -14 and -16 from the deeper part of the massif's history (Figs 57a and

57b). These strain rates are extrapolated under a constant-stress assumption, which may not be a valid for the entire massif's history. The observation of fast strain rates in the latter part of the massif's history is in accordance with independent thermal and chronological evidence indicating fast exhumation (Platt et al., 2003). Our new data are in accordance with this interpretation and provide additional support fast exhumation in the later part of the massif's history.

Finally, the conditions inferred for our samples indicate that deformation is close to the transition between diffusion and dislocation dominated deformation (Fig 57c and 57d). We consider it likely that the observed weak LPO patterns are a result of the influence of the diffusion creep mechanism. Intuitively one would assume, as observed that the LPO records the latest deformation event in the dislocation creep regime and overprints older fabrics.

The above mentioned relationship on deformation mechanism and P-T conditions can additionally be illustrated in a P-T diagram if grain size and stress are considered constant over the investigated P-T conditions (Figure 58). We used the inferred P-T path of Beni Bousera (Gysi et al., in prep) with additional constraints from the surrounding rocks (Piasecki, 2009) and Ronda (Platt et al., 2003) to compare the P-T path of the massif and the inferred deformation conditions. In accordance with above observations from deformation mechanism maps, the inferred deformation conditions along the P-T path indicate that the massif during the higher pressure evolution part resided in the diffusion creep range, which would not induce a LPO. However, any increase in temperature in the range of 100-150°C, for instance triggered by the influx of a hot melt, could have pushed the massif into

the dislocation creep regime resulting in LPO formation. This is observed for the melt infiltration event that produced the Cr-spinel websterites. It may have equally occurred in deeper parts during the evolution history, but if so, ambient temperatures where colder so that the massif cooled and reequilibrated in the

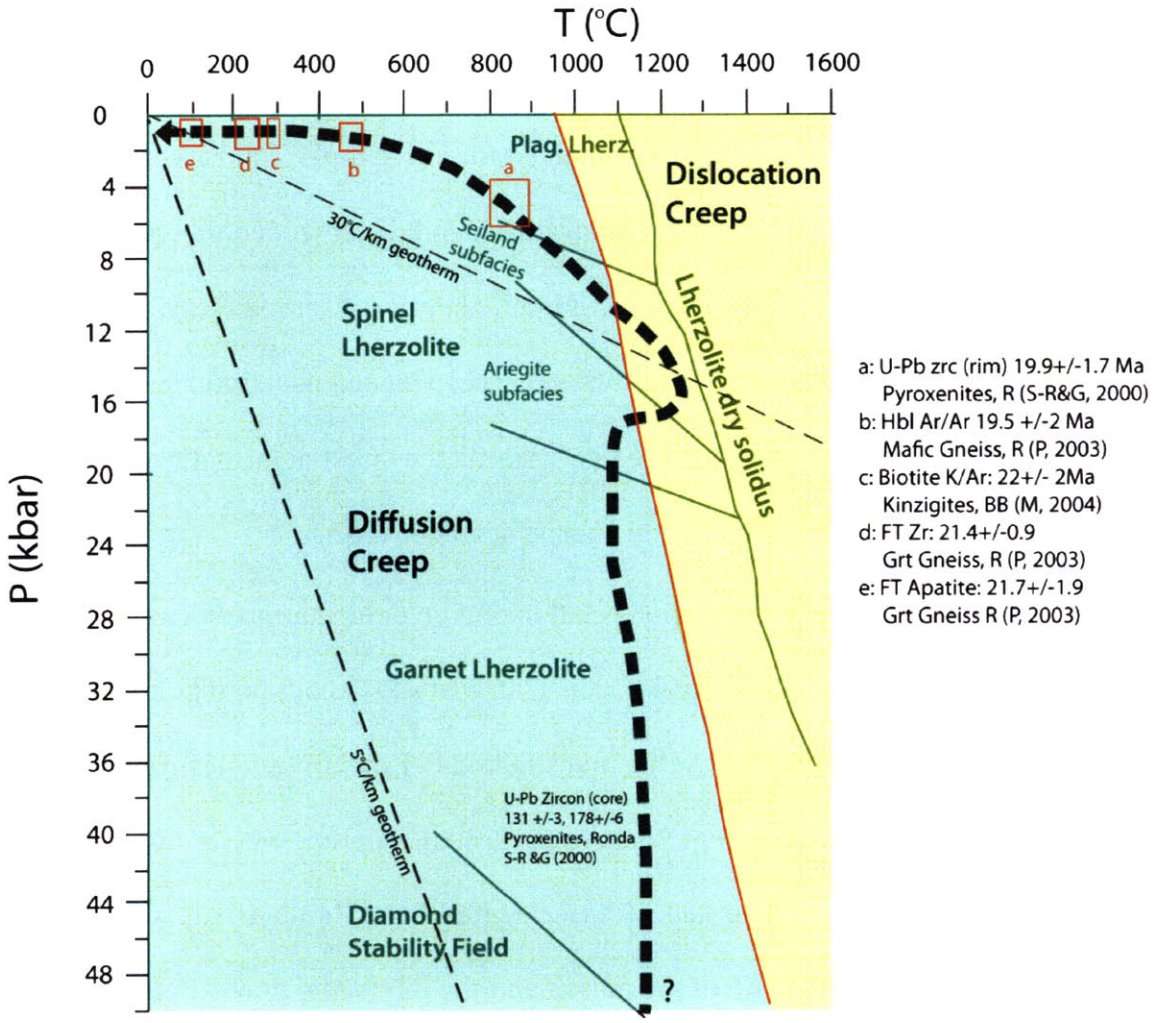

Figure 58. Pressure Temperature diagram with inferred path of Beni Bousera, inspired by P-T data from Gysi et al. (in prep), Platt et al. (2003), and Piasecki (2009). Also shown are the fields for dislocation Creep and diffusion creep for grain sizes 0.4 to 0.9 mm, stress of about 10 MPa (calculated from OlivineDeformationMaps ©2007 by J.M. Warren). The massif mostly remains in the diffusion creep regime, only when the temperature increases does it enter the dislocation creep regime (LPO forming). Exhumation to the surface was fast, shown are dates from Beni Bousera (BB) and Ronda (R) massifs from Sanchez-Rodriguez and Gebauer (2000), Montigny et al. (2004) and Platt et al. (2003). The Area where path veers into dislocation creep regime is associated with temperatures from the Cr-diopside patches.

diffusion creep regime. Our results indicate that LPO in Beni Bousera only formed in association with the influx of melt with subsequent rise of the ambient temperature of the massif. Thus the record of the LPO relies on melt presence. As mentioned the generally observed weak LPO pattern could be related to the close proximity of the massif P-T conditions to the transition between dislocation and diffusion creep regime.

This calculated relationship between P-T and deformation regime is counterintuitive as diffusion creep is generally thought to be active at higher temperatures, the opposite of what is shown in Figure 58. A more commonly viewed coordinate frame, temperature-stress (Fig. 58), indicate similar relationship when viewed in P-T space. Even so the deformation map presented in Figure 58 is not calibrated specifically for the conditions inferred for Beni Bousera, it illustrates that for a given stress, an increase in temperature results in the transition from diffusion creep to dislocation creep (labeled power-law creep on the diagram). The pressure dependence of the field boundary in Figure 57 is a strongly dependant on the choice of V*, the activation volume, for both diffusion and dislocation creep, neither of which are extremely well constrained. The relationship between temperature and deformation mechanism in Figure 57 arises from the fixed grain size and, most importantly, stress. The calculated stress relies on the paleopiezometer, that may not be valid thought the massif's entire history, but we consider it appropriate for the conditions where the LPO formed in the measured samples.

Geochronologic evidence indicates that Beni Bousera (and Ronda) were exhumed very quickly, with thermochronometers over a full range of closure

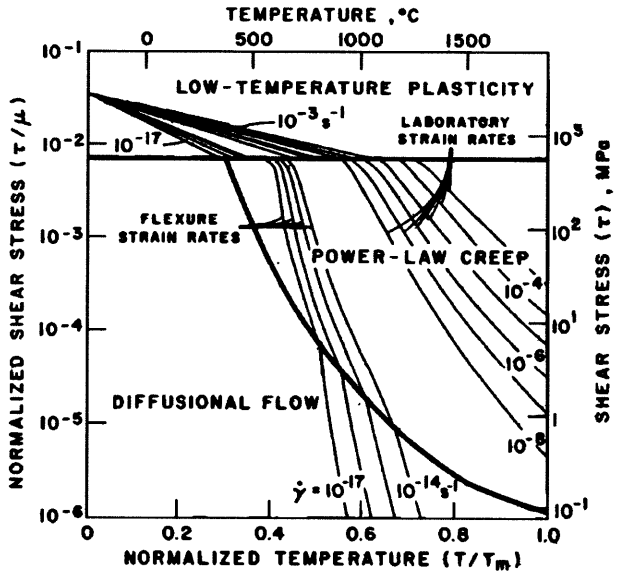

Figure 59. Deformation mechanism map in temperature-stress space. This plot is given for an average grain size of 1mm, slightly larger than that in the Beni Bousera samples. Shear stress is normalized by the shear modulus (μ), and temperature is normalized by the melt temperature (T_m). It is likely that different constants were used to calculate these fields than the deformation mechanism maps shown in Figure *, but this map indicates that for a given stress, increasing temperature moves towards the dislocation creep (power law creep) field. From Kirby (1983) after Ashby and Verrall (1978)

temperatures giving ages between 18 and 23 Ma (Fig 7)(Montel et al., 2000; Platt et al., 2003). Platt et al. (2003) estimate an exhumation rate of at least 15 km/Ma for the garnet gneisses surrounding Ronda. Some of the early attempts to constrain the ascent rate of the ultramafite by Obata (1980) yielded ascent rates of more than 1 m/yr based on recrystallization front thickness and Al zoning in pyroxene, though this estimate is generally considered very high. In the Beni Bousera ultramafite the plagioclase lherzolite is absent, indicating that the massif did not reequlibrate in that pressure range. In combination with the thermochronologic evidence for fast exhumation to the surface, we can infer that Beni Bousera was exhumed rapidly from the spinel lherzolite stability field (~10-20 kbar) to the surface. This is in accordance with the fact that the LPO formed during melt infiltration in the spinel

lherzolite field. Since olivine LPO is a high-temperature fabric, above ~800°C, it is unlikely that the olivine LPO was overprinted by near surface tectonics.

Relation to Melt Transport

Melt driven buoyancy might provide an explanation for the change in shear sense across the melt zone. The higher melt content in the channel would cause it to be more buoyant than the surrounding peridotites and move upward. In this situation we would expect opposite senses of shear on either side of the channel, as shown by our LPO patterns.

Jagoutz et al. (2006) proposed a model for the emplacement of zoned ultramafic complexes (ZUC) in which they are buoyed up by melt filled channels that extend down into the mantle. Surface expressions of these ZUC with evidence for mantle diapirism can be found emplaced in the lower crust in the Kohistan Arc (Jagoutz et al., 2006) and even up into un-metamorphosed sediments in the

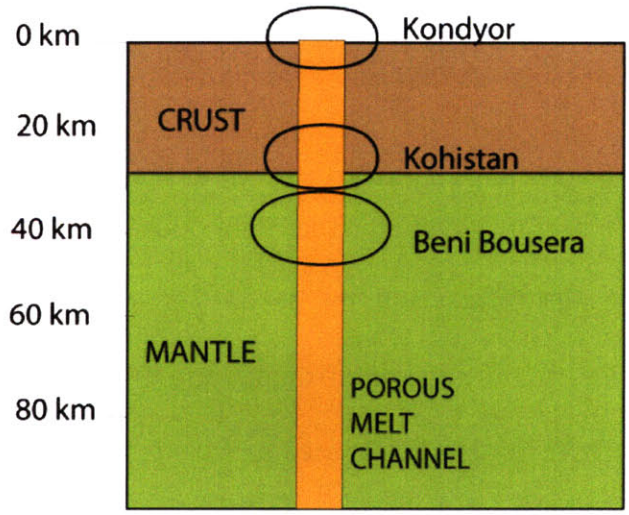

Figure 60. Diagram showing how Beni Bousera might relate to ZUC such as the Kondyor massif (Burg et al. 2009) or those found in Kohistan by Jagoutz et al (2006). The melt channels in Beni Bousea may represent the channels at depths of 30-70 km.

Kondyor massif (Burg et al., 2009). The melt channel examined at Beni Bousera similarly has melt infiltrated material moving relative to its surroundings, but within the surrounding mantle rather than though the crust. One might speculate that this is representative of a similar mechanism at depth, and perhaps and what one might expect to find in the mantle below one of these ZUCs (Figure 60).

Holtzman and Kholstedt (2007) show in the laboratory setting that stress causes the segregation of melt rich bands which form an anastamosing channel network. They indicate that this could operate under geologic conditions with channel spacing on the order of 10 to 1000 meters. They observe that strain is partitioned into these melt rich bands. Similarly, we find melt channels that have a large amount strain, indicated by the a-axis alignment of LPO patterns and isoclinally folded and boudinaged pyroxenite layers. If Holtzman and Kohlstedt's (2007) model is applicable to geologic scales, than melt channels such as the one investigated here may be related to larger scale stresses. They present a cartoon of what a section of stress-driven melt segregation might look like beneath a mid-ocean ridge (Figure 61), and it is interesting to compare it to the cross section of Beni Bousera (Plate 2). It could be that Beni Bousera represents the footwall of one of these large scale systems, with the Border Facies being analogous to the high strain region close to the edge of the diapir, and the channel studied in detail with EBSD analysis representing one of the more central channels. Kaczmarek and Müntener (2008) make similar speculations about the shear zone they inspected in the Lanzo Peridotie Body in Italy. Obviously much more detailed fieldwork and

understanding of the deformation and emplacement would be necessary understand if this were truly the case.

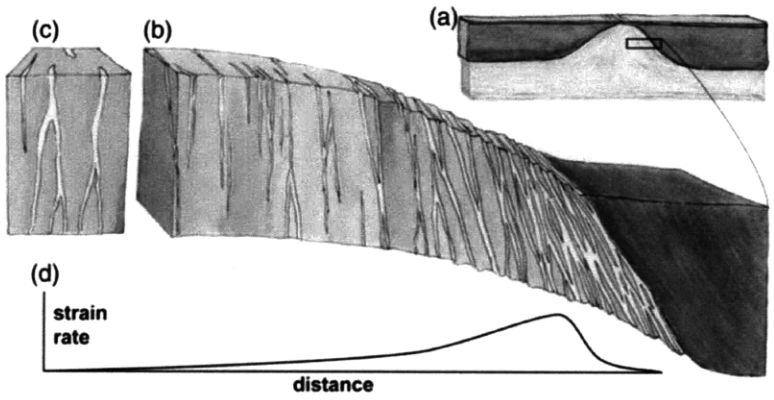

Figure 61. Illustration from Holtzman and Kohlstedt (2007) of a hypothetical stress-driven melt segregation zone under a mid ocean ridge. It is interesting to compare this to observations from Beni Bousera, perhaps the Border facies represents something similar to the edge of this drawing, and the channel investigated in detail with EBSD might represent one of the more interior channels.

6. Conclusion and Further Studies

This study of the Beni Bousera Ultramafic Massif, Northern Morocco has indicated that there was significant amounts of melt infiltration in the massif's history, some of which segregated into channels of focused flow. The LPO for the peridotites in the massif give fabrics indicating dislocation under dry, high temperature conditions on the [100](010) slip system. The LPO pattern for the dunite indicates slip on the [001](010) system, producing a pattern that is normally associated with significant melt or water content. The LPO indicates a change in shear sense across a paleo-melt channel and an increase in strain toward the center of the channel. This indication of high strain is supported by field evidence showing significant deformation in the melt channels such as boudinaged and isoclinally folded pyroxenites. Additionally, Deformation mechanism maps indicate that the massif deforms in the dislocation creep regime more readily when hot melt raises the ambient temperature of the massif. This indicates melt-induced deformation; buoyancy driven forces from rising melts induce a high strain within the melt zone and cause a change in shear sense across the zone. This has broader implications for melt extraction processes and the effects of stress on melt segregation.

There are many directions for further studies. In the field, the massif could be mapped in more detail with attention towards the distribution of pyroxenites and melt channels. For the microstructural study, it would be interesting to measure the LPO of orthopyroxene and compare it to the LPO of olivine. The samples however, are so coarse-grained that this would require analysis several thin sections to achieve a statistically significant analysis. It would be interesting to

see if the dunite from the heterogeneous zone studied in depth was similar to the peridotite patterns from that melt zone or more similar to the dunite pattern from elsewhere in the massif. Additional LPO patterns from other samples of granular textures would also be useful in understanding the consistency or variability of the more homogeneous-textured rocks. Additionally "decorating" thin sections to expose dislocations would indicate whether there was a lot of deformation in the dislocation creep regime. The next step with the LPO is to understand what effect it has on seismic anisotropy and whether such melt-rich channels or peridotite bodies would be distinguishable seismically.

Eventually a more complete understanding of the chemistry, deformation, and emplacement mechanism of Beni Bousera would be the ultimate goal, as well as an understanding of the why so many large peridotite bodies exist in the western Mediterranean, but that is far beyond the scope of this project.

Works Cited

Agard, P., Jullien, M., Goffe, B., Baronnet, A. and Bouybaouene, M., 1999. TEM evidence for high-temperature (300 degrees C) smectite in multistage clay-mineral pseudomorphs in pelitic rocks (Rif, Morocco). European Journal of Mineralogy, 11(4): 655-668.

Allerton, S., Reicherter, K. and Platt, J.P., 1994. A Structural and Paleomagnetic Study of a Section through the Eastern Subbetic, Southern Spain. Journal of the Geological Society, 151: 659-668.

Andrieux, J., Fontbote, J.M. and Mattauer, M., 1971. An explanatory model for the Gibralter Arc. Earth and Planetary Science Letters, 12: 191-198.

Argles, T.W., Platt, J.P. and Waters, D.J., 1999. Attenuation and excision of a crustal section during extensional exhumation: The Carratraca Massif, Betic Cordillera, southern Spain. Journal of the Geological Society, 156: 149-162.

Ashby, M.F. and Verrall, R.A., 1978. MICRO-MECHANISMS OF FLOW AND FRACTURE, AND THEIR RELEVANCE TO RHEOLOGY OF UPPER MANTLE. Philosophical Transactions of the Royal Society of London Series a-Mathematical Physical and Engineering Sciences, 288(1350): 59-95.

Bai, Q., Mackwell, S.J. and Kohlstedt, D.L., 1991. High-Temperature Creep of Olivine Single-Crystals .1. Mechanical Results for Buffered Samples. Journal of Geophysical Research-Solid Earth and Planets, 96(B2): 2441-2463.

Balling, N. and Banda, E., 1992. Europe's lithosphere, recent activity. In: D. Blundel, R. Freeman and S. Mueller (Editors), A Continent Revealed: The European Geotraverse. Cambridge University Press, pp. 111-135.

Beslier, M.O. and Brun, J.P., 1991. Boudinage of the Lithosphere as a New Model of Passive Continental-Margin Formation. Comptes Rendus De L Academie Des Sciences Serie Ii, 313(8): 951-958.

Beyer, E.E., Griffin, W.L. and O'Reilly, S.Y., 2006. Transformation of archaean lithospheric mantle by refertilization: Evidence from exposed peridotites in the Western Gneiss Region, Norway. Journal of Petrology, 47(8): 1611-1636.

Bouillin, J.P., Durand-Delga, M. and Olivier, P., 1986. Betic-Rifian and Tyrrhenian Arcs: Distinctive features, genesis and development stages. In: F.C. Wezel (Editor), The Orgin of Arcs. Elsevier Sci. Publ., Amsterdam, pp. 218-304.

Bouillin, J.P. et al., 1998. Preliminary thermochronological data on the submerged Sardinian and Kabylian-Peloritan insular shelves in the Sardinia Channel (western Mediterranean). Comptes Rendus De L Academie Des Sciences Serie Ii Fascicule a-Sciences De La Terre Et Des Planetes, 326(8): 561-566.

Bouybaouene, M., Michard, A. and Goffe, B., 1998. High-pressure granulites on top of the Beni Bousera peridotites, Rif belt, Morocco: a record of an ancient thickened crust in the Alboran domain. Bulletin De La Societe Geologique De France, 169(2): 153-162.

Bouybaouene, M.L., 1993. Etude petrologique des metapelites des sebtides superierues, Rif interne, Maroc, Univ. Mohamed V, Rabat, 160 pp.

Brey, G.P. and Kohler, T., 1990. GEOTHERMOBAROMETRY IN 4-PHASE LHERZOLITES .2. NEW THERMOBAROMETERS, AND PRACTICAL

ASSESSMENT OF EXISTING THERMOBAROMETERS. Journal of Petrology, 31(6): 1353-1378.
Buforn, E., Degaldeano, C.S. and Udias, A., 1995. Seismotectonics of the Ibero-Maghrebian Region. Tectonophysics, 248(3-4): 247-261.
Bunge, H., 1982. Texture Analysis in Materials Science: Mathematical Models. Butterworths, London.
Burg, J.P. et al., 2009. Translithospheric Mantle Diapirism: Geological Evidence and Numerical Modelling of the Kondyor Zoned Ultramafic Complex (Russian Far-East). Journal of Petrology, 50(2): 289-321.
Bystricky, M., Kunze, K., Burlini, L. and Burg, J.P., 2000. High shear strain of olivine aggregates: Rheological and seismic consequences. Science, 290(5496): 1564-1567.
Caby, R., Hammor, D. and Delor, C., 2001. Metamorphic evolution, partial melting and Miocene exhumation of lower crust in the Edough metamorphic core complex, west Mediterranean orogen, eastern Algeria. Tectonophysics, 342(3-4): 239-273.
Calvert, A. et al., 2000. Geodynamic evolution of the lithosphere and upper mantle beneath the Alboran region of the western Mediterranean: Constraints from travel time tomography. Journal of Geophysical Research-Solid Earth, 105(B5): 10871-10898.
Calvo, M., Cuevas, J. and Tubia, J.M., 2001. Preliminary palaeomagnetic results on Oligocene-early Miocene mafic dykes from southern Spain. Tectonophysics, 332(3): 333-345.
Calvo, M., Vegas, R. and Osete, M.L., 1997. Palaeomagnetic results from Upper Miocene and Pliocene rocks from the Internal Zone of the eastern Betic Cordilleras (southern Spain). Tectonophysics, 277(4): 271-283.
Chalouan, A. and Michard, A., 2004. The Alpine Rif belt (Morocco): A case of mountain building in a subduction-subduction-transform fault triple junction. Pure and Applied Geophysics, 161(3): 489-519.
Chalouan, A., Michard, A., Feinberg, H., Montigny, R.A. and Saddiqi, O., 2001. The Rif mountain building (Morocco): a new tectonic scenario. Bulletin De La Societe Geologique De France, 172(5): 603-616.
Chalouan, A., Saji, R., Michard, A. and Bally, A.W., 1997. Neogene tectonic evolution of the southwestern Alboran basin as inferred from seismic data off Morocco. Aapg Bulletin-American Association of Petroleum Geologists, 81(7): 1161-1184.
Comas, M.C., Platt, J.P., Soto, J.I. and Watts, A.B., 1999. The orgin and tectonic history of the Alboran basin: Insights from ODP leg 161 results. In: R. Zahn, M.C. Comas and A. Klaus (Editors), Proc. Ocean Drill. Program Sci. Tesults 161, pp. 555-580.
de Lamotte, D.F., 1985. La structure du Rif oriental (Maroc). Role de la tectonique longitudinale et importance des fluides. Mem. Sci. Terre Univ. P. et M. Curie, 85(03).
de Lamotte, D.F., Saint Bezar, B.A., Bracene, R. and Mercier, E., 2000. The two main steps of the Atlas building and geodynamics of the western Mediterranean. Tectonics, 19(4): 740-761.

Delamotte, D.F., Andrieux, J. and Guezou, J.C., 1991. KINEMATICS OF THE NEOGENE THRUSTING IN THE BETIC-RIF OROCLINE - A REVIEW. Bulletin De La Societe Geologique De France, 162(4): 611-626.

Dercourt, J., Ricou, L.E. and Vrielinck, B. (Editors), 1993. Atlas of Tethys Environmental Maps. Gauthier-Villars, Paris, 307 pp.

Doglioni, C., Fernandez, M., Gueguen, E. and Sabat, F., 1999. On the interface btween the early Apennines-Maghrebides backarc extension and the Alps-Betics Orogen in the Negogene gyeodynamics of wht Western Mediterranean. Bull. Soc. geol. It., 118: 75-89.

Doglioni, C., Mongelli, F. and Pialli, G., 1998. Boudinage of the Alpine Belti in the Apenninic Backarc. Mem. Soc. Geol. It., 52: 457-468.

Draoui, M., 1992. Etude petro-structurale du massif ultrabasique de Beni Bousera (Rif Interne, Maroc): un module de mise en place, Universite Cadi Ayyad.

Durand-Delga, M. and Fontbote, J.M., 1980. Le cadre structural de la Mediterranee occidentale, 26th Inter. Geol. Congr. , Paris, pp. 67-85.

Durand-Delga, M., Rossi, P., Olivier, P. and Puglisi, D., 2000. Structural setting and ophiolitic nature of Jurassic basic rocks associated with the Maghrebian flyschs in the Rif (Morocco) and Sicily (Italy). Comptes Rendus De L Academie Des Sciences Serie Ii Fascicule a-Sciences De La Terre Et Des Planetes, 331(1): 29-38.

Elazzab, D. and Feinberg, H., 1994. Paleomagnetism of External Rif Ultrabasic Rocks (Morocco). Comptes Rendus De L Academie Des Sciences Serie Ii, 318(3): 351-357.

Ellis, D.J. and Green, D.H., 1979. Experimental-Study of the Effect of Ca Upon Garnet-Clinopyroxene Fe-Mg Exchange Equilibria. Contributions to Mineralogy and Petrology, 71(1): 13-22.

Evans, B. and Goetze, C., 1979. Temperature-Variation of Hardness of Olivine and Its Implication for Polycrystalline Yield Stress. Journal of Geophysical Research, 84(Nb10): 5505-5524.

Faccenna, C., Mattei, M., Funiciello, R. and Jolivet, L., 1997. Styles of back-arc extension in the Central Mediterranean. Terra Nova, 9(3): 126-130.

Favre, P., 1995. Quantitative-Analysis of Rifting and Thermal Relaxation in the Western Part of the North-African Transform Margin - External Rif (Morocco). Geodinamica Acta, 8(2): 59-81.

Froitzheim, N., Schmid, S.M. and Frey, M., 1996. Mesozoic paleogeography and the timing of eclogite-facies metamorphism in the Alps: A working hypothesis. Birkhauser Verlag Ag, pp. 81-&.

Garciaduenas, V., Balanya, J.C. and Martinezmartinez, J.M., 1992. Miocene Extensional Detachments in the Outcropping Basement of the Northern Alboran Basin (Betics) and Their Tectonic Implications. Geo-Marine Letters, 12(2-3): 88-95.

Goffe, B., Azanon, J.M., Bouybaouene, M.L. and Jullien, M., 1996. Metamorphic Cookeite in Alpine Metapelites from Rif (Northern Morocco) and Betic Chains (Southern Spain). Eur. J. Mineral., 6: 897-911.

Gueguen, E., Doglioni, C. and Fernandez, M., 1997. Lithospheric boudinage in the western Mediterranean back-arc basin. Terra Nova, 9(4): 184-187.

Guerrera, F., Martinalgarra, A. and Perrone, V., 1993. LATE OLIGOCENE-MIOCENE SYN-/-LATE-OROGENIC SUCCESSIONS IN WESTERN AND CENTRAL MEDITERRANEAN CHAINS FROM THE BETIC CORDILLERA TO THE SOUTHERN APENNINES. Terra Nova, 5(6): 525-544.

Gysi, A., 2007. Petrogenesis of Pyrozenites and Melt Infiltrations in the Ultramafic Complex of Beni Bousera, Northern Morocco, ETH Zurich, Zurich, Switzerland, 182 pp.

Gysi, A., Jagoutz, O., Schmidt, M. and Targuisti, K., in prep. Petrogenisis of pyroxenites and melt infiltrations in the ultramafic complex of Beni Bousera, northern Morocco.

Hirth, G., 2002. Laboratory constraints on the rheology of the upper mantle In: S. Karato and H.R. Wenk (Editors), Conference on Plastic Deformation of Minerals and Rocks. Mineralogical Soc America, Berkeley, Ca, pp. 97-120.

Hirth, G. and Kohlstedt, D.L., 1995. Experimental Constraints on the Dynamics of the Partially Molten Upper-Mantle .2. Deformation in the Dislocation Creep Regime. Journal of Geophysical Research-Solid Earth, 100(B8): 15441-15449.

Hirth, G. and Kohlstedt, D.L., 2003. Rheology of the Upper Mantle and the Mantle Wedge: A View from Experimentalists. In: J. Eiler (Editor), The Subduction Factory. American Geophysical Union Geophysical Monograph, pp. 83-105.

Hitchings, R.S., Paterson, M.S. and Bitmead, J., 1989. Effects of Iron and Magnetite Additions in Olivine Pyroxene Rheology. Physics of the Earth and Planetary Interiors, 55(3-4): 277-291.

Holtzman, B.K. et al., 2003. Melt segregation and strain partitioning: Implications for seismic anisotropy and mantle flow. Science, 301(5637): 1227-1230.

Hoyes, B., 1989. Le Numidien et les flyschs oligo-miocenes de la bordure sud de la Mediterranee occidentale, Universite Lille, Lille, 464 pp.

Jagoutz, O., Muntener, O., Burg, J.P., Ulmer, P. and Jagoutz, E., 2006. Lower continental crust formation through focused flow in km-scale melt conduits: The zoned ultramafic bodies of the Chilas complex in the Kohistan island arc (NW Pakistan). Earth and Planetary Science Letters, 242(3-4): 320-342.

Ji, S.C., Wang, Z.C. and Wirth, R., 2001. Bulk flow strength of forsterite-enstatite composites as a function of forsterite content. Tectonophysics, 341(1-4): 69-93.

Kaczmarek, M.A. and Muntener, O., 2008. Juxtaposition of Melt Impregnation and High-Temperature Shear Zones in the Upper Mantle; Field and Petrological Constraints from the Lanzo Peridotite (Northern Italy). Journal of Petrology, 49(12): 2187-2220.

Kaminski, E. and Ribe, N.M., 2001. A kinematic model for recrystallization and texture development in olivine polycrystals. Earth and Planetary Science Letters, 189(3-4): 253-267.

Karato, S., Jung, H., Katayama, I. and Skemer, P., 2008. Geodynamic significance of seismic anisotropy of the upper mantle: New insights from laboratory studies. Annual Review of Earth and Planetary Sciences, 36: 59-95.

Karato, S.I., Toriumi, M. and Fujii, T., 1980. Dynamic Recrystallization of Olivine Single-Crystals during High-Temperature Creep. Geophysical Research Letters, 7(9): 649-652.

Kelemen, P.B., 1990. Reaction between Ultramafic Rock and Fractionating Basaltic Magma .1. Phase-Relations, the Origin of Calc-Alkaline Magma Series, and the Formation of Discordant Dunite. Journal of Petrology, 31(1): 51-98.
Kelemen, P.B., Dick, H.J.B. and Quick, J.E., 1992. FORMATION OF HARZBURGITE BY PERVASIVE MELT ROCK REACTION IN THE UPPER MANTLE. Nature, 358(6388): 635-641.
Kelemen, P.B., Shimizu, N. and Salters, V.J.M., 1995. Extraction of Mid-Ocean-Ridge Basalt from the Upwelling Mantle by Focused Flow of Melt in Dunite Channels. Nature, 375(6534): 747-753.
Kirby, S.H., 1983. Rheology of the Lithosphere. Reviews of Geophysics, 21(6): 1458-1487.
Kornprobst, J., 1974. Contribution a l'etude petrographique et sturcurale de la zone interne du Rif (Maroc septentrional). Notes Mem. Serv. Geol. Maroc, 251: 256.
Kornprobst, J., Suter, G. and Wildi, W., 1975. Carte Geologique du Rif: Bou Ahmed. In: A. Boudda (Editor), Editions Du Service Geologique du Maroc, Notes et Memoires No. 289. Royaume du Maroc, Ministere de l'Energie et des Mines, Direction de la Geologie.
Kornprobst, J., Tabit, A., Targuisti, K., Draoui, M. and Woodland, A.B., 1995. A Trip to Beni Bousera Ultamafic Massif (Morocco): Structural and Petrological Data, 2nd Workshop on Orogenic Lherzolites.
Kornprobst, J. and Vielzeuf, D., 1984. Transcurrent crustal thinning: a mechanism for the uplift of deep continental crust/upper mantle associations. In: J. Kornprobst (Editor), Kimberlites and Related Rocks. Development in Petrology Series, pp. 347-359.
Le Roux, V. et al., 2007. The Lherz spinel lherzolite: Refertilized rather than pristine mantle. Earth and Planetary Science Letters, 259(3-4): 599-612.
Le Roux, V., Tommasi, A. and Vauchez, A., 2008. Feedback between melt percolation and deformation in an exhumed lithosphere-asthenosphere boundary. Earth and Planetary Science Letters, 274(3-4): 401-413.
Lonergan, L. and White, N., 1997. Origin of the Betic-Rif mountain belt. Tectonics, 16(3): 504-522.
Loomis, T.P., 1972. Diapiric Emplacement of the Ronda High-Temperature Ultramafic Intrusion, Southern Spain. Geological Society of America Bulletin, 83: 2475-2496.
Maldonado, A. et al., 1992. Alboran Sea Late Cenozoic Tectonic and Stratigraphic Evolution. Geo-Marine Letters, 12(2-3): 179-186.
Maldonado, A., Somoza, L. and Pallares, L., 1999. The Betic orogen and the Iberian-African boundary in the Gulf of Cadiz: geological evolution (central North Atlantic). Marine Geology, 155(1-2): 9-43.
MartinezMartinez, J.M. and Azanon, J.M., 1997. Mode of extensional tectonics in the southeastern Betics (SE Spain): Implications for the tectonic evolution of the peri-Alboran orogenic system. Tectonics, 16(2): 205-&.
Menvielle, M. and Lemouel, J.L., 1985. Existence of a Conductivity Anomaly in the High Atlas Area (Morocco) and Telluric Currents Concentration at a Regional Scale. Bulletin De La Societe Geologique De France, 1(4): 553-558.

Michard, A., Chalouan, A., Feinberg, H., Goffe, B. and Montigny, R., 2002. How does the Alpine belt end between Spain and Morocco? Bulletin De La Societe Geologique De France, 173(1): 3-15.
Michard, A., Chopin, C. and Henry, C., 1993. Compression Versus Extension in the Exhumation of the Dora-Maira Coesite-Bearing Unit, Western Alps, Italy. Tectonophysics, 221(2): 173-193.
Michard, A., Goffe, B., Bouybaouene, M.L. and Saddiqi, O., 1997. Late Hercynian-Mesozoic thinning in the Alboran Domain: Metamorphic data from the northern Rif, Morocco. Terra Nova, 9: 1-8.
Monie, P., Delamotte, D.F. and Leikine, M., 1984. AN AR-39-AR-10 PRELIMINARY-STUDY OF THE ALPINE METAMORPHISM WITHIN THE EXTERNAL RIF (MOROCCO) - SOME PRECISIONS ABOUT ITS TERTIARY EVOLUTION. Revue De Geologie Dynamique Et De Geographie Physique, 25(4): 307-317.
Montel, J.M., Kornprobst, J. and Vielzeuf, D., 2000. Preservation of old U-Th-Pb ages in shielded monazite: example from the Beni Bousera Hercynian kinzigites (Morocco). Journal of Metamorphic Geology, 18(3): 335-342.
Montigny, R. et al., 2004. K-Ar and 40Ar/39Ar Study of Metamorphic Rocks from the Internal Rif (Morocco): Geochronological constraints on the Peridotite Emplacement and Exhumation Tectonics in the Gibraltar Arc, revisited. Bulletin De La Societe Geologique De France, 174, in press.
Muntener, O., Pettke, T., Desmurs, L., Meier, M. and Schaltegger, U., 2004. Refertilization of mantle peridotite in embryonic ocean basins: trace element and Nd isotopic evidence and implications for crust-mantle relationships. Earth and Planetary Science Letters, 221(1-4): 293-308.
Najid, D., Westphal, M. and Hernandez, J., 1981. Paleomagnetism of Quaternary and Miocene Lavas from Northeast and Central Morocco. Journal of Geophysics-Zeitschrift Fur Geophysik, 49(2): 149-152.
Obata, M., 1980. THE RONDA PERIDOTITE - GARNET-LHERZOLITE, SPINEL-LHERZOLITE, AND PLAGIOCLASE-LHERZOLITE FACIES AND THE P-T TRAJECTORIES OF A HIGH-TEMPERATURE MANTLE INTRUSION. Journal of Petrology, 21(3): 533-572.
Pearson, D.G., 1989. The petrogenesis of pyroxentites containing octahedral graphite and associated mafic and ultramafic rocks of the Beni Bousera Peridotite Massif, N. Morocco, University of Leeds, Leeds, UK, 413 pp.
Piasecki, A., 2009. The contact relationship between a large orogenic ultramafic massif and its surrounding units: Beni Bousera northern Morocco, Massachusetts Institute of Technology, Cambridge, MA, 36 pp.
Platt, J.P. et al., 2003. Exhumation of the Ronda peridotite and its crustal envelope: constraints from thermal modelling of a P-T-time array. Journal of the Geological Society, 160: 655-676.
Platt, J.P. and Vissers, R.L.M., 1989. Extensional Collapse of Thickened Continental Lithosphere - a Working Hypothesis for the Alboran Sea and Gibraltar Arc. Geology, 17(6): 540-543.
Platzman, E., Platt, J.P., Kelley, S.P. and Allerton, S., 2000. Large clockwise rotations in an extensional allochthon, Alboran Domain (southern Spain). Journal of the Geological Society, 157: 1187-1197.

Platzman, E.S., 1992. Paleomagnetic Rotations and the Kinetmatics of the Gibraltar Arc. Geology, 20(4): 311-314.
Platzman, E.S., Platt, J.P. and Olivier, P., 1993. Paleomagnetic Rotations and Fault Kinematics in the Rif Arc of Morocco. Journal of the Geological Society, 150: 707-718.
Prior, D.J. et al., 1999. The application of electron backscatter diffraction and orientation contrast imaging in the SEM to textural problems in rocks. American Mineralogist, 84(11-12): 1741-1759.
Rehault, J.P., Boillot, G. and Mauffret, A., 1984. THE WESTERN MEDITERRANEAN BASIN GEOLOGICAL EVOLUTION. Marine Geology, 55(3-4): 447-477.
Reuber, I., Michard, A., Chalouan, A., Juteau, T. and Jermoumi, B., 1982. Structure and Emplacement of the Alpine-Type Peridotites from Beni Bousera, Rif, Morocco - a Polyphase Tectonic Interpretation. Tectonophysics, 82(3-4): 231-251.
Roest, W.R. and Srivastava, S.P., 1991. KINEMATICS OF THE PLATE BOUNDARIES BETWEEN EURASIA, IBERIA, AND AFRICA IN THE NORTH-ATLANTIC FROM THE LATE CRETACEOUS TO THE PRESENT. Geology, 19(6): 613-616.
Rosenberg, C.L. and Handy, M.R., 2001. Mechanisms and orientation of melt segregation paths during pure shearing of a partially molten rock analog (norcamphor-benzamide). Journal of Structural Geology, 23(12): 1917-1932.
Saddiqi, O., Feinberg, H., Elazzab, D. and Michard, A., 1995. Paleomagnetism of the Beni-Bousera Peridotites (Internal Rif, Morocco) - Consequences for the Miocene Evolution of the Gibraltar Arc. Comptes Rendus De L Academie Des Sciences Serie Ii Fascicule a-Sciences De La Terre Et Des Planetes, 321(5): 361-368.
Sanchez-Rodriguez, L. and Gebauer, D., 2000. Mesozoic formation of pyroxenites and gabbros in the Ronda area (southern Spain), followed by Early Miocene subduction metamorphism and emplacement into the middle crust: U-Pb sensitive high-resolution ion microprobe dating of zircon. Tectonophysics, 316(1-2): 19-44.
Savostin, L.A., Sibuet, J.C., Zonenshain, L.P., Lepichon, X. and Roulet, M.J., 1986. KINEMATIC EVOLUTION OF THE TETHYS BELT FROM THE ATLANTIC-OCEAN TO THE PAMIRS SINCE THE TRIASSIC. Tectonophysics, 123(1-4): 1-35.
Scott, T. and Kohlstedt, D.L., 2006. The effect of large melt fraction on the deformation behavior of peridotite. Earth and Planetary Science Letters, 246(3-4): 177-187.
Skemer, P., Katayama, B., Jiang, Z.T. and Karato, S., 2005. The misorientation index: Development of a new method for calculating the strength of lattice-preferred orientation. Tectonophysics, 411(1-4): 157-167.
Slodkevitch, V.V., 1982. Paramorphosis of diamond into graphite. Mineralogical Society of USSR, 1: 13-33.
Stampfli, G.M. et al., 1998. Subduction and obduction processes in the Swiss Alps. Elsevier Science Bv, pp. 159-204.
Stolper, E., 1980. A PHASE-DIAGRAM FOR MID-OCEAN RIDGE BASALTS - PRELIMINARY-RESULTS AND IMPLICATIONS FOR PETROGENESIS. Contributions to Mineralogy and Petrology, 74(1): 13-27.

Streckeisen, A., 1976. To Each Plutonic Rock Its Proper Name. Earth-Science Reviews, 12(1): 1-33.
Suhr, G., 1999. Melt migration under oceanic ridges: Inferences from reactive transport modelling of upper mantle hosted dunites. Journal of Petrology, 40(4): 575-599.
Sundberg, M. and Cooper, R.F., 2008. Crystallographic preferred orientation produced by diffusional creep of harzburgite: Effects of chemical interactions among phases during plastic flow. Journal of Geophysical Research-Solid Earth, 113(B12): -.
Tommasi, A., Mainprice, D., Canova, G. and Chastel, Y., 2000. Viscoplastic self-consistent and equilibrium-based modeling of olivine lattice preferred orientations: Implications for the upper mantle seismic anisotropy. Journal of Geophysical Research-Solid Earth, 105(B4): 7893-7908.
Tommasi, A., Vauchez, A., Godard, M. and Belley, F., 2006. Deformation and melt transport in a highly depleted peridotite massif from the Canadian Cordillera: Implications to seismic anisotropy above subduction zones. Earth and Planetary Science Letters, 252(3-4): 245-259.
Torresroldan, R.L., Poli, G. and Peccerillo, A., 1986. AN EARLY MIOCENE ARC-THOLEIITIC MAGMATIC DIKE EVENT FROM THE ALBORAN SEA - EVIDENCE FOR PRECOLLISIONAL SUBDUCTION AND BACK-ARC CRUSTAL EXTENSION IN THE WESTERNMOST MEDITERRANEAN. Geologische Rundschau, 75(1): 219-234.
Turner, S.P. et al., 1999. Magmatism associated with orogenic collapse of the Betic-Alboran Domain, SE Spain. Journal of Petrology, 40(6): 1011-1036.
Underwood, E., 1970. Quantitative Stereology. Addison-Welsley Pub. Co., Reading, Massachusetts.
Vanderwal, D., Chopra, P., Drury, M. and Fitz Gerald, J.D., 1993. Relationships between Dynamically Recrystallized Grain-Size and Deformation Conditions in Experimentally Deformed Olivine Rocks. Geophysical Research Letters, 20(14): 1479-1482.
Vanderwal, D. and Vissers, R.L.M., 1993. Uplift and Emplacement of Upper-Mantle Rocks in the Western Mediterranean. Geology, 21(12): 1119-1122.
Verges, J. and Sabat, F., 1999. Constraints on the Neogene Mediterranean kenematic evolution along a 1000km transect from Iberia to Aftrica. In: B. Durand, l. Jolivet, F. Horvath and M. Seranne (Editors), The Mediterranean basins: Tertiary Extension withing the Alpine Orogen. Geol. Soc. Spec. Publ., London, pp. 63-80.
Vidal, O., Goffe, B., Bousquet, R. and Parra, T., 1999. Calibration and testing of an empirical chloritoid-chlorite Mg-Fe exchange thermometer and thermodynamic data for daphnite. Journal of Metamorphic Geology, 17(1): 25-39.
Warren, J.M., Hirth, G. and Kelemen, P.B., 2008. Evolution of olivine lattice preferred orientation during simple shear in the mantle. Earth and Planetary Science Letters, 272(3-4): 501-512.
Watts, A.B., Platt, J.P. and Buhl, P., 1993. Tectonic Evolution fo the Alboran Sea Basin. Basin Research, 5: 153-177.

Wenk, H.R., 2002. Texture and anisotropy. In: S. Karato and H.R. Wenk (Editors). Mineralogical Soc America, pp. 291-329.
Wenk, H.R. and Tome, C.N., 1999. Modeling dynamic recrystallization of olivine aggregates deformed in simple shear. Journal of Geophysical Research-Solid Earth, 104(B11): 25513-25527.
Wildi, W., 1983. The Orogenic Belt of the Rif (Morocco) and the Tell (Algeria, Tunisia) - Structure, Stratigraphy, Paleogeographic and Tectonic Evolution from Triassic to the Miocene. Revue De Geologie Dynamique Et De Geographie Physique, 24(3): 201-297.
Wood, B.J. and Banno, S., 1973. Garnet-Orthopyroxene and Orthopyroxene-Clinopyroxene Relationships in Simple and Complex Systems. Contributions to Mineralogy and Petrology, 42(2): 109-124.
Zeck, H.P., 1996. Betic-Rif orogeny: Subduction of Mesozoic Tethys lithosphere under eastward drifting Iberia, slab detachment shortly before 22Ma, and subsequent uplift and extensional tectonics. Tectonophysics, 254(1-2): 1-16.
Zhang, S.Q. and Karato, S., 1995. Lattice Preferred Orientation of Olivine Aggregates Deformed in Simple Shear. Nature, 375(6534): 774-777.

Appendix 1: Sample Locations

SAMPLE	NORTHING	EASTING	DESCRIPTION
BB-08-9	35°17'02.412" N	4°53'46.176" W	Honeycomb lherzolite near the center of the heterogeneous zone.
BB-08-10	35°16'38.604" N	4°53'52.770" W	Nich Lherzolite
BB-08-13	35°16'50.772" N	4°53'50.532" W	Strongly foliated lherzolite
BB-08-18	35°16'54.732" N	4°53'48.894" W	Transitional lherzolite/ harzburgite within the heterogeneous zone
BB-08-23	35°16'53.502" N	4°53'48.462" W	Honeycomb lherzolite within the heterogeneous zone
BB-08-31	35°17'11.588" N	4°53'39.540" W	Strongly foliated lherzolite
BB-08-35	35°17'11.130" N	4°53'41.154" W	Strongly foliated lherzolite
BB-08-45	35°15'48.132" N	4°53'59.496" W	Dunite within Porphyric harzburgite
BB-08-47	35°16'04.260" N	4°54'02.190" W	Porphyric harzburgite
BB-08-49	35°16'17.496" N	4°5401.290" W	Nich lherzolite

Beni Bousera Massif

Northern Morocco

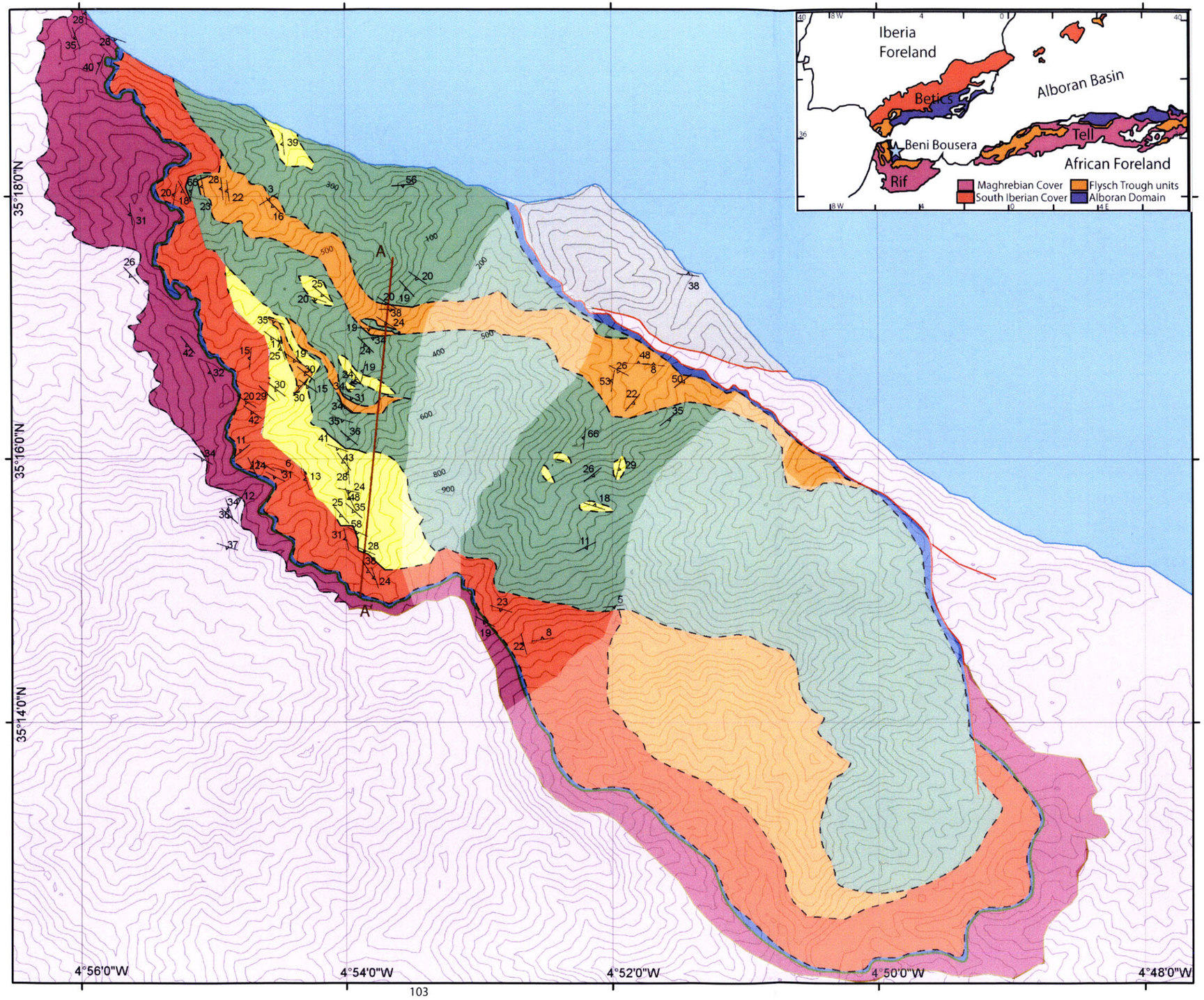

Legend

Foliation strike and dip
contour interval 50 meters

Contacts

- Massif Edge
- coast
- fault
- inferred
- known

Geologic Units

- Nich Lherzolite
- Porphyric Harzburgite
- Heterogeneous Zone
- Border Facies
- Kinzingites
- Serpentinite
- Ghomeride Shale
- Sebtide Gneisses and Schists
- Mediterranean Sea

N

0 0.5 1 2 3 4

Kilometers

Plate 1: Geologic Map

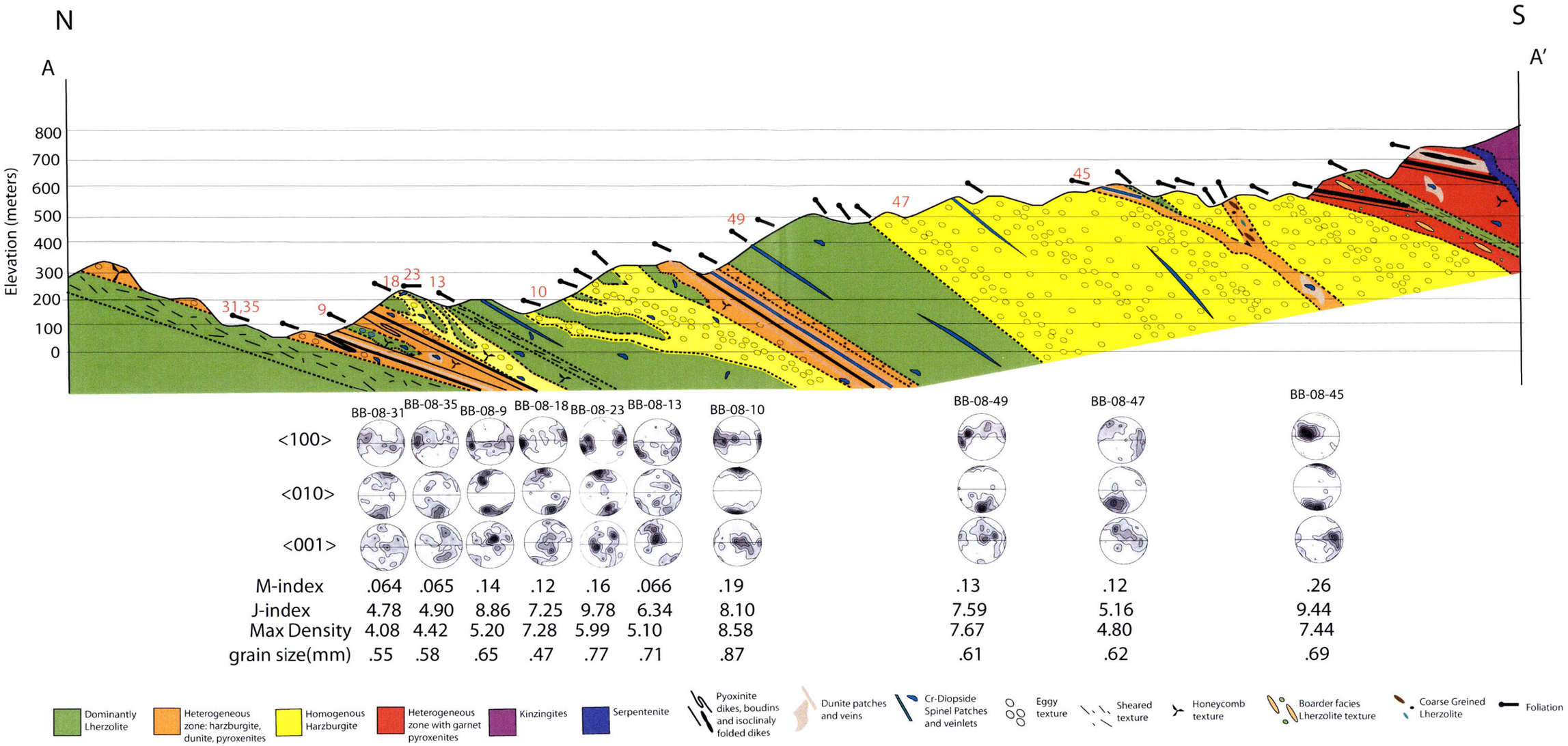

Plate 2. Cross section of massif with LPO pole figures shown with respect to geology. Pole figures are shown wiht foliation horizontal, north to the left, and upwards up. Red numbers above foliation symbols correspond to approximate sample location. Contour interval on all pole figures is 1 multiple of a uniform distribution. No vertical exaggeration in cross section.